A SIMPLIFIED SYNTHESIS OF LOSSLESS TWO-PORT WAVE DIGITAL AND ANALOG FILTERS

by

Mark R. Jarmasz

A thesis presented to the Faculty of Graduate Studies
University of Manitoba
in partial fulfillment of the requirements for the degree
Doctor of Philosophy

February 1990, Winnipeg, Manitoba

ISBN 0-315-63272-0

Canada

A SIMPLIFIED SYNTHESIS OF LOSSLESS TWO-PORT WAVE DIGITAL AND ANALOG FILTERS

BY

MARK R. JARMASZ

A thesis submitted to the Faculty of Graduate Studies of the University of Manitoba in partial fulfillment of the requirements of the degree of

DOCTOR OF PHILOSOPHY

I hereby declare that I am the sole author of this thesis.

I authorize the University of Manitoba to lend this thesis to other institutions or individuals for the purpose of scholarly research.

Mark R. Jarmasz

I further authorize the University of Manitoba to reproduce this thesis by photocopying or by other means, in total or in part, at the request of other institutions or individuals for the purpose of scholarly research.

Mark R. Jarmasz

ABSTRACT

A synthesis algorithm of lossless 2-port networks is presented which is based on a simplified characterization of elementary sections and on an extraction step that eliminates the need for performing basic polynomial operations such as polynomial multiplication and division, zero finding, continued fraction expansion, solution of non-trivial simultaneous equations and rational interpolation. Each elementary section is characterized using a triplet of numbers $\{\psi_i , \rho(\psi_i) , d(\psi_i)\}$, where ψ_i is the location of the transmission zero, $\rho(\psi_i)$ is the value of the reflectance at the transmission zero, and $d(\psi_i)$ is the value of the return group delay at the transmission zero and is only required for reciprocal sections. During the extraction of a section that realizes a particular transmission zero, the triplets that characterize the remaining transmission zeros are recomputed using a pair of simple algebraic expressions that only require complex multiplications and divisions. If the extracted section is chosen appropriately, the recomputed triplets characterize a lower-order network and the resulting realization is canonic. The extraction step is repeated after selecting the next transmission zero.

It is shown that a cascade (chain) decomposition of lossless and real two-port networks characterized using scattering variables can be completed to within a constant section by applying the above procedure. In the disctrete-time domain, the triplet characterizing every elementary section is, analogous to the analog domain, given by $\{z_i , \rho(z_i) , \delta(z_i)\}$, where $z_i = (1 + \psi_i)/(1 - \psi_i)$. It is shown that $\rho(z_i) = \rho(\psi_i)$ and $\delta(z_i)$ and $d(\psi_i)$ are related by a constant. It follows that the synthesis algorithm is applicable to both the continuous-time (analog) domain in the form of lumped LC and commensurate distributed networks and to the discrete-time domain in the form of wave digital filters. All types and multiplicities of transmission zeros are allowed, with multiple zeros handled in a slightly different way from distinct zeros.

It is shown that all elementary sections of degree one and two can be derived systematically from a basic 4-port topology that is matched (i.e., has zero reflectance) at each port. By terminating two of the ports with basic reactances – which, in the wave digital (WD) domain, map to allpass sections – all elementary 1st- and 2nd-order sections can be obtained such that the corresponding WD circuits consist of only one basic building block – called the 2-port adaptor. A 2-port adaptor is the WD equivalent of an ideal transformer and its normalized scattering matrix corresponds to a planar rotation. The above derivation is an independent verification of the fact that every orthogonal scattering matrix can be factored non-uniquely into a product of planar rotation operators.

A computable WD circuit for the general 2nd-order reciprocal and nonreciprocal sections is derived via the factorization of the scattering hybrid matrix. It is shown that the underlying topology is still that of the matched 4-port with the two allpass terminations forming a

coupling network. Giving up one degree of freedom by setting $\rho(z_i) = z_i$, results in a simplified WD circuit that has a single-multiplier control of the transmission zero and is structurally lossless, i.e., the circuit allows a canonic number of quantizations and remains ideally lossless after the quantizations have been performed. Structural losslessness leads to low sensitivity of the filter response to parameter variations.

By terminating two other ports with allpass sections, canonic sections are derived that are structurally lossless and consist of a minimum number of 2-port adaptors. It is shown, however, that these sections cannot be made reflection-free without giving up crucial degrees of freedom. However, these sections are still useful, but to ensure computability, they must be terminated on both sides by reflection-free sections, as shown in an example. Other examples are presented that demonstrate the numerical robustness and relative immunity to roundoff error accumulation of the synthesis algorithm. They also show the effect of interchanging the reflectance and transmittance, as well as using voltage versus power wave 2-port adaptors, on the sensitivity of the filter response to parameter quantizations.

ACKNOWLEDGEMENTS

The author wishes to express his sincere appreciation to Professor G.O. Martens for his untiring, always-available, and ever-helpful guidance throughout the course of this work. Thanks also are due to R. Smith and V. Cheng for doing some of the simulation and programming work. Many helpful discussions with G. Scarth, L. Leung, and X. Liang are also much appreciated.

Special thanks to Kristina and Jessica for allowing me the privilege of this intellectual vacation.

TABLE OF CONTENTS

I. INTRODUCTION

Canonic decomposition of lossless two-port networks in the continuous-time domain is a classical problem that, due to its importance, has received a great deal of attention over the years [1]-[9]. An elegant and efficient solution to this problem is of great interest since filtering, as realized using an electrical circuit or network, is a frequently occuring operation in most electrical engineering applications. Also, due to the remarkable advances in VLSI technology in recent years, the problem has resurfaced in the discrete-time domain in the form of wave digital filters [11],[14]-[16]. However, as will become clear in this thesis, the two problems are essentially equivalent due to the close relationship that exists between wave digital filters (WDFs) and their analog counterparts.

Filter design based on inserting a lossless 2-port network between two resistive terminations has received most of the attention since such networks exhibit the best properties. Among these, low response sensitivity to element variations is of great importance. In this area, the pioneering work of Cauer [7] and Darlington [8] deserve special mention. They proved a critical result, namely:

> A given rational function $Z(\psi)$ is realizable as the driving-point impedance of a lossless 2-port network terminated in a (1Ω) resistor (see Fig. 1.1), if and only if $Z(\psi)$ is a positive real (p.r.) function (i.e., $Z(\psi)$ is real for real ψ and $\mathrm{Re}\{ Z(\psi) \} > 0$ for $\mathrm{Re}\{ \psi \} > 0$).

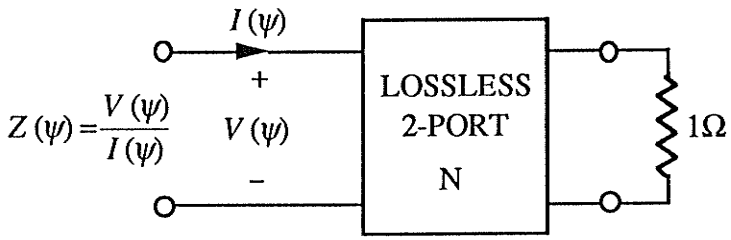

Fig. 1.1. Realization of an arbitrary positive real impedance $Z(\psi)$.

The main problem of network cascade synthesis can be stated as follows: starting from $Z(\psi)$ or some other equivalent characterization, extract low-order realizable lossless subnetworks such that the overall cascade connection terminated in a 1Ω resistor has the prescribed $Z(\psi)$. (See Fig. 1.2). Each subnetwork N_i in Fig. 1.2 realizes a particular transmission zero. The mechanics of extracting (or removing) a subnetwork N_i can be quite involved and, generally, depend on the nature of the transmission zero being extracted. For example, if all the transmission zeros are at infinity, then a continued fraction expansion of $Z(\psi)$, or its

reciprocal $Y(\psi)$, is sufficient to complete the synthesis [2]. This covers the classical Butterworth and Chebyshev response cases. If the transmission zeros are all distinct, which is the usual case for transfer functions that are highly selective, then general 2nd-order reciprocal (Brune) sections are required. If, in addition, the transfer function has transmission zeros with non-zero real part, which can result from an attempt to optimize the phase response, then the extraction of nonreciprocal sections is necessary. This thesis deals with transfer functions of the most general type.

Upon completion of the extraction step, the remainder impedance $Z_i(\psi)$ is obtained (see Fig. 1.2) and the process is repeated until $Z_L = 1$.

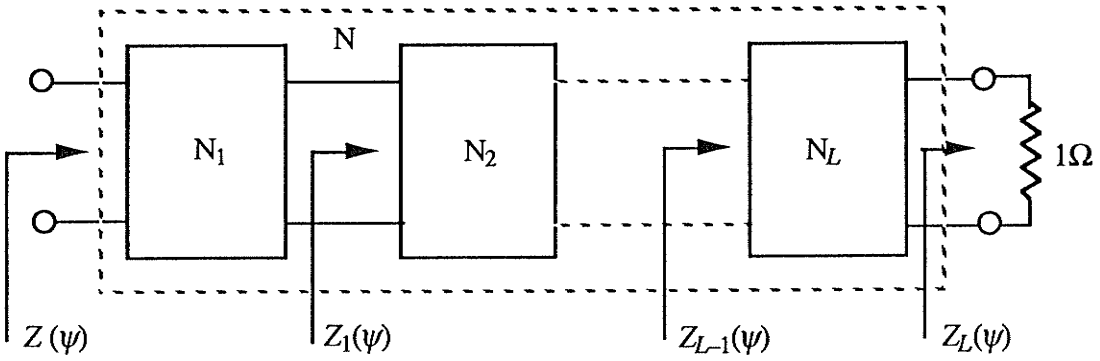

Fig. 1.2. Network cascade synthesis.

For the process to be successful each extraction step must satisfy the following:

(a) The extracted subnetwork must be realizable with physical elements.

(b) The positive real property of the remainders $Z_i(\psi)$ must be maintained.

(c) The remainder $Z_i(\psi)$ must be of lower degree than $Z_{i-1}(\psi)$ unless a zeroth-order section is being extracted.

If the order of the extracted N_i is the difference of orders of $Z_i(\psi)$ and $Z_{i-1}(\psi)$ $\forall i$, then the process is canonic, i.e., the sum of orders of N_i equals the order of N. This thesis deals with canonic cascade synthesis of real networks only.

Most of the practical difficulties encountered during the extraction step stem from the particular representation of the subnetwork N_i , i.e., the choice of signal variables and the form of polynomials. Traditionally, one used the chain matrix representation [2], [28], as shown in Fig. 1.3a, where the overall chain matrix **K** is a product of all the subnetwork chain matrices $\mathbf{K}_i$. An alternative due to Belevitch [1], [9] uses wave quantities for signal variables (see Fig. 1.3b), and the cascade decomposition can be accomplished by factoring the scattering transfer matrix **T** (henceforth simply called the transfer matrix). It is now generally accepted that the transfer matrix **T** is a better tool for network synthesis because its representation requires only three polynomials - referred to as Belevitch's representation - whereas four rational functions are needed for the chain matrix **K** (see Fig. 1.3). In passing,

we should note that in order to derive computable digital filters that are modelled on analog filters, one must use wave quantities for signal variables instead of the more obvious voltage and current signals [10]. Hence, synthesis based on the **T** matrix is applicable to both the analog and digital domains.

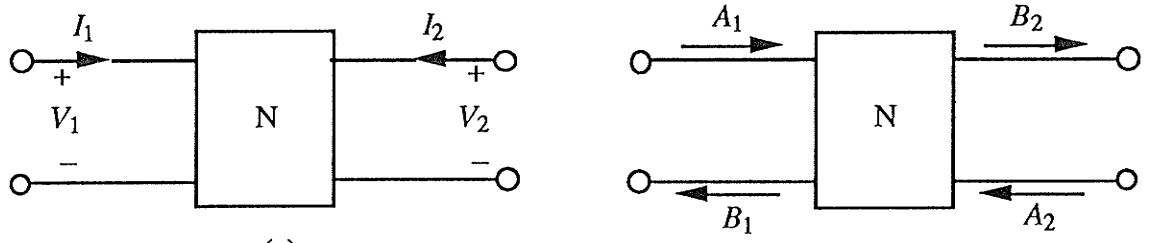

$$\begin{bmatrix} V_1 \\ I_1 \end{bmatrix} = \begin{bmatrix} A & B \\ C & D \end{bmatrix} = \begin{bmatrix} -I_2 \\ V_2 \end{bmatrix} = \mathbf{K} \begin{bmatrix} V_2 \\ -I_2 \end{bmatrix} \qquad \begin{bmatrix} B_1 \\ A_1 \end{bmatrix} = \frac{1}{f(\psi)} \begin{bmatrix} \pm g(-\psi) & h(\psi) \\ \pm h(-\psi) & g(\psi) \end{bmatrix} \begin{bmatrix} A_2 \\ B_2 \end{bmatrix} = \mathbf{T} \begin{bmatrix} A_2 \\ B_2 \end{bmatrix}$$

Fig. 1.3 Network characterization using (a) chain matrix **K** and (b) transfer matrix **T.**

The factorization problem can be formulated in many different ways. One possibility is to solve a set of simultaneous equations which are obtained from the coefficients of the canonic polynomials $f(\psi)$, $g(\psi)$, and $h(\psi)$ [3],[4]. However, it is known that the coefficient form representation is inappropriate for highly selective filters, i.e. ones with a high degree and a narrow band, due to the high sensitivity of element values to variations in the coefficient values [5]. This problem is usually circumvented by using the zero form representation for the polynomials. Williamson successfully used this form in his reformulation of the factorization problem as a rational interpolation problem [31]. However, as is the case for most zero-form algorithms, an efficient and reliable zero-finding routine is required. Such an operation consumes a lot of computer time, is not always reliable, and generates roundoff error which can accumulate to excessive levels unless an elaborate extraction method is employed that at each stage uses only the input data [31]. It is shown in this thesis that comparable results can be achieved using much simpler techniques.

An alternative method, which simplifies the mechanics of the extraction step somewhat, operates on the input reflectance

$$\rho(\psi) \equiv \frac{h(\psi)}{g(\psi)} = \frac{Z(\psi) - 1}{Z(\psi) + 1} \tag{1.1}$$

which, for positive real $Z(\psi)$, can be shown to be bounded real (passive) [1]. In this approach, the remainder reflectance is obtained by forcing cancelling common factors between the numerator and denominator (see Fig. 1.4) [16],[19],[20]. However, in order to

force the cancellation of common factors, it is usually necessary to either find the zeros of or perform long division on both the numerator and denominator polynomials. These operations are computationally intensive and again generate roundoff errors.

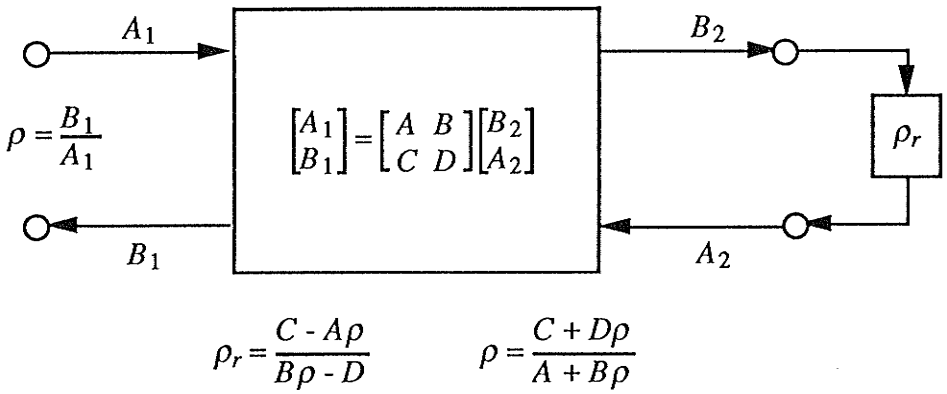

Fig. 1.4 Basic two-port (pair) extraction step from [16],[20].

In this thesis, a novel synthesis algorithm is presented that eliminates the need for performing all basic polynonial operations, particularly zero finding, as well as solving a set of simultaneous equations. It is shown that instead of the usual polynomial representations, only values of the reflectance and, for reciprocal sections, the return group delay (henceforth simply called the delay) evaluated at all the transmission zeros are required to complete the synthesis. These values form an equivalent characterization of the overall network as well as of each individual elementary section. It is mainly due to this characterization that a simplification can take place. During the extraction step, a canonic section is removed that realizes a chosen transmission zero, followed by the recomputation of reflectance and delay values at the remaining transmission zeros. By appropriately selecting the extracted section, the process of recomputation generates new reflectance and delay values that correspond to a lower-order network. This step is accomplished by applying two simple formulae, as derived in Chapter IV, that require only simple polynomial evaluations. Synthesis is completed by iterating the basic extraction step. The algorithm can synthesize lossless filters in the ψ-domain in the form of lumped LC and commensurate distributed networks, and in the $z = (\psi + 1)/(\psi - 1)$ - domain in the form of WDFs. All locations and multiplicities of transmission zeros are allowed. Since the algorithm is free of elaborate logical procedures and sophisticated computational tools, it is ideally suited for a first time user in need of a quick solution. The relative speed with which a particular solution can be obtained allows for experimentation and optimization of the final realization.

The prototype used throughout is the lossless two-port network inserted between resistive terminations. It is well known that such a structure offers very low sensitivities to element variations in both the continuous- and discrete-time domains [11, p. 273],[43].

Other terminations are possible; eg, the load-port can be open-circuited [24], or an ideal source can be applied to the source-port [25]. However, these prototypes have been shown to suffer from higher sensitivities [26].

As already mentioned, with the advent of the transistor and the subsequent microchip, the focus has shifted from continuous-time to discrete-time filtering (or digital filtering), where the continuous-time signals are sampled and the sample values are represented and processed using binary arithmetic. Digital filters are recursive numerical algorithms, and in this sense, can be said to have been invented by mathematicians in the 19th century [32], thus predating continuous-time filters. Advantages of digital filters are many, some of which include: reduced cost, flexibility of implementation, filter parameters are independent of temperature variations and ageing, complete design methodologies are available, cf [32], [33]. With modern super-efficient digital signal processors (DSPs) that can perform an addition and multiplication step in 200 ns, digital filters have become a viable alternative to analog filters for most real-time applications. For very high sampling frequencies, specialized VLSI circuits can be designed [34],[35].

However, the most important advance in digital filtering came when it was discovered that the superior and desirable properties of doubly-terminated lossless analog filters, such as low sensitivity and passivity, can also be achieved in the digital domain by imitating the topology of analog filters. The resulting class of digital filters is called wave digital, and was originated by Fettweis [10]. The term wave refers to the fact that, instead of voltage and current variables, incident and reflected wave quantities

$$a = v + Ri \quad , \quad b = v - Ri \qquad R \text{ an arbitrary positive reference}$$

must be used to ensure computability, i.e., no delay-free loops. Wave digital building blocks, also called adaptors, are lossless under linear (infinite precision) operating conditions and can be made passive under nonlinear (finite arithmetic) operating conditions if an appropriate truncation scheme is employed. Normally, magnitude truncation [12] and overflow saturation [13] of the signals between the adaptors are sufficient for the suppression of zero-input granularity oscillations and forced-response overflow oscillations, respectively. These nonlinear functions can be easily implemented with most digital signal processors. In addition to eliminating parasitic oscillations, WDFs consisting of a simple interconnection of passive building blocks also enjoy low sensitivity to parameter quantizations in the passband. If the transmission zeros are distributed independently among the cascade of canonic sections, then low sensititivity is also present in the stopband.

Properties of losslessness and passivity lead to many other desirable properties [11] and make WDFs the primary choice for many applications; eg. WDFs provide two complementary transfer functions, the reflectance and the transmittance, without additional cost and are ideally suited as branching filters in polyphase arrangements in subband coders

[36],[37], and in PCM/FDM transmultiplexers [38]; WD bandpass filters have been designed for isolating the harmonic voltage and current signals in a control loop of a self-tuning reactor that eliminates unwanted harmonics in a power station [39]. Although WDFs require more additions than the conventional digital filters [40], such a criterion is no longer as important due to the efficiency of modern DSPs. Instead, properties such as nonlinear stability, low sensitivity, modularity, pipelineability (parallelism) are of greater importance [15],[41]. WDFs have been shown to possess all these properties [11]. A comprehensive survey of wave digital filters along with a 400 item reference list can be found in [11].

Recently, there has been a lot of attention directed towards the so called orthogonal filters which possess similar properties [14]-[16]. However, these structures have been shown to be normalized voltage WDFs, otherwise known as power WDFs [11],[17],[18]. Voltage WDFs are normally preferable since they require fewer multipliers, remain lossless even with quantized multipliers, have lower sensitivity, and make better use of the dynamic range. Power WDFs, on the other hand, are optimally scaled to minimize the probability of overflow but, with quantized coefficients, can only be made passive with the result that the transmission zeros move off the unit circle. This problem diminishes as more bits are used for the multipliers.

In Chapter II, we reiterate some of the conclusions reached in [11] and present some additional properties of the reflectance and the return group delay of lossless, real two-port networks that pertain to the synthesis problem. Belevitch's representation theory is presented which forms a minimal set of necessary and sufficient conditions for a lossless scattering matrix to be realizable [1]. A derivation of basic wave digital building blocks is given. Finally, a connection between continuous and discrete-time domains is discussed.

Chapter III deals with the characterization of elementary sections using values of the reflectance and delay evaluated at the location of the transmission zero. It is shown that starting from a basic 4-port topology, all the 1st and 2nd-order sections can be derived in a systematic way for both the continuous and discrete-time domains. A 2nd-order section with one degree of freedom less but some very desirable features [29] is analyzed where the additional constraint is imposed using a nonlinear optimization algorithm [42]. A network equivalence is applied that equates the transfer matrix with the hybrid matrix and allows a simple derivation of WD sections comprised of only delays and one basic building block, called the 2-port adaptor, whose scattering matrix is given by

$$S_\theta = \begin{bmatrix} -\cos\theta & \sin\theta \\ \sin\theta & \cos\theta \end{bmatrix} \tag{1.2}$$

and is clearly related to the planar rotator. A class of similar WD sections are derived based on the factorization of the scattering matrix. However, it is shown that these sections have some practical limitations.

One of the more desirable properties of digital circuits with quantized multipliers is the

confinement of transmission zeros of reciprocal elementary sections to the unit circle where they contribute most efficiently towards the overall attenuation. It is shown in Chapter III that this property does not hold for passive WD circuits, i.e. where two quantized multipliers (see eq. (1.2)) are used for each power wave 2-port adaptor (this includes orthogonal filters). Passivity stems from the fact that $\sin^2\theta + \cos^2\theta = 1$ cannot be satisfied with binary fractions. However, the confinement property does hold for lossless WD circuits comprised of voltage wave 2-port adaptors with only one quantized multiplier and the scattering matrix given by

$$S_v = \begin{bmatrix} -\cos\theta & 1+\cos\theta \\ 1-\cos\theta & \cos\theta \end{bmatrix} = P\, S_\theta\, P^{-1} \quad \text{where} \quad P = \begin{bmatrix} 1 & 0 \\ 0 & \cot\theta/2 \end{bmatrix} \tag{1.3}$$

where, it is assumed, the multiplier in P in (1.3) can be shifted out of the circuit. This condition is satisfied by most circuits. The use of voltage wave adaptors also reduces the amount of passivity (loss) that is generated by each section (if lossy elements are still present), which in turn improves passband sensitivity.

A simplified synthesis algorithm is presented in Chapter IV. It is shown that for distinct transmission zeros, the algorithm takes on a particularly simple form. If some of the transmission zeros are multiple, the reflectance and delay functions are evaluated instead on a circle centered at the location of the multiple transmission zero – a representation referred to as the sample characterization. Although this representation is more elaborate, it can be recomputed during the extraction step using essentially the same formulae as for the distinct zero case. A two-stage extraction step is described where a primitive canonic section is extracted first, followed by an ideal transformer $\leftrightarrow$ 2-port adaptor that induces a desired property for the overall section; e.g., reflection-free port, straight-through connection at some frequency, etc. (Note: we use the character $\leftrightarrow$ to denote the bilinear mapping between the analog and WD domains.) Finally, several methods, and their relative merits, of extracting the final ideal transformer (2-port adaptor) are described.

Several design examples are presented in Chapter V which illustrate the important aspects of the synthesis algorithm as well as general properties of WDFs. A very narrow-band 14th-order bandpass filter [22] has been selected to demonstrate the low rate of roundoff error accumulation. Another example shows the practical differences of realizing a given transfer function as a transmittance and as a reflectance. A comparison is made between quantized structures realized using power and voltage wave 2-port adaptors. Other examples demonstrate the feasibility of obtaining simplified designs where each 2nd-order section has one degree of freedom less.

II. ANALOG AND DIGITAL LOSSLESS TWO–PORT NETWORKS

This chapter deals mainly with the characterization of lossless and real two-port networks using scattering parameters. Such a characterization is most natural for doubly-terminated analog networks and, more importantly, leads to computable (wave) digital networks. Because of the close link, it is possible to present this characterization without making explicit reference to the complex frequency variable being used.

2.1 On the Connection between Continuous and Discrete–Time Domains

Signals in digital circuits are discrete-time signals and, as a first step, can be expressed as impulse -train modulated continuous-time signals, i.e.

$$x_s(t) := x(t) \sum_{n=-\infty}^{\infty} \delta(t-nT) = \sum_{n=-\infty}^{\infty} x(nT)\, \delta(t-nT) \tag{2.1}$$

where T is the sampling period. A discrete-time signal is defined as the sequence of numbers, $\{x(n)\}$, which correspond to the areas under the impulses in (2.1) [33]. The definition of the z-transform of a discrete-time signal follows from the Laplace transform of $x_s(t)$ and the mapping $z = e^{sT}$, i.e.

$$\begin{aligned} \mathrm{L}[x_s(t)] &:= \sum_{n=-\infty}^{\infty} x(nT) \int_{-\infty}^{\infty} \delta(t-nT)\, e^{-st}\, dt \\ &= \sum_{n=-\infty}^{\infty} x(nT)\, e^{-sTn} = \sum_{n=-\infty}^{\infty} x(n)\, z^{-n} =: X(z) \end{aligned} \tag{2.2}$$

The Fourier Transform ($s = j\omega$) of $x_s(t)$ is periodic in ω, i.e., the frequency response of an analog network with the impulse response $x_s(t)$ is periodic. A class of analog networks with an impulse response that can be expressed as $x_s(t)$ are the commensurate distributed microwave networks [2]. Since $x_s(t)$ can be identified via (2.1) with $\{x(n)\}$, it follows that the corresponding discrete-time network has an identical frequency response. A class of discrete-time networks which are derived this way is called wave digital, and was originated by A. Fettweis in 1971 [10].

The mapping $z = e^{sT}$ implies that wave digital filters (WDFs) follow from the process of discretization of commensurate distributed networks which, as we shall shortly see, are closely allied with the lumped-element networks. As a result, WDFs can be viewed as

numerical simulations of analog networks. Desirable properties of analog networks, such as losslessness and low sensitivity, are mapped directly to the digital domain.

The process of discretization and subsequent mapping to the wave digital domain can be seen most clearly by considering a section of uniform lossless transmission line of characteristic impedance R and a one-way delay of τ seconds, as shown in Fig. 2.1a.

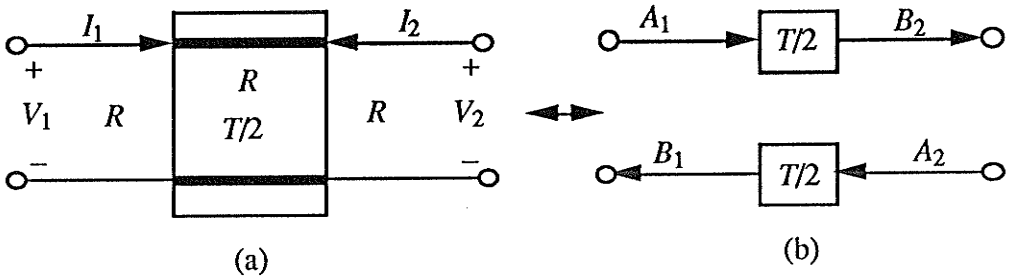

Fig. 2.1 (a) Unit element and (b) its wave digital image.

The chain parameters for this section are given by

$$\begin{bmatrix} V_1 \\ I_1 \end{bmatrix} = \begin{bmatrix} \cosh(s\tau) & R\sinh(s\tau) \\ \frac{1}{R}\sinh(s\tau) & \cosh(s\tau) \end{bmatrix} \begin{bmatrix} V_2 \\ -I_2 \end{bmatrix} = \mathbf{K} \begin{bmatrix} V_2 \\ -I_2 \end{bmatrix} . \tag{2.3a}$$

An alternative characterization which leads to simple and computable digital circuits uses wave quantities for port variables, as shown in Fig. 2.2a.

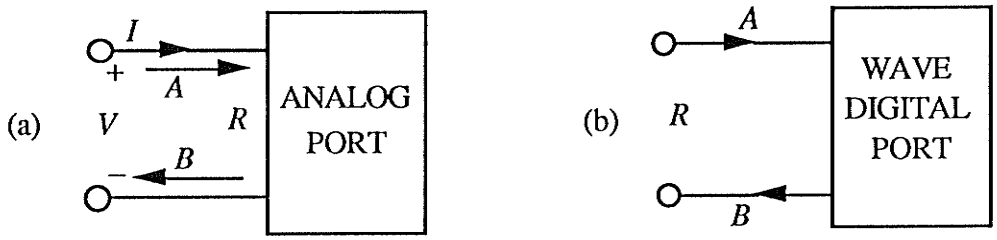

Fig. 2.2 Wave quantities as port variables.

In general, for each port i

$$A_i = V_i + R_i I_i \qquad \text{and} \qquad B_i = V_i - R_i I_i \tag{2.4}$$

are the incident and reflected voltage waves, respectively, and R_i is an arbitrary positive port reference. WD circuits can usually be simplified by a judicious choice of port references R_i.

A WD "port" corresponding to an analog port is shown in Fig.2.2b. Conceptually, the two ports differ greatly since, for the analog port, the port variables share the two leads and cannot be physically separated, whereas for the WD port, port variables are partitioned between two independent uni-directional signal-flow paths.

Applying (2.4) to (2.3a) yields the scattering transfer representation

$$\begin{bmatrix} B_1 \\ A_1 \end{bmatrix} = \begin{bmatrix} \cosh(s\tau) - \sinh(s\tau) & 0 \\ 0 & \cosh(s\tau) + \sinh(s\tau) \end{bmatrix} \begin{bmatrix} A_2 \\ B_2 \end{bmatrix} = \mathbf{T} \begin{bmatrix} A_2 \\ B_2 \end{bmatrix} \tag{2.3b}$$

with port references $R_1 = R_2 = R$. For this choice, the chain and transfer matrices are related through a similarity transformation:

$$\mathbf{T} = \mathbf{P}\,\mathbf{K}\mathbf{P}^{-1} \quad \text{where} \quad \mathbf{P} = \begin{bmatrix} 1 & -R \\ 1 & R \end{bmatrix} . \tag{2.5}$$

The two-port in Fig. 2.1a is referred to as the unit element (UE), and the term "commensurate" means that all the elements in a particular distributed network have one-way delays that are an integer multiple of the basic delay τ [2]. Expressions such as (2.3b) can be simplified by using a complex frequency variable defined by

$$\psi = \tanh\left(\frac{sT}{2}\right) = \frac{e^{sT} - 1}{e^{sT} + 1} = \frac{z - 1}{z + 1} \qquad , \qquad \tau = \frac{T}{2} \quad z = e^{sT} \tag{2.6}$$

which is referred to as the Richards variable [2]. This mapping allows distributed networks to be described using polynomials in ψ. Substituting ψ in (2.3b) yields the scattering transfer matrix characterization of a unit element:

$$\begin{bmatrix} B_1 \\ A_1 \end{bmatrix} = \begin{bmatrix} \sqrt{\dfrac{1-\psi}{1+\psi}} & 0 \\ 0 & \sqrt{\dfrac{1+\psi}{1-\psi}} \end{bmatrix} \begin{bmatrix} A_2 \\ B_2 \end{bmatrix} = \begin{bmatrix} z^{-1/2} & 0 \\ 0 & z^{1/2} \end{bmatrix} \begin{bmatrix} A_2 \\ B_2 \end{bmatrix} . \tag{2.7}$$

A WD equivalent of a unit element is shown in Fig. 2.1b. (Note: the words image, equivalent, translation, and correspondent are used interchangibly when referring to the range of the mapping between analog and WD domains).

The key property of the mapping in (2.6) is that rational transfer functions in ψ are mapped to rational transfer functions in z, and vice versa. This means that the approximation and synthesis problems can be solved in either domain. Moreover, it is known that a distributed network which is a simple interconnection of UEs can be formally equated with a corresponding lumped-element LC circuit because the two share the same

two-port scattering matrix representation in ψ [2]. This can be seen most readily by considering the driving point impedence of a UE with open and short-circuit terminations at port 2, i.e., from (2.3), (2.4) and (2.6) we have

$$Z_1 = \frac{V_1}{I_1} = \frac{R}{\tanh sT/2} = \frac{R}{\psi} \qquad \text{for} \quad I_2 = 0 \quad (A_2 = B_2) \tag{2.8a}$$

$$Z_1 = \frac{V_1}{I_1} = R \tanh sT/2 = R\psi \qquad \text{for} \quad V_2 = 0 \quad (A_2 = -B_2) \ . \tag{2.8b}$$

A UE terminated according to (2.8a, b) is called an open- and short-circuited stub, respectively, and clearly has the same formal properties with respect to ψ as do a capacitor and an inductor, respectively. The corresponding wave digital circuits obtained from Fig. 2.1 are shown in Fig.2.3.

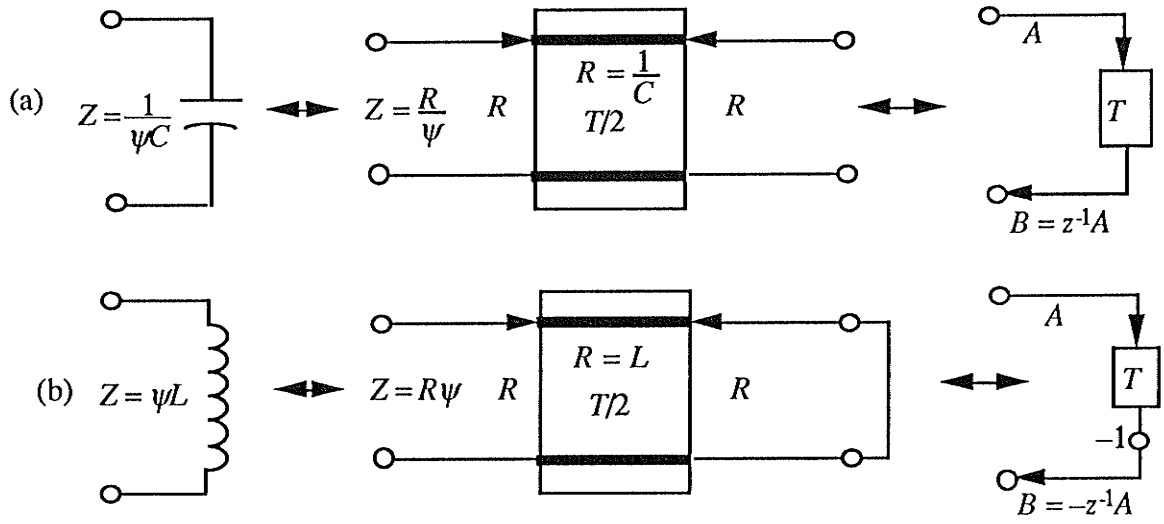

Fig. 2.3 Symbolic representations of (a) a capacitor and (b) an inductor in the ψ, s, and z domains, respectively.

It follows that a formal equivalence can be established between distributed networks with open- and short-circuited stubs (UEs) and lumped networks with capacitors and inductors, respectively. In fact, most authors prefer to use the simpler lumped symbols for capacitors and inductors when deriving a prototype for a WDF, with the understanding that the actual complex frequency variable being used is the Richards variable ψ and the resulting filter response is periodic in ω.

The mapping in (2.6) has some additional properties [11],[44] which are listed below:

1. The imaginary axis $\psi = j\phi$ is mapped onto the imaginary axis $s = j\omega$ and one-to-

one onto the unit circle $z = e^{j\omega T}$, where

$$\phi = \tan\left(\frac{\omega T}{2}\right) \tag{2.9}$$

and ϕ, ω, and ωT represent the real frequencies for the lumped, distributed, and WD networks, respectively.

2. The Nyquist range $0 \le \omega \le \pi/T$ is mapped one-to-one and onto the range $0 \le \phi \le \infty$. It follows that the frequency responses of WDFs and their corresponding lumped filters are the same with the frequency variables related by (2.9).

3. Stable filters in whichever domain are mapped to stable filters in the image domain, i.e.

$$\begin{aligned} \text{Re}\,\psi > 0 \;&\Leftrightarrow\; \text{Re}\,s > 0 \;\Leftrightarrow\; |z| > 1 \\ \text{Re}\,\psi < 0 \;&\Leftrightarrow\; \text{Re}\,s < 0 \;\Leftrightarrow\; |z| < 1 \end{aligned} \tag{2.10}$$

A two-port closely related to the UE is the quasi-reciprocal line (QUARL), which, as the name implies, does not have the same delay in both transfer directions, but their sum is equal to T [11]. Two instances of a QUARL which are of importance for WDFs are shown in Fig. 2.4.

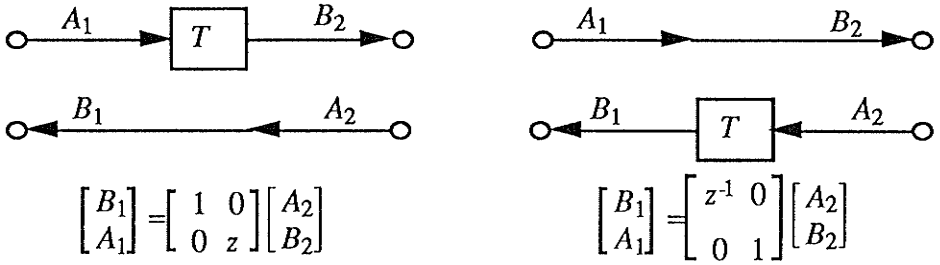

Fig. 2.4 Two instances of a QUARL.

The other important one-port terminations are the resistor and a resistor in series with a voltage source. These can be derived using (2.4), and are shown in Fig. 2.5.

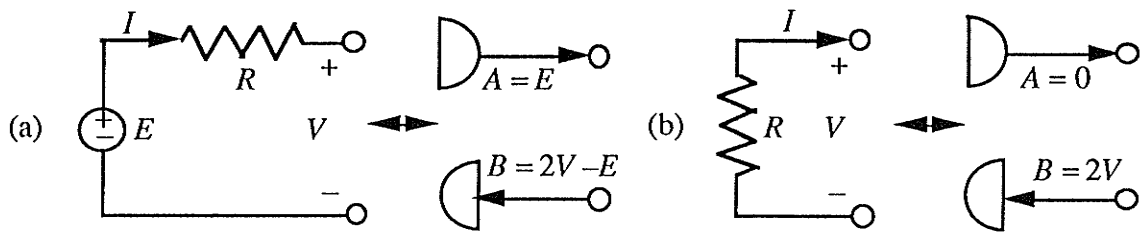

Fig. 2.5 Resistive terminations and their WD images.

2.2 Ideal Transformer and its Wave Digital Equivalent – the 2-port Adaptor

Basic one-port terminations and their WD equivalents were derived in the previous section. In this section, we derive a WD equivalent of the most basic and ubiquitous zeroth-order two-port – the ideal transformer. WD equivalents of analog multi-port networks which do not store or dissipate energy (i.e. nonenergic) are called adaptors, and their purpose is to ensure that laws equivalent to Kirchhoff's voltage and current laws hold in the wave domain. In order to derive a flowgraph (i.e., a digital circuit made up of adders and multipliers) for an adaptor, it is convenient to start from the scattering matrix representation which, in general, is related to the transfer matrix by

$$\begin{bmatrix} B_1 \\ B_2 \end{bmatrix} = \begin{bmatrix} S_{11} & S_{12} \\ S_{21} & S_{22} \end{bmatrix} \begin{bmatrix} A_1 \\ A_2 \end{bmatrix} = \frac{1}{T_{22}} \begin{bmatrix} T_{12} & T_{11}T_{22} - T_{12}T_{21} \\ 1 & -T_{21} \end{bmatrix} \begin{bmatrix} A_1 \\ A_2 \end{bmatrix} = \mathbf{S} \begin{bmatrix} A_1 \\ A_2 \end{bmatrix} \tag{2.11a}$$

$$\begin{bmatrix} B_1 \\ A_1 \end{bmatrix} = \begin{bmatrix} T_{11} & T_{12} \\ T_{21} & T_{22} \end{bmatrix} \begin{bmatrix} A_2 \\ B_2 \end{bmatrix} = \frac{1}{S_{21}} \begin{bmatrix} S_{12}S_{21} - S_{11}S_{22} & S_{11} \\ -S_{22} & 1 \end{bmatrix} \begin{bmatrix} A_2 \\ B_2 \end{bmatrix} = \mathbf{T} \begin{bmatrix} A_2 \\ B_2 \end{bmatrix} \tag{2.11b}$$

An ideal transformer and its chain matrix are shown in Fig. 2.6.

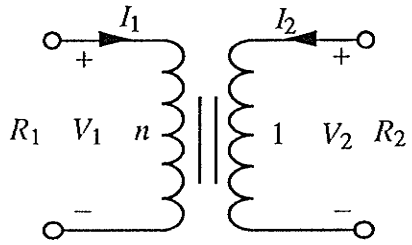

$$\begin{bmatrix} V_1 \\ I_1 \end{bmatrix} = \begin{bmatrix} n & 0 \\ 0 & 1/n \end{bmatrix} \begin{bmatrix} V_2 \\ -I_2 \end{bmatrix}$$

Fig. 2.6 An ideal transformer and its chain matrix.

The corresponding voltage wave scattering and transfer matrices obtained from (2.11) and (2.4) for general port references R_1 and R_2 are given by

$$\begin{bmatrix} B_1 \\ B_2 \end{bmatrix} = \frac{1}{n^2 + \frac{R_1}{R_2}} \begin{bmatrix} n^2 - \frac{R_1}{R_2} & 2n\frac{R_1}{R_2} \\ 2n & \frac{R_1}{R_2} - n^2 \end{bmatrix} \begin{bmatrix} A_1 \\ A_2 \end{bmatrix} = \mathbf{S} \begin{bmatrix} A_1 \\ A_2 \end{bmatrix}, \qquad \begin{bmatrix} B_1 \\ A_1 \end{bmatrix} = \frac{1}{2n} \begin{bmatrix} n^2 + \frac{R_1}{R_2} & n^2 - \frac{R_1}{R_2} \\ n^2 - \frac{R_1}{R_2} & n^2 + \frac{R_1}{R_2} \end{bmatrix} \begin{bmatrix} A_2 \\ B_2 \end{bmatrix} = \mathbf{T} \begin{bmatrix} A_2 \\ B_2 \end{bmatrix} \tag{2.12}$$

There are three instances of (2.12) that are of interest: (1) For $n = 1$, the circuit in Fig. 2.6 is equivalent to a simple direct connection of two ports with different port references, and

(2.12) reduces to

$$\mathbf{S}_\gamma = \begin{bmatrix} -\gamma & 1+\gamma \\ 1-\gamma & \gamma \end{bmatrix} \quad , \quad \mathbf{T}_\gamma = \frac{1}{1-\gamma}\begin{bmatrix} 1 & -\gamma \\ -\gamma & 1 \end{bmatrix} \quad \text{where} \quad \gamma := \frac{R_1 - R_2}{R_1 + R_2} \tag{2.13}$$

A flowgraph corresponding to (2.13) is called the 2-port adaptor; (2) The case $R_1 = R_2$ corresponds to the normalized voltage (power) waves, and (2.12) can be expressed as

$$\mathbf{S}_\theta = \begin{bmatrix} -\cos\theta & \sin\theta \\ \sin\theta & \cos\theta \end{bmatrix} \quad , \quad \mathbf{T}_\theta = \frac{1}{\sin\theta}\begin{bmatrix} 1 & -\cos\theta \\ -\cos\theta & 1 \end{bmatrix} \tag{2.14a}$$

where $$\cos\theta = \frac{1-n^2}{1+n^2} \qquad \sin\theta = \frac{2n}{1+n^2} \qquad \Rightarrow \quad n = \tan\left(\frac{\theta}{2}\right) \tag{2.14b}$$

$\mathbf{S}_\theta$ is essentially equivalent to the planar rotation (Givens) operator [18]. (3) Finally, for $n^2 = R_1/R_2$, expressions in (2.12) reduce to

$$\mathbf{S}_n = \begin{bmatrix} 0 & n \\ 1/n & 0 \end{bmatrix} = \mathbf{P}^{-1}\begin{bmatrix} 0 & 1 \\ 1 & 0 \end{bmatrix}\mathbf{P} \quad \mathbf{P} = \begin{bmatrix} 1 & 0 \\ 0 & n \end{bmatrix} \quad , \quad \mathbf{T}_n = n\begin{bmatrix} 1 & 0 \\ 0 & 1 \end{bmatrix} \tag{2.15}$$

$\mathbf{S}_n$ corresponds to a pair of inverse multipliers ($b_1 = na_2$ and $b_2 = a_1/n$) that introduces a frequency-independent scaling factor when placed in front of a one-port or as part of the overall cascade. As such, they are usually referred to as scaling multipliers.

By letting $\gamma = \cos\theta$, which implies $n^2 = R_2/R_1$, eqs. (2.13)-(2.15) can be combined as

$$\mathbf{S}_\theta = \mathbf{P}^{-1}\,\mathbf{S}_\gamma\,\mathbf{P} \quad , \quad \mathbf{T}_\theta = \mathbf{T}_\gamma\mathbf{T}_n = \mathbf{T}_n\,\mathbf{T}_\gamma \tag{2.16}$$

i.e., a normalized 2-port adaptor is equivalent to a voltage wave 2-port adaptor cascaded with a pair of inverse multipliers. (Note that n in (2.15) is now given by $n^2 = R_2/R_1$.) This equivalence is depicted symbolically in Fig. 2.7a, and the corresponding flowgraphs are shown in Fig. 2.7b. In Fig. 2.7a, we use the convention of placing the rotation angle θ and the heavy bar on the side belonging to port 1. The flowgraph of the 2-port adaptor (henceforth, the prefix voltage wave will be omitted) in Fig. 2.7b is not unique. Many other flowgraphs can be derived and some of these can be found in [11],[45]. A particular choice of flowgraph is usually dictated by the properties of the DSP that implements the filter [46].

The main feature of the 2-port adaptor in Fig. 2.7 is that the number of multipliers that must be quantized in order to ensure realizability equals the number of degrees of freedom, which in this case is one. Consequently, the 2-port adaptor is structurally lossless. This is in contrast to the normalized 2-port adaptor which requires two independent quantizations. The flowgraph of the 2-port adaptor in Fig. 2.7 was first derived in 1971 [10].

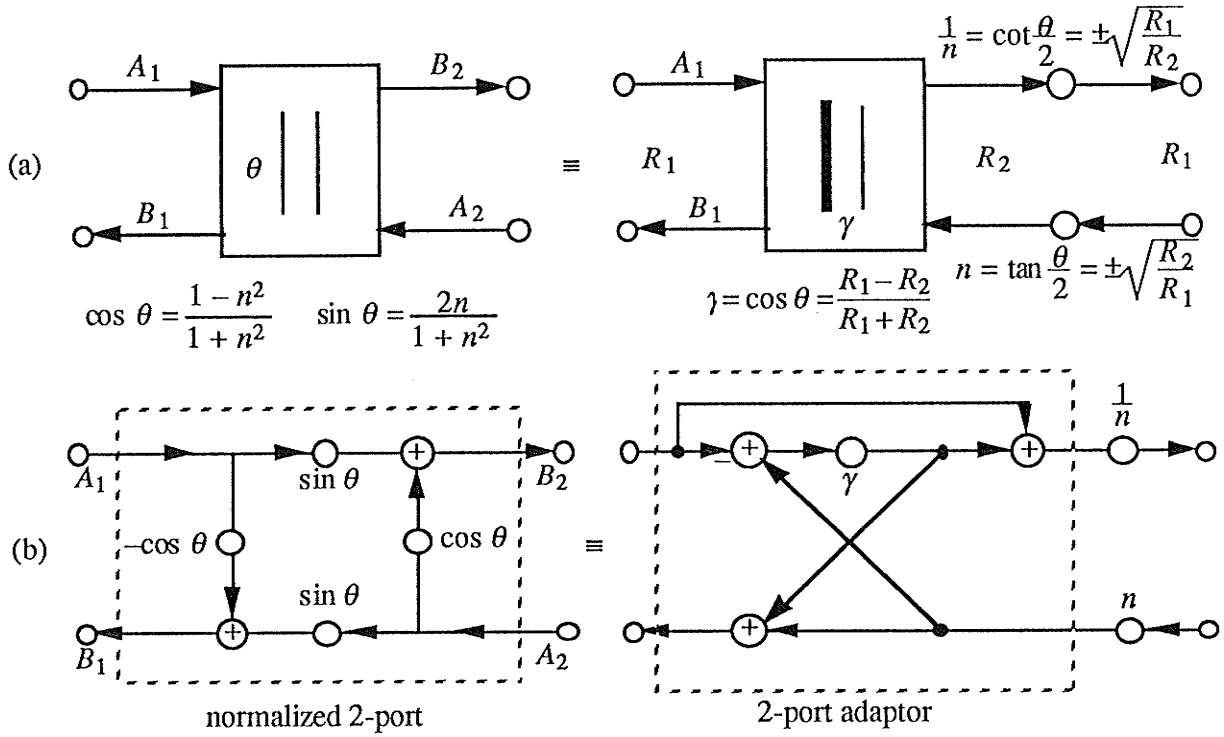

Fig. 2.7 (a) Symbolic representation of the decomposition of a normalized (power wave) 2-port adaptor into a (voltage wave) 2-port adaptor and a pair of inverse multipliers; (b) the corresponding flowgraphs.

Another zeroth-order two-port of interest is the gyrator which, along with its WD equivalent, is shown in Fig. 2.8.

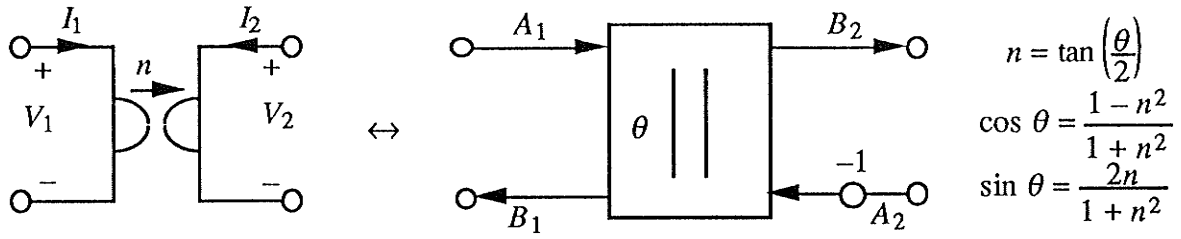

Fig. 2.8 A gyrator and its WD image.

Clearly, WD flowgraphs of the gyrator and the ideal transformer are equivalent except for the

negation of A_2 in Fig. 2.8. Note also that, for both cases, the flowgraphs are of a simple nature, requiring only 4 (1) multiplications and 2 (3) additions for the normalized and voltage wave 2-port adaptors, respectively. The relative ease of realizing such two-ports in the WD domain is in direct contrast to the difficulty of realizing an ideal transformer or a gyrator in the analog domain. Indeed, many analog structures that were only of passing or academic interest due to realization problems, have resurfaced in the WD domain [17]. Moreover, as will be shown in Chapter III, WDFs can be so structured that they consist of only 2-port adaptors and delays, thus achieving a high degree of modularity.

In practice, the pair of inverse multipliers in Fig. 2.7 can usually, but not always, be ignored. Their effect in such cases is to change signal levels within the flowgraph without affecting (except for a frequency independent shift) relevent transfer functions. However, for the normalized 2-port adaptor, two independent quantizations are required (see Fig. 2.7) for realizability, i.e., (2.14a) in fact corresponds to

$$\mathbf{S}_{\alpha\beta} = \begin{bmatrix} -\alpha & \beta \\ \beta & \alpha \end{bmatrix} \quad \Rightarrow \quad \mathbf{T}_{\alpha\beta} = \frac{1}{\beta}\begin{bmatrix} \alpha^2 + \beta^2 & -\alpha \\ -\alpha & 1 \end{bmatrix} \tag{2.17}$$

where the transfer matrix was obtained using (2.11b). Consequently, more quantizations are performed than the available number of degrees of freedom, and the resulting WDF can no longer be mapped to a lossless analog network. For this reason, a voltage wave 2-port adaptor is preferable to its power wave counterpart since the former preserves losslessness $\left(\mathbf{S}_\gamma \mathbf{R}\, \mathbf{S}_\gamma^{\mathrm{T}} = \mathbf{R}\,,\ \mathbf{R} = \mathrm{diag}\,\{R_1, R_2\}\right)$ even when γ is quantized to a binary fraction, whereas the latter requires two independent quantizations of $\alpha = \cos\,\theta$ and $\beta = \sin\,\theta$ such that, at best, passivity (i.e. $\mathbf{S}_{\alpha\beta}^{\mathrm{T}}\mathbf{S}_{\alpha\beta} < \mathbf{I}$) can be achieved. This is so because $\alpha^2 + \beta^2 = 1$ cannot be satisfied using only binary fractions, and therefore power wave 2-port adaptors cannot be made lossless. Losslessness, however, is a very desirable property since it leads to low-sensitivity and, consequently, to low roundoff noise power [11]. We should point out that WDFs comprised of normalized 2-port adaptors can be made to approach lossless structures with arbitrary closeness by simply allowing more bits for the multipliers. With today's 32-bit digital signal processors that allow 16 bits for multipliers, virtual losslessness can be achieved in most cases, but each case must be examined on an individual basis. However, for a microprocessor implementation, it is still desirable to keep the number of multiplications to a minimum. One advantage power wave adaptors in general do possess is that they make efficient use of the dynamic range, thereby maximizing the signal-to-noise ratio.

2.3 Elementary Allpass Sections

WDFs are an interconnection of ports that topologically match the ports of classical analog filters. Most of the ports are terminated in elementary one-port sections, with two such terminations shown in Fig. 2.3. Most of the one-port terminations in the analog domain are Foster functions (i.e. reactances) [2], which map to allpass sections in the WD domain. In this section, some of the elementary allpass sections are presented with lumped analog circuits used as prototypes.

In the wave domain, a one-port is characterized by its reflectance (see Fig. 2.2):

$$S = \frac{B}{A} = \frac{Z - R}{Z + R} \tag{2.18}$$

where Z is the driving-point impedence of the one-port. If Z is a Foster function, then for $\psi = j\phi \leftrightarrow z = e^{j\omega T}$, $Z = jX(\phi)$ and $|S| = 1$, i.e., S is an allpass function. The 1st-order allpass sections in Fig. 2.3 can be generalized by allowing reference R_1 to be independent of the element value; the results are shown in Fig. 2.9.

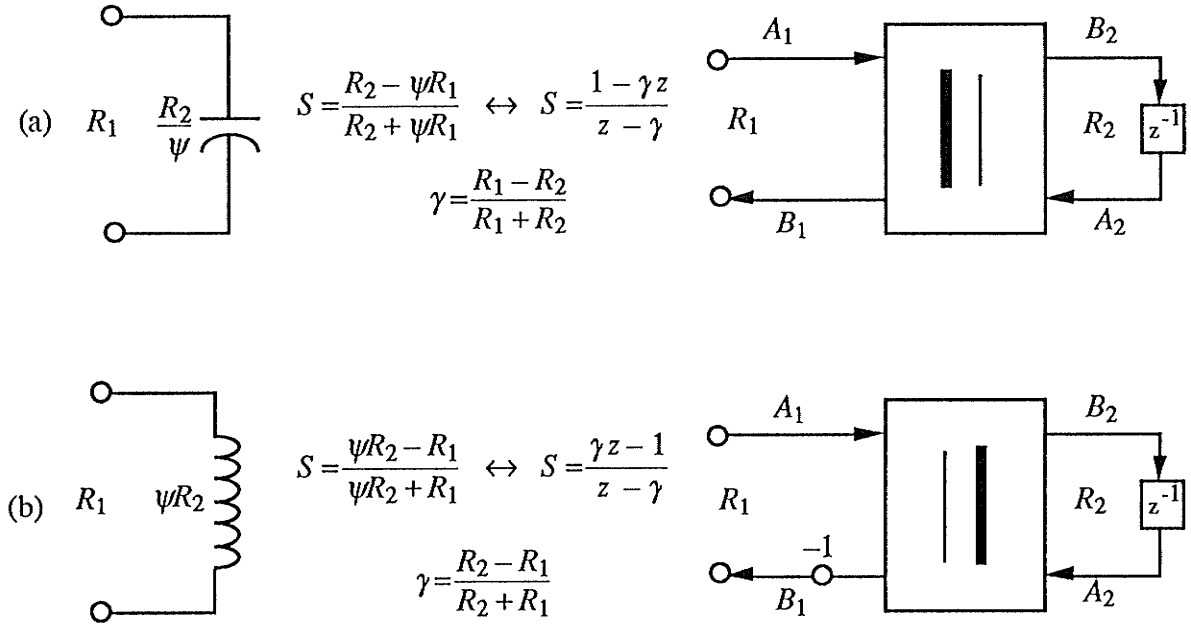

Fig. 2.9 Elementary 1st-order allpass sections.

It follows from the denominator of S in Fig. 2.9 that to guarantee stability it is necessary and sufficient that $\frac{R_2}{R_1} > 0 \leftrightarrow |\gamma| < 1$. It can be shown [45]-[47] that for the circuits in Fig. 2.9

$$\left\|\frac{B_2}{A_1}\right\|_2^2 = \frac{1-\gamma}{1+\gamma} \qquad \text{and} \qquad \left\|\frac{B_2}{A_1}\right\|_\infty = \frac{1-\gamma}{1-|\gamma|} \tag{2.19}$$

where $\|F\|_2^2 := \frac{1}{2\pi}\int_0^{2\pi} |F(e^{j\theta})|^2\, d\theta$ and $\|F\|_\infty := \max |F(e^{j\theta})|_{0 \le \theta \le \pi}$ are referred to as the L_2 and L_∞-norms, respectively [33]. For scaling that minimizes the probability of overflow, all the L_∞-norms are set to one, i.e., the amplitude of B_2 at steady state in Fig. 2.9 is never larger than that of A_1. This is true in (2.19) for $\gamma > 0$, which can always be ensured by applying the equivalence [11] shown in Fig. 2.10.

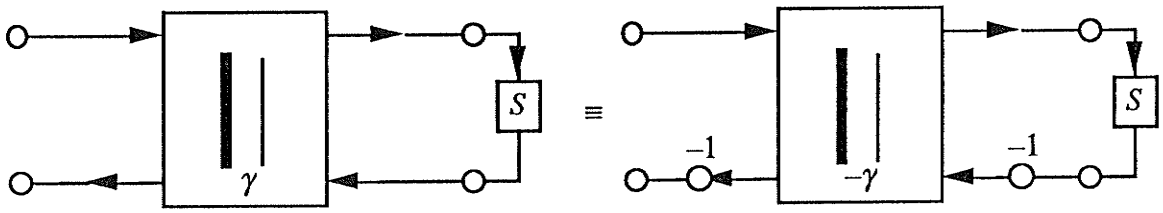

Fig. 2.10 2-port adaptor equivalence when one of the ports is terminated.

As $\gamma \to 1$ in (2.19) $L_2 \to 0$, and the allpass section has poor dynamic range, i.e., the amplitude of B_2 at steady state, for a majority of input frequencies, is nearly zero. In such cases, it is better to use the normalized 2-port adaptor, and (2.19) changes to

$$\left\|\frac{B_2}{A_1}\right\|_2^2 = 1 \qquad \text{and} \qquad \left\|\frac{B_2}{A_1}\right\|_\infty = \sqrt{\frac{1+|\gamma|}{1-|\gamma|}} \quad \text{at } z = 1 \text{ or } z = -1 \ . \tag{2.20}$$

It has been shown that such scaling minimizes roundoff noise [45]-[47].

Elementary 2nd-order allpass sections can be obtained from cascading two UEs from Fig. 2.1, with the second UE terminated in either an open or short-circuit. The two possibilities are shown in Fig. 2.11. Note that the reflectances of the two allpass sections differ by a minus sign which means the two circuits are duals of each other. The L_2 and L_∞-norms for B_2/A_1 are the same as in (2.19), and for B_4/A_1 can be found in [46].

In general, allpass sections comprised of normalized 2-port adaptors have all L_2-norms equal to one, whereas 2-port adaptor realizations with positive γ's have all L_∞-norms ≤ 1. From the point of view of scaling, the latter choice is usually too conservative and makes poor use of the dynamic range, which is another way of saying that the signal-to-noise ratio is low. Normally, a pair of inverse multipliers are inserted at port 2 in Fig. 2.11 to improve the dynamic range.

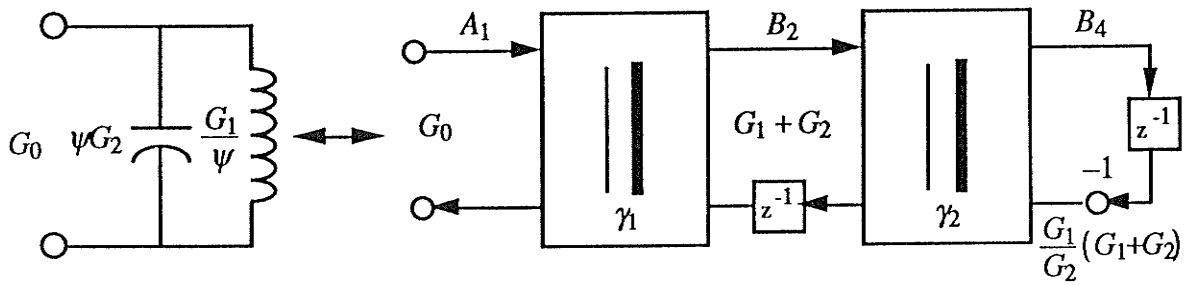

(a) $$S(z)=\frac{\gamma_1 z^2+\gamma_2(1-\gamma_1)z-1}{z^2-\gamma_2(1-\gamma_1)z-\gamma_1} \qquad \gamma_1=\frac{G_0-(G_1+G_2)}{G_0+G_1+G_2} \qquad \gamma_2=\frac{G_2-G_1}{G_2+G_1}$$

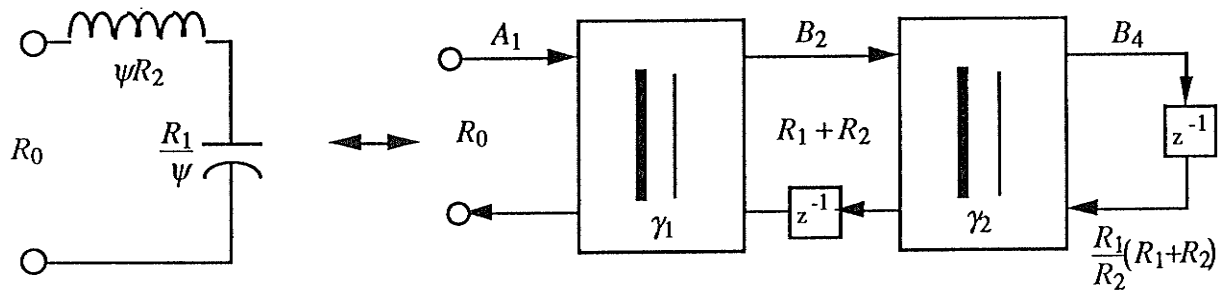

(b) $$S(z)=\frac{-\gamma_1 z^2-\gamma_2(1-\gamma_1)z+1}{z^2-\gamma_2(1-\gamma_1)z-\gamma_1} \qquad \gamma_1=\frac{R_0-(R_1+R_2)}{R_0+R_1+R_2} \qquad \gamma_2=\frac{R_2-R_1}{R_2+R_1}$$

Fig. 2.11 Elementary 2nd-order allpass sections.

It is known that many transfer functions of interest can be expressed as a difference of two allpass terms [11],[48]. If WD allpass sections are used to realize such a transfer function, the resulting digital filter is called a WD lattice filter. The corresponding analog filter has a symmetric lattice structure, and its canonic equivalent is shown in Fig. 2.12.

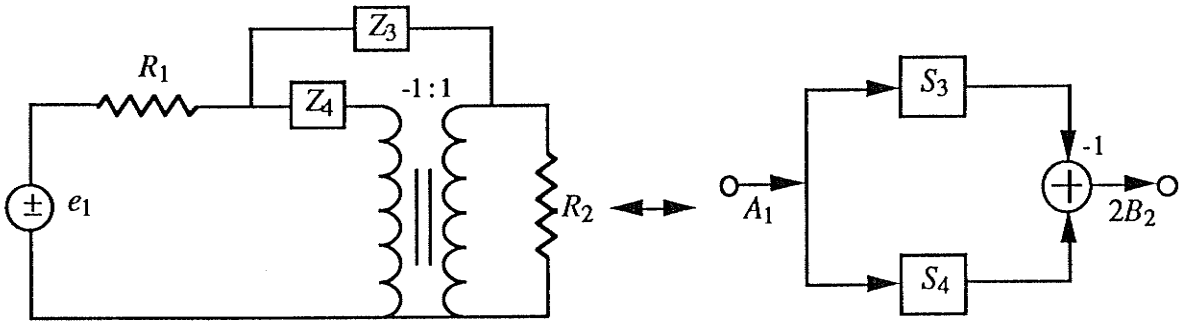

$$S_i=\frac{Z_i-1}{Z_i+1} \qquad i=3,4 \qquad \frac{B_2}{A_1}=\frac{S_4-S_3}{2}$$

Fig. 2.12 Symmetric lattice filter and its WD equivalent.

In many ways, WD lattice filters are the most efficient WDF structures available – the main drawback being increased sensitivity in the stopband due to the requirement that the two allpass outputs be exactly in phase to create a transmission zero (see Fig. 2.12). However, for most applications, acceptable stopband behaviour can be found via optimization of the binary-fraction-valued coefficients.

A simple example, that has found a practical application [39], can be constructed from a 2nd-order allpass section, say S_3, in Fig. 2.11a, and a 1st-order allpass section, say S_4 with γ_3 as the coefficient, in Fig. 2.9a. The resulting lowpass filter can be transformed to a bandpass filter by applying the simplest lowpass-to-bandpass mapping $z^{-1} \rightarrow -z^{-2}$ [33]. The resulting allpass sections are shown in Fig. 2.13. The bandpass transfer function is given by $2T_{BP}(z) = S_4(-z^2) - S_3(-z^2)$ whose response on the unit circle is shown in Fig. 2.14 for the following set of coefficients:

$$\cos\theta_1 = 1 - \frac{91}{2048} \qquad \cos\theta_2 = \frac{3}{2048} - 1 \qquad \cos\theta_3 = 1 - \frac{23}{512}$$

This filter was designed to isolate a chosen harmonic voltage and current signals in a power generating station. A phase comparison of the filtered signals is then used to control a tuning reactor that provides a path to ground for the unwanted harmonic.

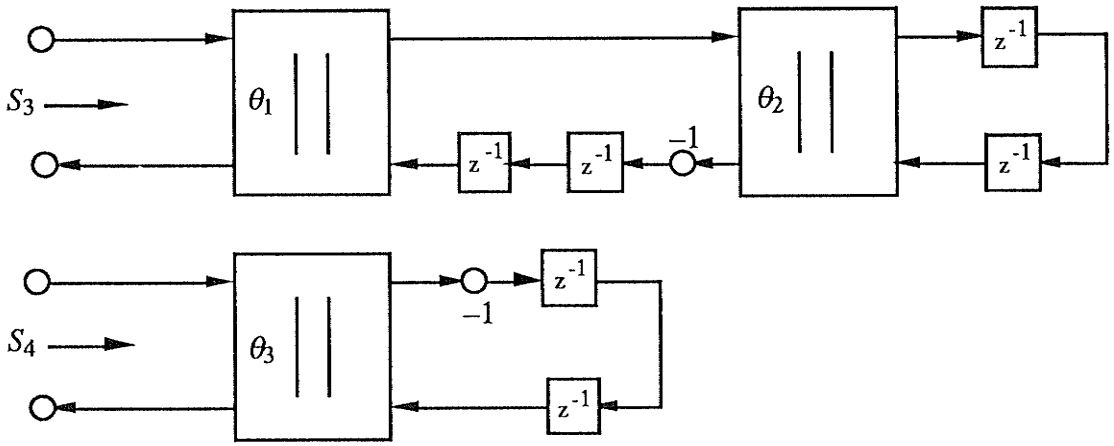

Fig. 2.13 Allpass sections for the example filter.

Since all the multipliers are close to one in magnitude, it is imperative that the normalized 2-port adaptors are used to achieve acceptable dynamic range. Overflow oscillations are eliminated using saturation arithmetic [11],[13]. That such a simple method can guarantee suppression of overflow nonlinearities is one of the most important features of WDFs. Although a conservative scaling criterion, such as L_∞, could be used to eliminate overflow in most digital filters, it provides no guarantee that the filter can recover from an internal,

randomly-induced overflow that may occur during a prolonged operation – which is an important feature of the present application. In such cases, it is important to guarantee that no overflow oscillations persist. Saturation arithmetic has been shown to be sufficient in WDFs for this purpose.

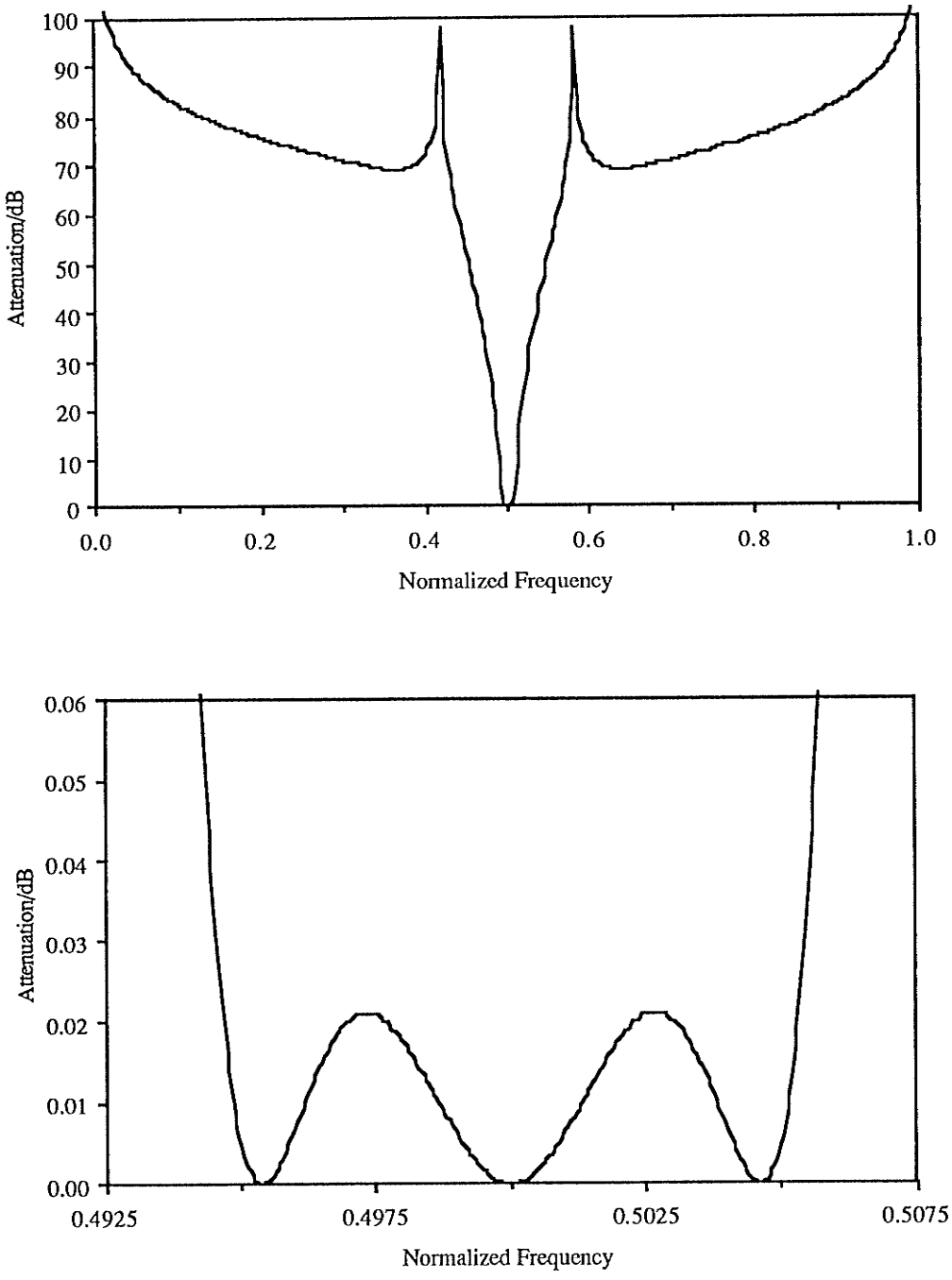

Fig. 2.14 Stopband and passband responses of a bandpass filter.

2.4 Belevitch's Representation of Lossless Two-Port Networks

A lossless two-port network with port references R_1 and R_2 is shown in Fig. 2.15a. A natural way of characterizing such a two-port is to use normalized scattering variables

$$A_i = \frac{V_i + R_i I_i}{2\sqrt{R_i}} \qquad B_i = \frac{V_i - R_i I_i}{2\sqrt{R_i}} \qquad i = 1, 2 \tag{2.21}$$

which are known as the incident and reflected power waves, respectively [1]. Power waves are simply normalized voltage waves (see (2.4)), and are used here for convenience. One can convert from one to the other by inserting an ideal transformer (a pair of inverse multipliers n and $1/n$ (see 2.15)) where $n^2 = R_1/R_2$. It is customary for power WD circuits not to explicitly show the port references, as they may all be set to one, and any difference between the resistive terminations is accounted for with an insertion of an appropriate ideal transformer.

There are three useful groupings of the scattering variables:

$$\begin{bmatrix} B_1 \\ B_2 \end{bmatrix} = \begin{bmatrix} S_{11} & S_{12} \\ S_{21} & S_{22} \end{bmatrix} \begin{bmatrix} A_1 \\ A_2 \end{bmatrix} = \mathbf{S} \begin{bmatrix} A_1 \\ A_2 \end{bmatrix} \quad , \quad \begin{bmatrix} B_1 \\ A_1 \end{bmatrix} = \mathbf{T} \begin{bmatrix} A_2 \\ B_2 \end{bmatrix} \quad , \quad \begin{bmatrix} B_1 \\ A_2 \end{bmatrix} = \mathbf{H} \begin{bmatrix} A_1 \\ B_2 \end{bmatrix} \tag{2.22a,b,c}$$

where **S**, **T** and **H** are 2×2 matrices referred to as the scattering, transfer and hybrid matrix, respectively. For the resistive terminations shown in Fig. 2.15a, the entries of the **S** matrix – called the scattering coefficients – can be obtained using (2.21) and Fig. 2.5:

$$S_{11} = \frac{Z_1 - R_1}{Z_1 + R_1} \qquad S_{22} = \frac{Z_2 - R_2}{Z_2 + R_2} \qquad S_{21} = 2\sqrt{\frac{R_1}{R_2}}\frac{V_2}{E_1} \qquad S_{12} = 2\sqrt{\frac{R_2}{R_1}}\frac{V_1}{E_2} \tag{2.23}$$

where Z_1 and Z_2 are the input driving-point impedences at ports 1 and 2, respectively. S_{11} (S_{22}) is called a reflectance (or a reflection coefficient), and it corresponds to the fraction of maximum power available from source E_1 (E_2) that is reflected by the interconnecting network and dissipated in R_1 (R_2). S_{21} (S_{12}) is called a transmittance (or a transmission coefficient) and it corresponds to the remaining fraction of maximum power available from source E_1 (E_2) that is transmitted by the lossless interconnecting network N and dissipated in R_2 (R_1). Normally, we identify the transfer function with the transmittance, but WDFs have the additional advantage of allowing the transfer function to be identified with the reflectance. Since only one circuit is used, WDFs are by far the most efficient means of generating two complementary transfer functions. In the analog domain, such an advantage is not readily available due to the difficulty of extracting the reflected signal. Note also that the transmittances are proportional to voltage transfer functions.

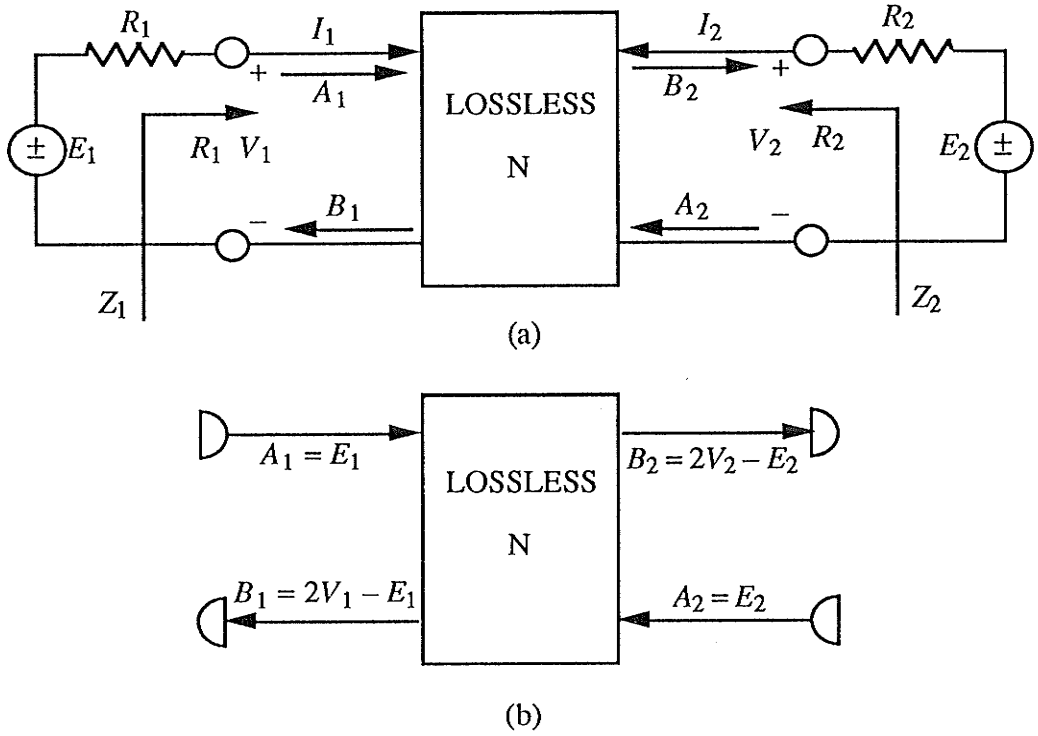

Fig. 2.15 (a) A lossless two-port N inserted between resistive terminations and (b) its wave digital equivalent.

A significant and practical simplification in the characterization of lossless two-port networks was achieved by Belevitch who showed that the scattering coefficients can be expressed using only three polynomials and a unimodular constant [1]. He proved that for real, realizable and lossless two-port networks, matrices in (2.22) necessarily take on the following forms:

$$\mathbf{S} = \frac{1}{g}\begin{bmatrix} h & \sigma f_* \\ f & -\sigma h_* \end{bmatrix} \quad , \quad \mathbf{T} = \frac{1}{f}\begin{bmatrix} \sigma g_* & h \\ \sigma h_* & g \end{bmatrix} \quad , \quad \mathbf{H} = \frac{1}{-\sigma h_*}\begin{bmatrix} -\sigma g_* & \sigma f_* \\ -f & g \end{bmatrix} \qquad (2.24a,b,c)$$

and the polynomials f, g and h satisfy the following necessary and sufficient conditions:

1. Polynomials f, g and h are real in some complex frequency variable, say ψ, and the subscript asterisk denotes paraconjugation, i.e., for a real polynomial $f_*(\psi) \equiv f(-\psi)$, which is also referred to as Hurwitz conjugation.

2. $g(\psi)$ is a (Hurwitz) polynomial with all its zeros strictly in the left-hand plane.

3. σ is either +1 or -1 for real two-ports. For reciprocal two-ports, σ is specified by the ratio f/f_*, whereas for nonreciprocal two-ports it can take on either value.

4. The scattering matrix $\mathbf{S}$ for real lossless two-ports is paraunitary, i.e., $\mathbf{S}_*\mathbf{S} = \mathbf{I}$, where matrix paraconjugation also includes transposition and $\mathbf{I}$ is the identity matrix. Given the canonic form in (2.24), the paraunitary property is equivalent to

$$gg_* = hh_* + ff_* \tag{2.25}$$

which is the analytic continuation of the Feldkeller equation.

Due to the conformal nature of the mapping $\psi = \dfrac{z-1}{z+1}$, Belevitch's representation also holds for the WD domain except that now paraconjugation $\psi \to -\psi \Leftrightarrow z \to z^{-1}$, and

$$f_*\left(z^{-1}\right) := z^{-m} f(z), \quad h_*\left(z^{-1}\right) := z^{-m} h(z), \quad g_*\left(z^{-1}\right) := z^{-m} g(z), \quad \text{where } m = \deg g(z). \tag{2.26}$$

Also, $g(z)$ has all its zeros strictly inside the unit circle. For both domains, eq. (2.25) is equivalent to

$$1 = \left|\frac{h}{g}\right|^2 + \left|\frac{f}{g}\right|^2 \text{ for } \psi = j\phi \leftrightarrow z = e^{j\omega T} \text{ where } \phi = \tan\left(\frac{\omega T}{2}\right) \tag{2.27}$$

which is known as the Feldkeller equation and which clearly displays the complementary nature of the scattering coefficients. We conclude that, except for spacial consequences of the mapping, WD two-ports are formally equivalent to their analog counterparts. It follows that the network problems of synthesis and transfer function approximation can be conducted in either domain.

A WD circuit equivalent to the analog circuit in Fig. 2.15a is shown in Fig. 2.15b. In practice, the circuit is driven with a single source, i.e., $E_2 = A_2 = 0$. We continue now with further properties and definitions.

For a nonenergic multi-port interconnection of wires, ideal transformers, gyrators and circulators, the scattering matrix is orthogonal [18], i.e.

$$\mathbf{S}^T\mathbf{S} = \mathbf{I} \quad \text{, and for voltage waves} \quad \hat{\mathbf{S}}^T\mathbf{G}\hat{\mathbf{S}} = \mathbf{G} \quad , \quad \hat{\mathbf{S}} = \mathbf{G}^{-1/2}\mathbf{S}\,\mathbf{G}^{1/2} \tag{2.28a,b,c}$$

where $\mathbf{G}$ is a diagonal matrix of port reference conductances (reciprocal resistances). Clearly, the voltage wave scattering matrix $\hat{\mathbf{S}}$ is orthogonal to within a diagonal similarity transformation – usually referred to as scaling. The steady-state power absorbed by a nonenergic multi-port is given by [18]

$$\mathbf{P} = \mathbf{A}*\mathbf{A} - \mathbf{B}*\mathbf{B} = \mathbf{A}*(\mathbf{I} - \mathbf{S}^{\mathrm{T}}\mathbf{S})\mathbf{A} \tag{2.29}$$

where **A** and **B** are column vectors of incident and reflected power waves, respectively, and **B** = **S** **A**. It follows from (2.28a) that P = 0 $\forall$**A**, hence the term lossless. If some of the available ports are terminated in frequency-dependent one-ports, then **S** has entries that are functions of the complex frequency variable and (2.29) becomes

$$\mathbf{P} = \mathbf{A}*(\mathbf{I} - \mathbf{S}*\mathbf{S})\mathbf{A} \tag{2.30}$$

where dimensions of **A** and **S** have been accordingly decreased. If now $\mathbf{P} \geq 0$ (i.e. $\mathbf{I} - \mathbf{S}*\mathbf{S}$ is positive semi-definite) for Re $\psi \geq 0$ and $\forall$**A**, then the partially terminated multi-port is said to be passive. If, in addition, P = 0 (i.e. $\mathbf{I} - \mathbf{S}*\mathbf{S}$ is identically zero) for Re $\psi = 0$ and $\forall$**A**, then the multi-port is also said to be lossless. Thus, lossless networks are necessarily passive. If all of the available ports, except for an input and output port, are terminated in lossless elements, such as capacitances, inductances, unit elements, etc, then the resulting 2-port is paraunitary (strictly lossless) since $\mathbf{S}*\mathbf{S} = \mathbf{I}$ holds $\forall\psi$, and it follows that P = 0 $\forall$ ψ, **A**. Some additional properties of lossless two-ports follow:

5. Both the transmittance f/g and the reflectance h/g are passive (bounded) functions [1], i.e. g is realizable (Hurwitz) and

$$\left|\frac{f}{g}\right| \leq 1 \quad , \quad \left|\frac{h}{g}\right| \leq 1 \qquad \psi = j\phi \ \left(z = e^{j\omega T}\right) \tag{2.31}$$

which follows from (2.27). Note that the values of scattering coefficients are the same in both the ψ and z–domain (see Property 2 p. 12).

6. Zeros of f are called transmission zeros. For transmission zeros on the $\psi = j\phi$ $\left(z = e^{j\omega T}\right)$ axis (unit circle), we have for both domains $\left(\frac{h}{g}\right)_* = \left(\frac{h}{g}\right)^*$. It follows from (2.27) and the fact that all polynomials are real that

$$1 = \left|\frac{h}{g}\right|^2 \Leftrightarrow \frac{h}{g} = e^{j\alpha} \Rightarrow \frac{h}{g} = \pm 1 \quad \text{for} \quad \phi = 0 \ (z = 1) \ \text{ or } \ \phi = \infty \ (z = -1) \tag{2.32}$$

For transmission zeros with Re $\psi > 0$ ($|z| > 1$), the passivity property implies that

$$\left|\frac{h}{g}\right| < 1 \qquad , \qquad \left|\frac{h*}{g*}\right| > 1 \tag{2.33a,b}$$

where (2.33b) follows from (2.25) with $ff_* = 0$.

7. A function defined by

$$d(\psi) := \left[\ln\left(\frac{g}{h}\right)\right]' = \frac{g'}{g}(\psi) - \frac{h'}{h}(\psi) \tag{2.34}$$

will be referred to as the delay.

Lemma 2.1: $d(\psi)$ evaluated at $\psi = j\phi$ such that $f(j\phi) = 0$, is real, positive, and equal to the return group delay defined [2] by $\tau(\phi) := \mathrm{Ev}\left\{\left[\ln\left(\frac{g}{h}(\psi)\right)\right]'\right\}_{\psi = j\phi} = \mathrm{Ev}\{d(\psi)\}_{\psi = j\phi}$.

Proof: From the given $f(j\phi) = f_*(j\phi) = 0$, it follows from (2.25) that $g(j\phi)\, g(-j\phi) = h(j\phi)\, h(-j\phi)$. Differentiating (2.25) and substituting these results yields $d(j\phi) = d_*(j\phi) = d(-j\phi) = d^*(j\phi)$; hence $d(j\phi)$ is real.

For a function which is the quotient of two real polynomials the even part of the function, when evaluated at $\psi = j\phi$, is the same as the real part of the value of the function at $\psi = j\phi$. It follows that $d(j\phi) = \tau(\phi)$.

From $\frac{h}{g} = \frac{Z-1}{Z+1}$, we have $d = \frac{2Z'}{1-Z^2}$. The driving-point impedance of a lossless two-port terminated in a resistance R_2 is given in terms of the open-circuit parameters by

$$Z = \frac{z_{11}(R_2 + z_{22}) - z_{12}^2}{R_2 + z_{22}} \tag{2.34a}$$

At a $\psi = j\phi$ transmission zero, $z_{12}(j\phi) = z_{21}(j\phi) = 0$ [2], and it follows from (2.34a) that $Z(j\phi) = z_{11}(j\phi) = j X_{11}(\phi^2)$, where the 2nd equality follows from the fact that z_{11} is a Foster function. Differentiating (2.34a) and substituting $z_{12}(j\phi) = z_{21}(j\phi) = 0$ yields $Z'(j\phi) = z_{11}'(j\phi) > 0$, where the inequality is a property of Foster functions [2]. Substituting these results in the expression for d yields the required $d > 0$.

In the WD domain, $\psi = \frac{1-z^{-1}}{1+z^{-1}} \Rightarrow d\psi = \frac{-2dz^{-1}}{(1+z^{-1})^2}$, and it follows that

$$d(z^{-1}) := \left[\ln\left(\frac{g}{h}(z^{-1})\right)\right]' = \frac{g'}{g}(z^{-1}) - \frac{h'}{h}(z^{-1}) = \left[\frac{-2\,d(\psi)}{(1+z^{-1})^2}\right]_{\psi = \frac{1-z^{-1}}{1+z^{-1}}} \tag{2.35}$$

where differentiation is performed with respect to z^{-1}. For transmission zeros located on the unit circle $\left(z = e^{j\omega T}\right)$, it is more convenient to use

$$\delta\left(e^{-j\omega T}\right) := -e^{-j\omega T} d\left(e^{-j\omega T}\right) = \frac{d(j\phi)}{2\cos^2\left(\frac{\omega T}{2}\right)} \quad \text{where} \quad \phi = \tan\frac{\omega T}{2} \tag{2.36}$$

It follows from *Lemma* 2.1 that δ is also real, positive and, in an analogous way, equal to the digital return group delay.

As will be shown in the following chapters, judicious application of the above properties, together with Belevitch's representation, leads to a simplified synthesis algorithm which relies on the characterization of elementary sections using values of the reflectance and delay evaluated at the location of the transmission zero.

Finally, the conformal mapping that relates the analog and WD domains and allows a common usage of Belevitch's representation, strongly suggests that there is no real need in changing the terminology when passing over to the z-domain. Indeed, Fettweis [11] has chosen to retain most of the nomeclature from classical analog filters when referring to their WD images. This choice is illuminating and pedagogically sound since, in practice, the context is usually clear and allows for no misunderstanding. Unfortunately, in the development of orthogonal digital filters, which have been shown to be equivalent to power WDFs [18], mostly different terminology is being used [14]-[16],[19],[20],[25]. The main reason given is that many of the resulting digital circuits have no known analog counterparts. This is indeed the case but, as we have already remarked, the important point is that such analog counterparts do exist – although they may be of little practical use – thus establishing the formal link between the analog and WD domains. Another reason given is that familiarity with continuous-time filter synthesis techniques, particularly as applied to *LC* circuits, is unnecessary [25]. However, the main goal of filter synthesis is to split up an overall network characterization into a sequence of low-order sections. How these low-order sections are realized is a completely independent problem, and *LC* circuits do not have to come into play. It is true that in the past *LC* circuits were directly mapped into the z-domain, thus giving the mistaken impression that they were necessary. However, *LC* circuits as prototypes are simply sufficient and not necessary, and were used originally because they were readily available and could realize a majority of transfer functions of interest.

To eliminate any confusion that may arise due to different terminologies, we provide a correspondence list between the commonly used terms and the ones introduced for orthogonal digital filters:

(two)-port	digital (two)-pair
incident (reflected) wave	input (output) variable
$\mathbf{S} = \frac{1}{g}\begin{bmatrix} h & \sigma f_* \\ f & -\sigma h_* \end{bmatrix}$	$T = \begin{bmatrix} T_{11} & T_{12} \\ T_{21} & T_{22} \end{bmatrix}$
scattering (matrix) parameters	transfer (matrix) parameters
reflectance	input transfer function
transmittance	cross transfer function
$\begin{bmatrix} B_1 \\ A_1 \end{bmatrix} = \frac{1}{f}\begin{bmatrix} \sigma g_* & h \\ \sigma h_* & g \end{bmatrix}\begin{bmatrix} A_2 \\ B_2 \end{bmatrix} = \mathbf{T}\begin{bmatrix} A_2 \\ B_2 \end{bmatrix}$	$\begin{bmatrix} X_1 \\ Y_1 \end{bmatrix} = \begin{bmatrix} A & B \\ C & D \end{bmatrix}\begin{bmatrix} Y_2 \\ X_2 \end{bmatrix} = \Pi\begin{bmatrix} Y_2 \\ X_2 \end{bmatrix}$
scattering transfer matrix $\mathbf{T}$	chain matrix Π
passivity	structural boundedness
passive (bounded) function	bounded real (BR) function
paraunitarity	lossless bounded real (LBR)
reflection-free port 2	T_{22} - delay based
$gg_* = hh_* + ff_*$	$1+C_*C=A_*A$, $1+B_*B=D_*D$, $C_*D=A_*B$
reciprocity: $f = \sigma f_*$	$T_{12} = T_{21}$ or $AD - BC = 1$
power WDFs	orthogonal digital filters

The main practical difference between the two columns is in the economy of Belevitch's representation. Also, in a recent publication [18], Fettweis has pointed out that structural boundedness, which is necessary for low sensitivity, corresponds to only external passivity. Digital filters which are only externally passive, may not necessarily be amenable to the simple suppression schemes that guarantee various aspects of stability under finite-arithmetic conditions. On the other hand, computable digital circuits comprised of a simple interconnection of passive (lossless) building blocks that emulate Kirchhoff's voltage and current laws are internally passive. Such circuits are necessarily WDFs.

2.5 Reflection-Free Property

Two interconnected subnetworks N_1 and N_2 that share one common port are shown in Fig. 2.16. The port references at an interconnecting port are set equal, i.e. $R_i = R_j$, so that the corresponding analog port is a direct connection [11]. However, there is still a choice of what that value should be. As shown in Fig. 2.16, the interconnecting port creates a loop which, in order to ensure computability, must not be delay-free, i.e., at least one delay must interpose somewhere along the loop [32]. Computability allows an ordered sequence of computations to be written down for the filtering algorithm without creating infinite loops. The original solution for this problem involved inserting a WD equivalent of the UE (see Fig. 2.1) [10]. However, it was later realized that a simpler solution exists which assigns $R_i = Z_i(\psi=1)$ or $R_j = Z_j(\psi=1)$, where Z_i (Z_j) is the input impedance looking into port i (j) [49]. The reflectance looking into port i is given by $\frac{B_i}{A_i} = \frac{Z_i - R_i}{Z_i + R_i}$ (see 2.18),.and becomes zero at $\psi = 1$. Since $\psi = 1$ maps to $z^{-1} = 0$, it follows that $\frac{B_i}{A_i}$ has at least one factor of z^{-1}, thereby satisfying the necessary condition. The same procedure can be applied to port j instead. The assignment $R_i = Z_i(\psi=1)$ is equivalent to setting $s_{ii} = 0$ in the constant scattering matrix S_1 that represents the multi-port N_1, and is referred to as the reflection-free property since, if A_i is the only nonzero input into the adaptor S_1, then $B_i = 0$.

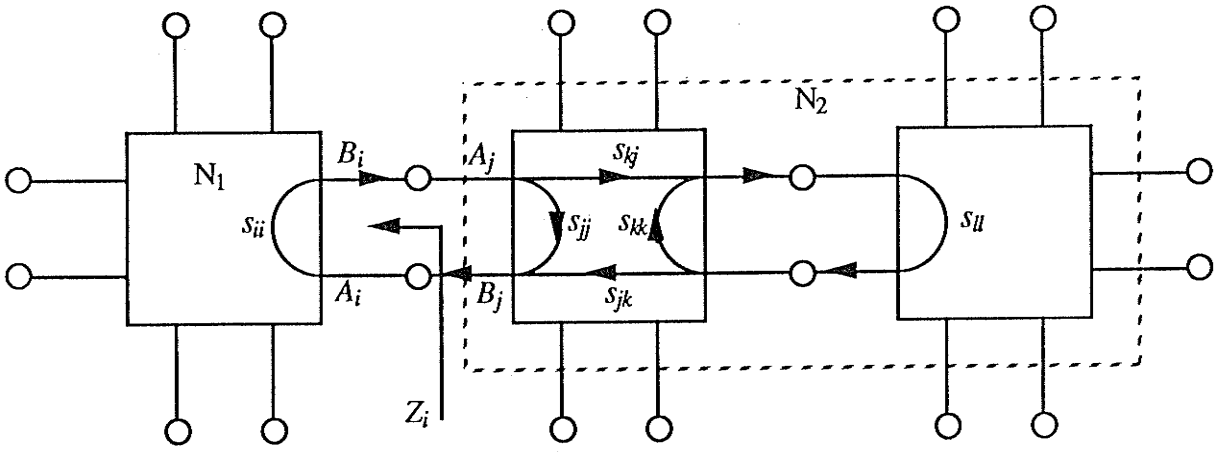

Fig. 2.16 Direct interconnection of WD adaptors.

The reflection-free property is necessary but not sufficient [11],[29]. This can be seen by examining a cascade connection of three multi-ports, as shown in Fig. 2.16. The loop created by a direct interconnection of ports i and j (k and l) can be broken by setting $s_{jj} = 0$ ($s_{kk} = 0$). However, a delay-free directed loop still exists via the off-diagonal terms s_{jk} and s_{kj}. For some adaptors, setting $s_{jj} = s_{kk} = 0$ also forces $s_{jk} = s_{kj} = 0$, and the flowgraph remains computable [29]. One such adaptor will be derived in Chapter III.

2.6 Two-port Network Decomposition using Belevitch's Representation

A cascade connection of two lossless two-ports N_a and N_b is shown in Fig. 2.17. Transfer matrices of N_a and N_b are given by

$$\begin{bmatrix} B_1 \\ A_1 \end{bmatrix} = \frac{1}{f_a}\begin{bmatrix} \sigma_a g_{a*} & h_a \\ \sigma_a h_{a*} & g_a \end{bmatrix}\begin{bmatrix} A_{2a} \\ B_{2a} \end{bmatrix} = \mathbf{T}_a \begin{bmatrix} A_{2a} \\ B_{2a} \end{bmatrix}, \quad \begin{bmatrix} B_{1b} \\ A_{1b} \end{bmatrix} = \frac{1}{f_b}\begin{bmatrix} \sigma_b g_{b*} & h_b \\ \sigma_b h_{b*} & g_b \end{bmatrix}\begin{bmatrix} A_2 \\ B_2 \end{bmatrix} = \mathbf{T}_b \begin{bmatrix} A_2 \\ B_2 \end{bmatrix} \tag{2.37}$$

At a direct interconnecting port $V_{2a} = V_{1b}$, $I_{2a} = -I_{1b}$ and $R_a = R_b$; it follows from (2.4) that $A_{2a} = B_{1b}$ and $B_{2a} = A_{1b}$ which, together with (2.37), implies that the transfer matrix for the combined network is given by

$$\mathbf{T} = \mathbf{T}_a \mathbf{T}_b = \frac{1}{f}\begin{bmatrix} \sigma g_* & h \\ \sigma h_* & g \end{bmatrix} \quad \text{where} \tag{2.38}$$

$$\sigma = \sigma_a \sigma_b \quad , \quad f = f_a f_b \quad , \quad g = g_a g_b + \sigma_a h_{a*} h_b \quad , \quad h = h_a g_b + \sigma_a g_{a*} h_b \tag{2.39a-d}$$

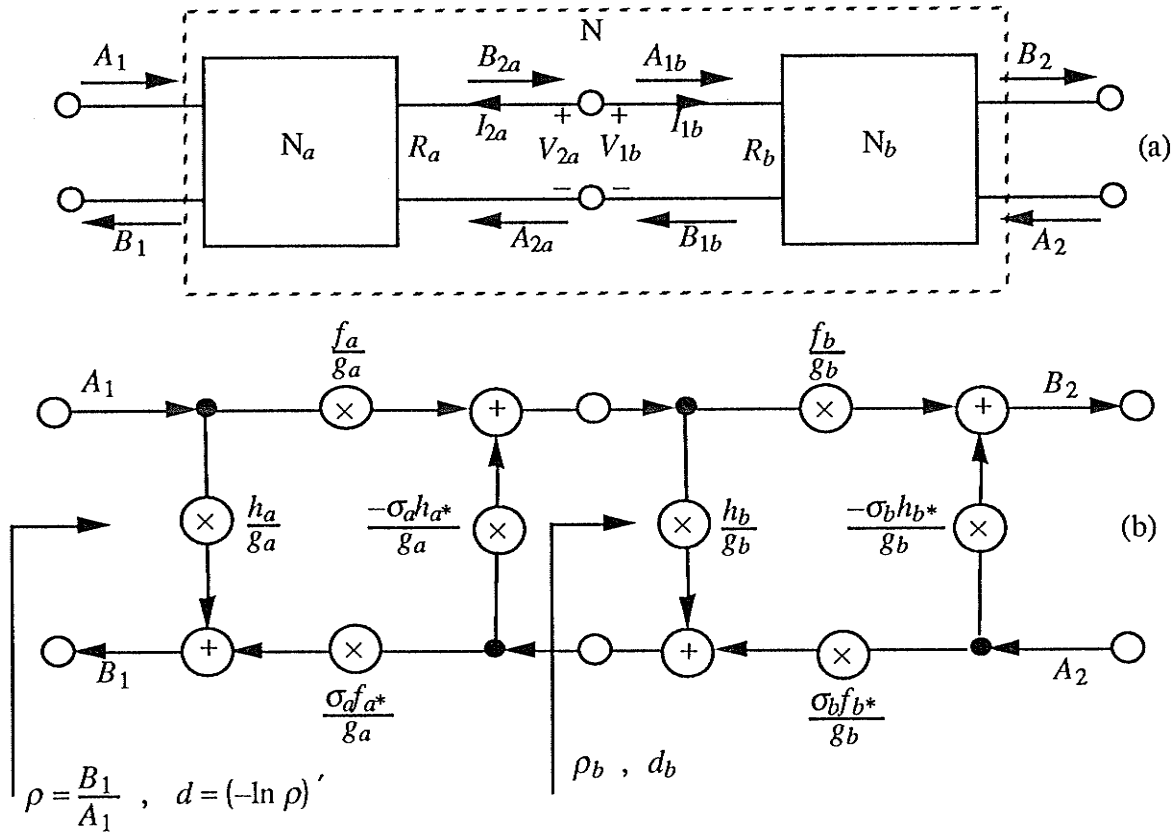

Fig. 2.17 (a) Cascade connection of N_a and N_b and (b) its signal flowgraph representation.

The problem of network cascade synthesis amounts to factoring the transfer matrix **T** into a product $\mathbf{T}_a\mathbf{T}_b$, with each factor corresponding to a realizable transfer matrix as in (2.37). Fettweis has shown that such a decomposition can always be found and, moreover, can be performed minimally [3]-[4], i.e.,

$$\deg g = \deg g_a + \deg g_b \tag{2.40}$$

The solution is unique to within a pair of inverse ideal transformers or a pair of identical gyrators inserted between N_a and N_b, as shown in Fig. 2.18.

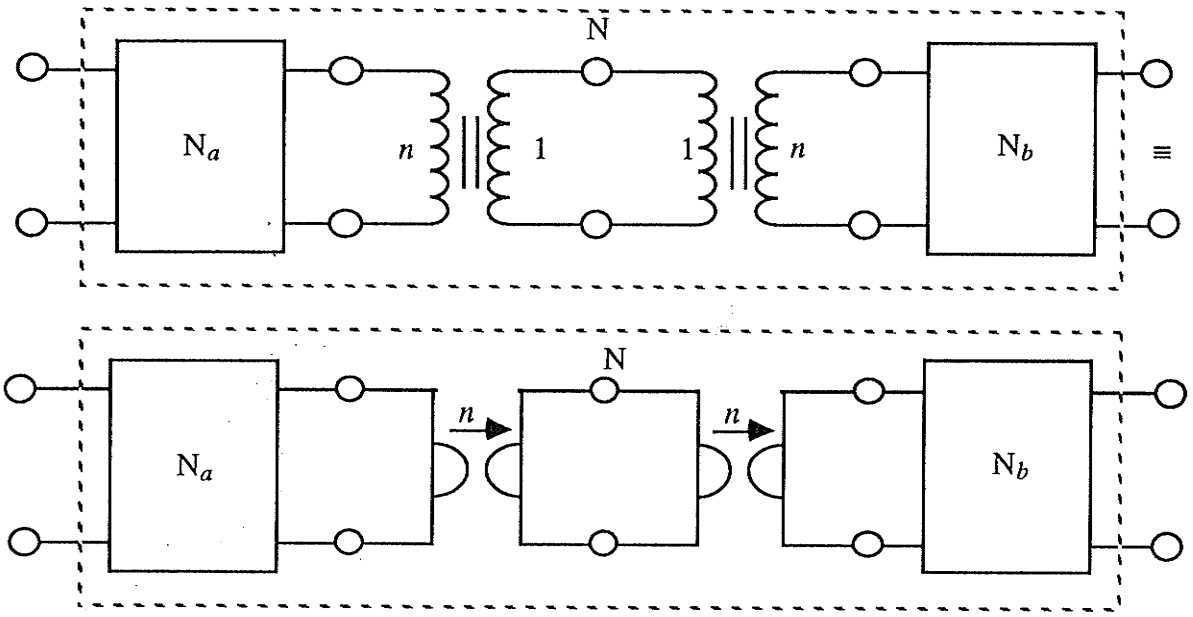

Fig. 2.18 Two equivalent solutions for the decomposition problem.

An important property of two-port networks arranged in a cascade can be seen by examining the signal flowgraph representation of the cascade connection as shown in Fig. 2.17b. At a transmission zero $\psi = \psi_a$ of N_a, we have $f_a(\psi_a) = 0$ which, together with the assumption that $A_2 = 0$, means that the only path from the input terminal A_1 to B_1 is through the branch with the multiplier $\frac{h_a}{g_a}$. It follows that for $A_1 = e^{\psi_a}$, we have $\frac{B_1}{A_1}(\psi_a) = \frac{h}{g}(\psi_a) = \frac{h_a}{g_a}(\psi_a)$. For a reciprocal two-port N_a we also have $f_{a*}(\psi_a) = 0$, and both transmittances that couple to N_b are zero, thus leaving N_b completely decoupled from N_a. In this case, we can show that we also have $d(\psi_a) = d_a(\psi_a)$. This we state in the form of a *Lemma*.

Lemma 2.2 : The values of the reflectance and delay functions of a lossless two-port network evaluated at a transmission zero of the first member of a cascade are equal to the corresponding values of that member, i.e.

$$\rho(\psi_a) := \frac{h}{g}(\psi_a) = \frac{h_a}{g_a}(\psi_a) =: \rho_a(\psi_a) \qquad \text{where} \quad f_a(\psi_a) = 0 \tag{2.41}$$

and

$$d(\psi_a) := \frac{g'}{g}(\psi_a) - \frac{h'}{h}(\psi_a) = \frac{g_a'}{g_a}(\psi_a) - \frac{h_a'}{h_a}(\psi_a) =: d_a(\psi_a) \quad \text{where } f_{a*}(\psi_a) = f_a(\psi_a) = 0 \ . \tag{2.42}$$

Proof: Starting from the definition of reflectance and substituting (2.39c,d) for g and h yields

$$\rho := \frac{B_1}{A_1} = \frac{h}{g} = \frac{h_a g_b + \sigma_a g_{a*} h_b}{g_a g_b + \sigma_a h_{a*} h_b} = \frac{h_a}{g_a}\left[\frac{g_b + \sigma_a \dfrac{g_{a*}}{h_a} h_b}{g_b + \sigma_a \dfrac{h_{a*}}{g_a} h_b}\right] . \tag{2.43}$$

From $g_{a*}g_a = h_{a*}h_a + f_{a*}f_a$ and the given $f_a(\psi_a) = 0$, we have $\dfrac{g_{a*}}{h_a} = \dfrac{h_{a*}}{g_a}$ at $\psi = \psi_a$. Substituting this result into (2.43) yields the desired (2.41).

Starting from the definition of delay from (2.34) and again substituting (2.39c,d) for g and h yields

$$\begin{aligned} d := \left[\ln \frac{g}{h}\right]' &= \left[\ln\left(\frac{g_a}{h_a}\left[\frac{1 + \sigma_a \dfrac{h_{a*}}{g_a}\dfrac{h_b}{g_b}}{1 + \sigma_a \dfrac{g_{a*}}{h_a}\dfrac{h_b}{g_b}}\right]\right)\right]' \\ &= d_a + \frac{(d_{*a})_* + d_b}{1 + \sigma_a \dfrac{h_a}{g_{a*}}\dfrac{g_b}{h_b}} - \frac{d_{*a} + d_b}{1 + \sigma_a \dfrac{g_a}{h_{a*}}\dfrac{g_b}{h_b}} \end{aligned} \tag{2.44}$$

where $$d_a := \frac{g_a'}{g_a} - \frac{h_a'}{h_a} \quad d_{*a} := \frac{g_a'}{g_a} + \frac{(h_a')_*}{h_{a*}} \quad d_b := \frac{g_b'}{g_b} - \frac{h_b'}{h_b} \ . \tag{2.45}$$

As before, we have $\dfrac{g_{a*}}{h_a} = \dfrac{h_{a*}}{g_a}$ but also $d_{*a} = (d_{*a})_*$, where the latter follows from the fact that d_{*a} as defined in (2.45) is the delay of N_a at port 2 and, due to reciprocity, has the same properties as d_a . By *Lemma* 2.1 , $d_{*a} = (d_{*a})_* = (d_{*a})^*$. Making appropriate substitutions in (2.44) results in (2.42).

In the above, we have used the fact that $(g_*(\psi))' = -(g'(\psi))_*$ which, in the z-domain, becomes $(g_*(z^{-1}))' := (z^{-m}g(z))' = mzg_*(z^{-1}) - z^2[g'(z^{-1})]_*$, where m = deg g and similarly for the h polynomial. *Lemma* 2.2 holds for both the ψ and z-domains. Note that (2.42)

holds if and only if the first member of a cascade is a reciprocal section. The significance of *Lemma* 2.2 will become apparent in Chapter III where it is shown that all 1st and 2nd-order elementary sections can be characterized using only the set of values $\{\psi_a\,,\ \rho_a\,,\ d_a\}$ in the ψ-domain and $\{z_a\,,\ \rho_a\,,\ \delta_a\}$ in the z-domain.

From (2.38) we have $\mathbf{T}_b = \mathbf{T}_a^{-1}\,\mathbf{T}$ which yields

$$h_b = \frac{g_a\,h - h_a\,g}{\sigma_a f_a f_{a*}} \quad , \quad g_b = \frac{g_{a*}\,g - h_{a*}\,h}{f_a f_{a*}} \tag{2.46a,b}$$

where we have used the general fact that

$$\mathbf{T}^{-1} = \frac{1}{\sigma f_*}\begin{bmatrix} g & -h \\ -\sigma h_* & \sigma g_* \end{bmatrix} \tag{2.47}$$

which is obtained from the definition of the transfer matrix (2.24b) and the Feldkeller equation (2.25). The cascade decomposition problem essentially reduces to the operation of forcing the factor $f_a f_{a*}$ to appear in both numerators of the expressions in (2.46). More formally: given $\{\sigma, f, g, h\}$, find $\{\sigma_a, f_a, g_a, h_a\}$ such that (2.39a,b) holds, h_b and g_b given by (2.46) are polynomials, g_b is realizable (Hurwitz), and deg $h_b \le$ deg g_b. Fettweis has demonstrated that a canonic solution always exists [3]-[4]. Moreover, he has shown that forcing the factor $f_a f_{a*}$ to appear in the numerator of (2.46b), implies that the same factor appears in the numerator of (2.46a) and vice versa, i.e., h_b is a polynomial if and only if g_b is a polynomial. However, the problem of forcing these factors can be formulated in many different ways: e.g., Fettweis [3],[4] derives a set of simultaneous equations with the coefficients of g_b and h_a as unknowns. However, sensitivity problems arise due to the coefficient-form representation of the polynomials. Other methods [16],[20] rely on finding the zeros of both numerators – an operation that requires an efficient and reliable zero-finding routine – once an appropriate section N_a has been selected. In Chapter IV, we propose a method that circumvents these basic operations.

III. CHARACTERIZATION OF ELEMENTARY SECTIONS

In this chapter, we derive the minimal characterizations of all 1st- and 2nd-order elementary sections for both the analog and WD domains. By minimal characterization we mean the specification of the coefficients of f, g and h using a minimal (canonic) set of parameters. The minimal set for all cases includes the location of the transmission zero that the section realizes, value of the reflectance at the transmission zero, and, for reciprocal sections, value of the delay at the transmission zero. It is shown that all elementary reciprocal WD sections can be realized with an appropriately terminated matched 4-port adaptor. Equivalent sections, comprised of only 2-port adaptors and delays, are derived using a network equivalence that allows the hybrid matrix **H** to be treated like a transfer matrix. Using this approach, the problem of finding structures for WD elementary sections reduces to a building-up process which starts from the most elementary zeroth-order section (2-port adaptor) and a delay (see Fig. 2.3). A 1st-order solution follows easily and is then used in deriving the 2nd-order solution. A second set of solutions is obtained from the factorization of the scattering matrix **S**. It is shown that these solutions cannot be made reflection-free without giving up crucial degrees of freedom.

3.1 Derivation of the Matched 4-Port Adaptor [29].

Consider the 4-port network shown in Fig. 3.1 which, with appropriate terminations, can realize all the 1st and 2nd-order reciprocal elementary sections. It is therefore of interest to find the corresponding WD 4-port adaptor – a problem that has received some attention [51], [52],[29]. Here, we derive a simplified version of this adaptor using a process of shifting parameters into the adjoining ports without compromising (except in one case) the known capabilities of this 4-port structure.

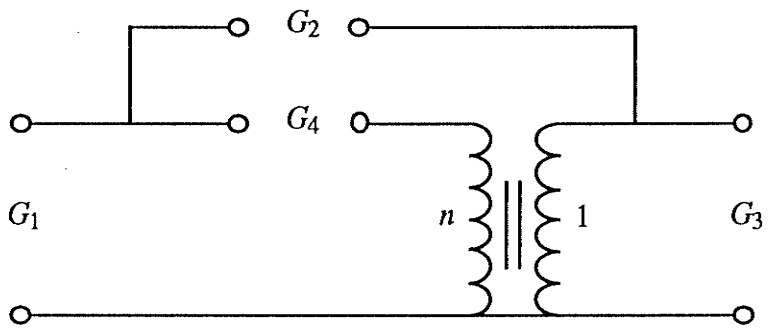

Fig. 3.1 A 4-port topology used in deriving the matched 4-port adaptor.

A WD adaptor is a signal flowgraph – with signal leads grouped into ports – that realizes

the matrix equation **B** = **SA** for some multi-port network using adders and multipliers. A simple example is the 2-port adaptor derived in Section 2.2. In general, the number of independent parameters that characterize an adaptor equals the number of ports minus one, plus the number of ideal transfomer turns-ratios (gyration ratios) within the network. There are four independent parameters for the network in Fig. 3.1.

The reflection-free property, described in Section 2.5, can often be used as a means of deriving simpler WD adaptors. The idea is to reduce the number of independent parameters by shifting them out of the structure and into the adjoining ports via 2-port adaptors. If the parameters are chosen to be the port reflectances, then the process of shifting is equivalent to making those ports reflection-free. This can be accomplished in a simple fashion by making proper choices for the the port references. In Section 2.5, it was shown that the diagonal elements of the scattering matrix that describes an adaptor are equal to the reflectances at those ports. For the 4-port in Fig. 3.1, we can select three independent reflectances as parameters:

$$s_{ii} = \frac{G_i - Y_i}{G_i + Y_i} \qquad i = 1, 2, 3 \tag{3.1}$$

where Y_i is the input conductance looking into port i with the remaining ports terminated in their port reference conductances. The fourth reflectance is dependent because, in general, for a nonsingular matrix S which is also lossless, $\Sigma\, s_{ii}$ = sum of the eigenvalues (which are either ± 1), which is equal to zero for the 4-port in Fig. 3.1 [29]. For the 4-port we have

$$Y_1 = \frac{G_2G_3 + (1-n)^2G_2G_4 + G_3G_4}{G_2 + G_3 + n^2G_4} \quad , \quad Y_2 = \frac{G_1G_3 + n^2G_1G_4 + G_3G_4}{G_1 + G_3 + (1-n)^2G_4} \quad . \tag{3.2a,b,c}$$

$$Y_3 = \frac{G_1G_2 + n^2G_1G_4 + (1-n)^2G_2G_4}{G_1 + G_2 + G_4}$$

The set $\{s_{11}\ ,\ s_{22}\ ,\ s_{33}\ ,\ n\}$ forms an independent set of parameters that characterizes the 4-port network. Adaptor structures based on 4 independent parameters plus a dependent multiplier have been derived elsewhere [29],[51],[52]. Here, we select $G_1 = Y_1 \Leftrightarrow s_{11} = 0$ in (3.1). The term G_1 in (3.2b and c) is then replaced with (3.2a). Next, we set $G_2 = Y_2 \Leftrightarrow s_{22} = 0$ in (3.1). From (3.2b), we solve for $G_2 = f(G_3, G_4, n)$ and substitute the result in (3.2c). Finally, we set $G_3 = Y_3 \Leftrightarrow s_{33} = 0$ and solve for $G_4 = f(n)$ from (3.2c). The resulting port references are given by:

$$G_1 \quad , \quad G_2 = \frac{nG_1}{1-n} \quad , \quad G_3 = nG_1 \quad , \quad G_4 = \frac{G_1}{1-n} \tag{3.3}$$

where n is the only independent parameter that remains. The port references in general must be positive which is ensured in (3.3) by $0 < n < 1$.

The 4-port scattering matrix, with port references from (3.3), can be derived by following the network analysis procedure developed by Martens and Meerkötter [50]. They have shown that the constant scattering matrix of a lossless multi-port network can be partitioned according to link and twig ports, i.e.,

$$\begin{bmatrix} b_l \\ b_t \end{bmatrix} = \begin{bmatrix} 2\mathbf{N}^{\mathrm{T}}\mathbf{K} - \mathbf{I} & 2\mathbf{N}^{\mathrm{T}}(\mathbf{I} - \mathbf{K}\mathbf{N}^{\mathrm{T}}) \\ 2\mathbf{K} & \mathbf{I} - 2\mathbf{K}\mathbf{N}^{\mathrm{T}} \end{bmatrix} \begin{bmatrix} a_l \\ a_t \end{bmatrix} \tag{3.4}$$

where $$v_l = \mathbf{N}^{\mathrm{T}} v_t \qquad v_t = \mathbf{K} e_l \ . \tag{3.5a,b}$$

$\mathbf{N}$ is a matrix of turns-ratios of an ideal-transformer multi-port network that reduces to the non-unit part of the fundamental cut-set matrix for a network consisting of "wire" interconnections only. $\mathbf{K}$ relates twig voltages to link voltage sources when all the ports are terminated in resistances with port reference values. A resistively terminated 4-port circuit for solving (3.5) with ports (1 and 2) and (3 and 4) chosen as link and twig ports respectively, is shown in Fig. 3.2.

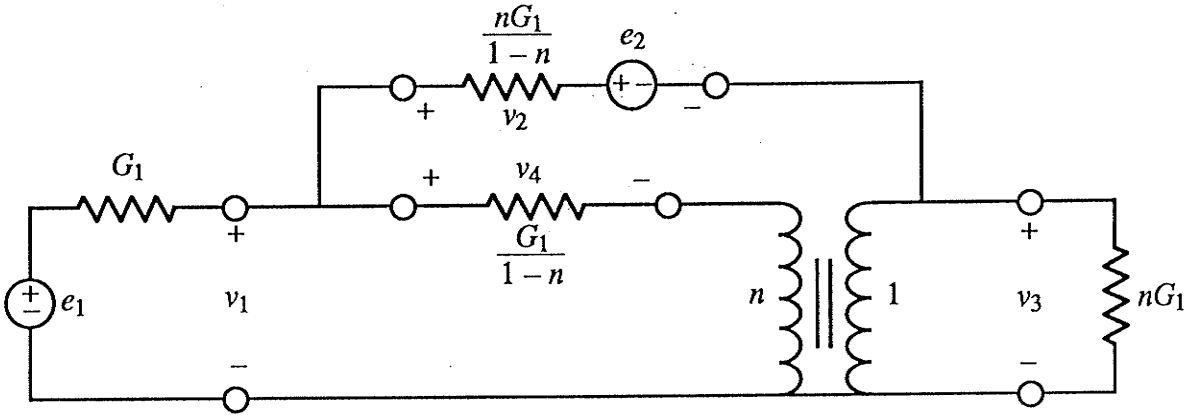

Fig. 3.2 A resistively terminated 4-port circuit used for solving (3.5) with ports (1 and 2) and (3 and 4) as link and twig ports, respectively.

The solutions of (3.5) using the circuit in Fig. 3.2 are given by

$$\begin{bmatrix} v_1 \\ v_2 \end{bmatrix} = \begin{bmatrix} n & 1 \\ n-1 & 1 \end{bmatrix} \begin{bmatrix} v_3 \\ v_4 \end{bmatrix} = \mathbf{N}^{\mathrm{T}} \begin{bmatrix} v_3 \\ v_4 \end{bmatrix} \quad , \quad 2\begin{bmatrix} v_3 \\ v_4 \end{bmatrix} = \begin{bmatrix} 1 & -1 \\ 1-n & n \end{bmatrix} \begin{bmatrix} e_1 \\ e_2 \end{bmatrix} = 2\mathbf{K} \begin{bmatrix} e_1 \\ e_2 \end{bmatrix} \ . \tag{3.6a,b}$$

It turns out that $2\mathbf{K} = (\mathbf{N}^{\mathrm{T}})^{-1}$. Sustituting (3.6) into (3.4) yields

$$\begin{bmatrix} b_1 \\ b_2 \\ b_3 \\ b_4 \end{bmatrix} = \begin{bmatrix} 0 & 0 & n & 1 \\ 0 & 0 & n-1 & 1 \\ 1 & -1 & 0 & 0 \\ 1-n & n & 0 & 0 \end{bmatrix} \begin{bmatrix} a_1 \\ a_2 \\ a_3 \\ a_4 \end{bmatrix} = \mathbf{S}_4 \begin{bmatrix} a_1 \\ a_2 \\ a_3 \\ a_4 \end{bmatrix} \tag{3.7}$$

As expected, the diagonal elements are all zero and, consequently, each port is individually reflection-free. However, in order to ensure computability, only ports 1 and 2 or ports 3 and 4 can simultaneously be treated as reflection-free, the reason being that only in these cases are the corresponding off-diagonal elements equal to zero – a necessary constraint which was described in Section 2.5. Since choosing a port reference to make the reflectance equal to zero is also called "matching", the adaptor corresponding to $\mathbf{S}_4$ is called the matched 4-port adaptor [29]. A signal flowgraph of the matched 4-port adaptor is shown in Fig. 3.3.

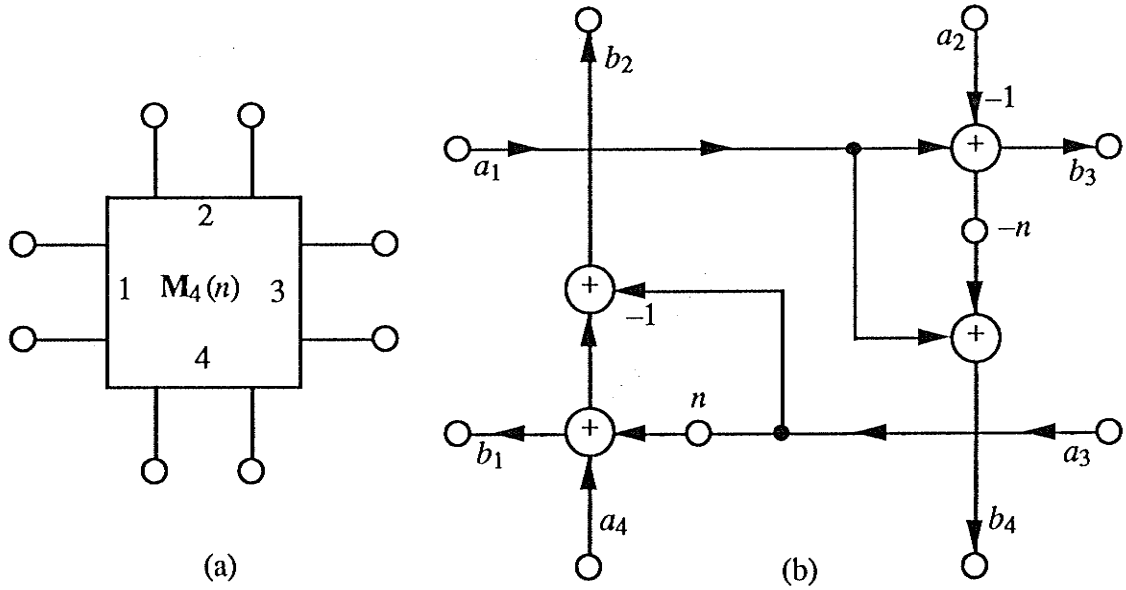

Fig. 3.3 (a) Symbolic designation and (b) signal-flow diagram of the matched 4-port adaptor.

By applying a diagonal similarity transformation (scaling), structures equivalent to Fig. 3.3 can be derived that consist of only 2-port adaptors. Let $\hat{\mathbf{S}}_4 = \mathbf{P}^{-1}\,\mathbf{S}_4\,\mathbf{P}$ where $\mathbf{P} = \left\{1\ ,\ \frac{1+\sqrt{n}}{\sqrt{n}}\ ,\ \frac{-1}{\sqrt{n}}\ ,\ 1+\sqrt{n}\right\}$. The resulting 4-port adaptor along with its scattering matrix is shown in Fig. 3.4a. Note that each nonzero block in the scattering matrix corresponds to the scattering matrix of a 2-port adaptor (see (2.13)). The 4-port scattering matrix $\mathbf{S}_4$ can be made orthogonal by choosing $\mathbf{P} = \left\{1\ ,\ \sqrt{\frac{1-n}{n}}\ ,\ \frac{-1}{\sqrt{n}}\ ,\ \sqrt{1-n}\right\}$. The resulting 4-port adaptor along with its scattering matrix is shown in Fig. 3.4b.

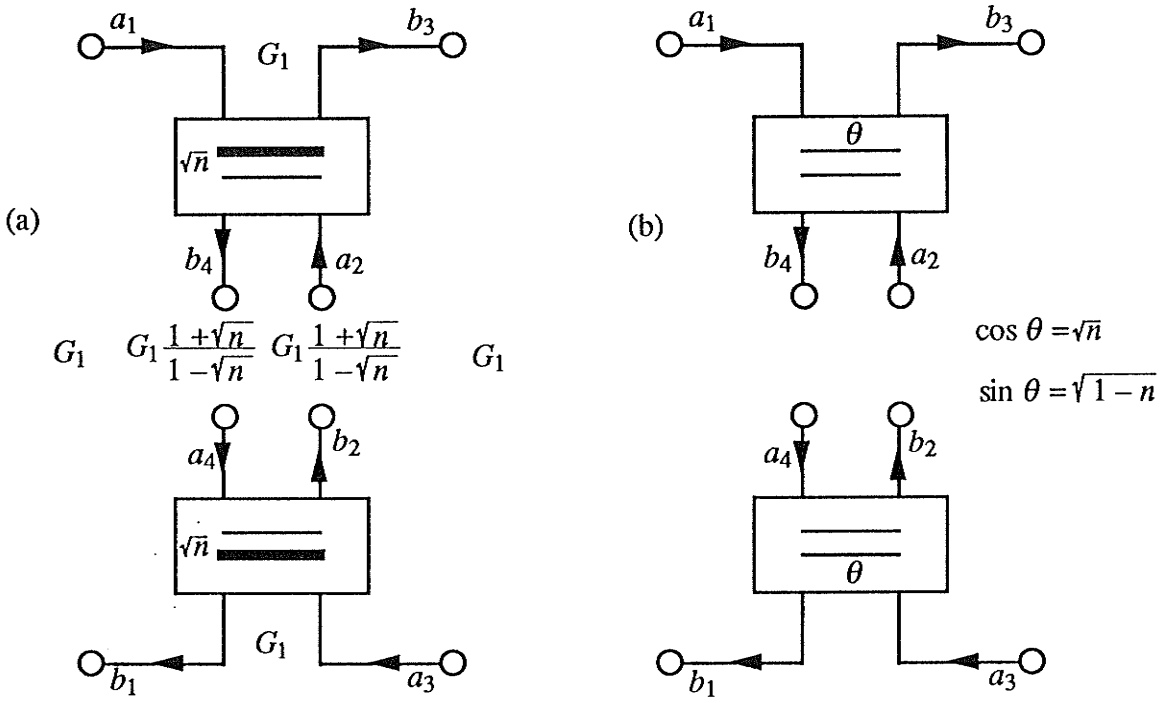

$$\hat{S}_4=\begin{bmatrix} 0 & 0 & -\sqrt{n} & 1+\sqrt{n} \\ 0 & 0 & 1-\sqrt{n} & \sqrt{n} \\ -\sqrt{n} & 1+\sqrt{n} & 0 & 0 \\ 1-\sqrt{n} & \sqrt{n} & 0 & 0 \end{bmatrix} \qquad \hat{S}_4=\begin{bmatrix} 0 & 0 & -\sqrt{n} & \sqrt{1-n} \\ 0 & 0 & \sqrt{1-n} & \sqrt{n} \\ -\sqrt{n} & \sqrt{1-n} & 0 & 0 \\ \sqrt{1-n} & \sqrt{n} & 0 & 0 \end{bmatrix}$$

Fig. 3.4 (a) 2-port adaptor and (b) normalized 2-port adaptor (orthogonal) versions of the matched 4-port adaptor in Fig. 3.3.

Of the three flowgraphs, the matched 4-port adaptor requires the fewest number of arithmetic operations; i.e., 4 additions and 2 multiplications as opposed to 6 and 2 in Fig. 3.4a, and 4 and 8 in Fig. 3.4b. Another equivalent circuit that is of interest can be derived by rewriting the normalized 2-port adaptor scattering matrix equation as

$$\begin{aligned} \begin{bmatrix} b_1 \\ b_2 \end{bmatrix} &= \begin{bmatrix} -\cos\theta & \sin\theta \\ \sin\theta & \cos\theta \end{bmatrix}\begin{bmatrix} a_1 \\ a_2 \end{bmatrix} = \begin{bmatrix} -\sin\theta & -\cos\theta \\ -\cos\theta & \sin\theta \end{bmatrix}\begin{bmatrix} 0 & -1 \\ 1 & 0 \end{bmatrix}\begin{bmatrix} a_1 \\ a_2 \end{bmatrix} \\ &= \begin{bmatrix} -\cos\theta_0 & \sin\theta_0 \\ \sin\theta_0 & \cos\theta_0 \end{bmatrix}\begin{bmatrix} 0 & -1 \\ 1 & 0 \end{bmatrix}\begin{bmatrix} a_1 \\ a_2 \end{bmatrix} \qquad \text{where} \quad \theta_0=\theta-\frac{\pi}{2} \end{aligned} \tag{3.8}$$

The decomposition in (3.8) corresponds to one of many network equivalences that exist between normalized 2-port adaptors. Some of these are shown in Fig. 3.5.

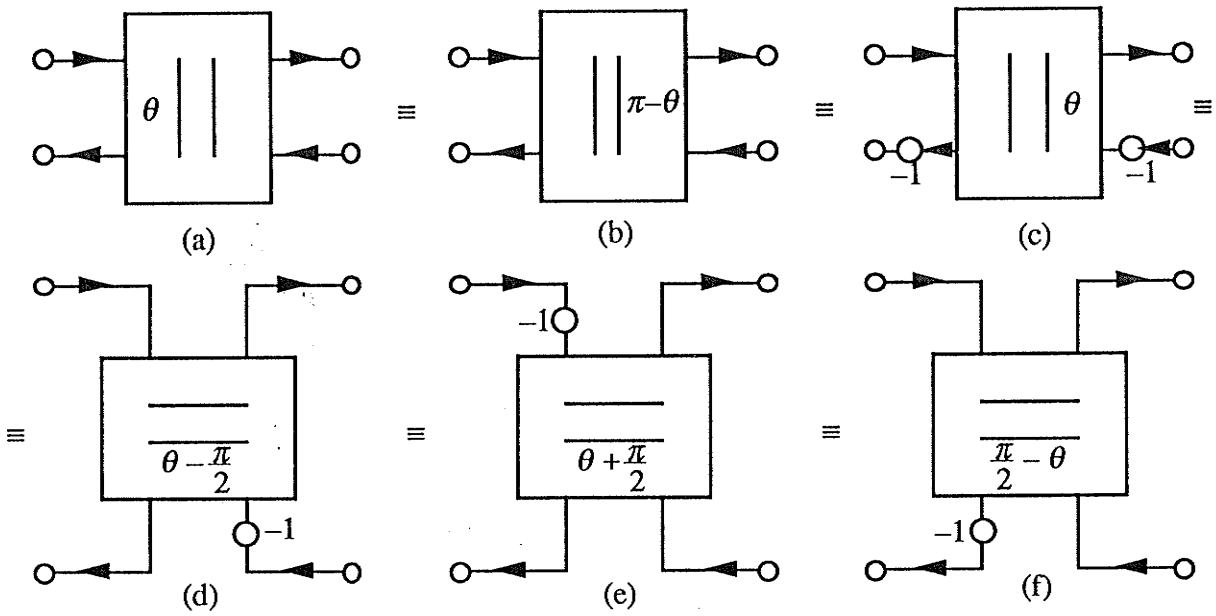

Fig. 3.5 Normalized 2-port adaptor equivalences.

Applying equivalences f and e from Fig 3.5 to Fig. 3.4b results in an equivalent flowgraph shown in Fig. 3.6.

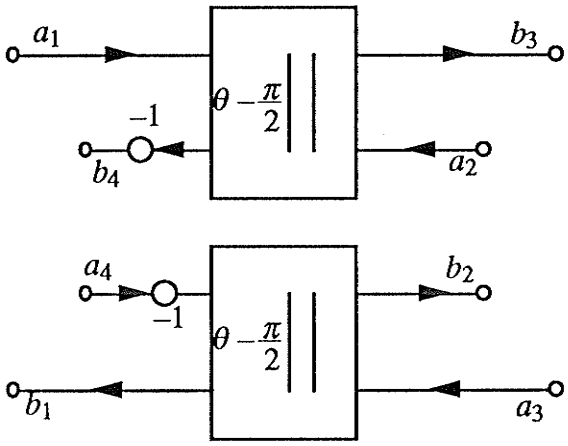

$$\hat{S}_4 = \begin{bmatrix} 0 & 0 & -\sqrt{1-n} & -\sqrt{n} \\ 0 & 0 & -\sqrt{n} & \sqrt{1-n} \\ -\sqrt{1-n} & -\sqrt{n} & 0 & 0 \\ -\sqrt{n} & \sqrt{1-n} & 0 & 0 \end{bmatrix}$$

$$\cos\theta = \sqrt{n} \qquad \sin\theta = \sqrt{1-n}$$

Fig. 3.6 A flowgraph equivalent to Fig. 3.4b.

The point of deriving the equivalent circuit in Fig. 3.6 is that when the normalized 2-port adaptors are converted to 2-port adaptors via Fig. 2.7a, the resulting multiplier is given by $\gamma = \cos(\theta - \pi/2) = \sin\theta = \sqrt{1-n}$, in contrast to Fig. 3.4a where $\gamma = \cos\theta = \sqrt{n}$. When the multipliers are quantized to binary fractions, it is usually the case that one or the other is a better approximation; e.g., $\theta = \pi/6$ where γ could be either 1/2 or $\sqrt{3}/2$. The difference,

however, becomes insignificant when a sufficient number of bits are used for the multipliers.

Two of the most important 3-port adaptors are the parallel and series adaptors [11], as shown in Fig. 3.7a and b, respectively.

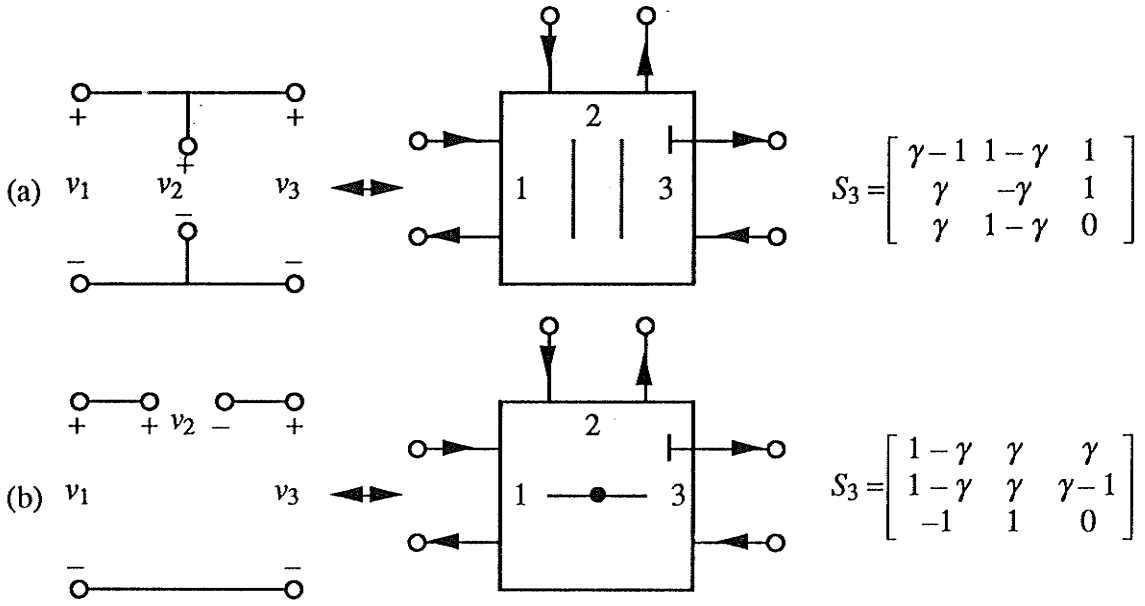

Fig. 3.7 (a) 3-port parallel and (b) series adaptors with port 3 reflection-free.

As their names imply, these adaptors allow a parallel and series interconnection of three ports in the wave domain. By terminating port 2 in the analog domain with an inductance or a capacitance, all 1st-order reciprocal sections can be obtained; if the terminating one-port is a resonant circuit from Fig. 2.11, two types of 2nd-order reciprocal sections can be obtained. The corresponding WD elementary sections are obtained by terminating port 2 in the 3-port adaptor with the corresponding allpass section from Fig. 2.9 and 2.11.

The 4-port network in Fig. 3.1 can be transformed to a 3-port network by terminating one of the ports with an open or short-circuit. For example, by open- or short-circuiting port 4, we have in the wave domain $b_4 = a_4$ and $b_4 = -a_4$, respectively, and (3.7) reduces to

$$\begin{bmatrix} b_1 \\ b_2 \\ b_3 \end{bmatrix} = \begin{bmatrix} 1-n & n & n \\ 1-n & n & n-1 \\ 1 & -1 & 0 \end{bmatrix} \begin{bmatrix} a_1 \\ a_2 \\ a_3 \end{bmatrix} \quad , \quad \begin{bmatrix} b_1 \\ b_2 \\ b_3 \end{bmatrix} = \begin{bmatrix} n-1 & -n & n \\ n-1 & -n & n-1 \\ 1 & -1 & 0 \end{bmatrix} \begin{bmatrix} a_1 \\ a_2 \\ a_3 \end{bmatrix} \qquad (3.9a,b)$$

A comparison of (3.9a,b) with the matrices in Fig. 3.7a and b shows that the matched 4-port adaptor can be made equivalent to within scaling to the 3-port parallel and series adaptors, respectively. It follows that the 4-port adaptor can also be used to realize 1st and 2nd-order elementary sections.

3.2 1st- and 2nd-order Elementary Reciprocal Sections

In the previous section, it was shown that an appropriately terminated 4-port adaptor can be used to realize all 1st-order and two types of 2nd-order reciprocal sections. If ports 2 and 4 in Fig. 3.1 are terminated in an inductance and a capacitance (or vice versa), respectively, then an additional type of 2nd-order reciprocal section, called the Brune section, can be obtained. All the above sections can be derived systematically by letting

$$a_2 = S_2 b_2 \qquad \text{and} \qquad a_4 = S_4 b_4 \tag{3.10}$$

where S_2 and S_4 are elementary allpass sections and ports 1 and 3 are the input and output ports, respectively. Fig. 3.4b can be redrawn, with ports 2 and 4 terminated according to (3.10), as shown in Fig. 3.8. In the course of deriving Fig. 3.4b, a pair of inverse multipliers $(-\sqrt{n}\,, -1/\sqrt{n}\,)$ has been introduced at port 3 which, in addition to normalizing the port reference, has also negated the voltage reference (see Fig. 3.2) at port 3. In Fig. 3.8, this voltage reference has been changed back to that in Fig. 3.2 by inserting a pair of minus signs at port 3 and using an equivalence from Fig. 3.5. In effect, ports 1 and 2 for both normalized 2-port adaptors have been interchanged.

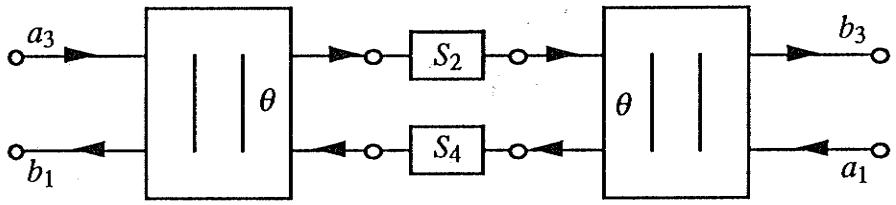

$$\cos\theta = \sqrt{n} \qquad \sin\theta = \sqrt{1-n}$$

Fig. 3.8 A redrawing of Fig. 2.4b with ports 2 and 4 terminated in allpass sections.

Fig. 3.8 illustrates that a particular two-port characterization factors in a natural way, i.e.,

$$\begin{aligned}\begin{bmatrix} b_1 \\ a_3 \end{bmatrix} &= \frac{1}{\sin\theta}\begin{bmatrix} 1 & \cos\theta \\ \cos\theta & 1 \end{bmatrix}\begin{bmatrix} S_4 & 0 \\ 0 & 1/S_2 \end{bmatrix}\frac{1}{\sin\theta}\begin{bmatrix} 1 & -\cos\theta \\ -\cos\theta & 1 \end{bmatrix}\begin{bmatrix} a_1 \\ b_3 \end{bmatrix} \\ &= \frac{1}{S_2\sin^2\theta}\begin{bmatrix} S_2S_4 - \cos^2\theta & (\cos\theta)(1 - S_2S_4) \\ (\cos\theta)(S_2S_4 - 1) & 1 - S_2S_4\cos^2\theta \end{bmatrix}\begin{bmatrix} a_1 \\ b_3 \end{bmatrix} = \mathbf{H}\begin{bmatrix} a_1 \\ b_3 \end{bmatrix}\end{aligned} \tag{3.11}$$

We recognize the grouping of wave variables in (3.11) as that corresponding to the hybrid representation (see eq. (2.22c)). Regrouping the wave variables according to (2.22a) and

(2.22b) yields the scattering and transfer matrices:

$$\begin{bmatrix} b_1 \\ b_3 \end{bmatrix} = \frac{1}{1 - S_2S_4\cos^2\theta} \begin{bmatrix} S_4 \sin^2\theta & (\cos\theta)(1 - S_2S_4) \\ (\cos\theta)(1 - S_2S_4) & S_2 \sin^2\theta \end{bmatrix} \begin{bmatrix} a_1 \\ a_3 \end{bmatrix} = \mathbf{S} \begin{bmatrix} a_1 \\ a_3 \end{bmatrix} \quad (3.12a)$$

$$\begin{bmatrix} b_1 \\ a_1 \end{bmatrix} = \frac{1}{(\cos\theta)(1 - S_2S_4)} \begin{bmatrix} \cos^2\theta - S_2S_4 & S_4 \sin^2\theta \\ -S_2 \sin^2\theta & 1 - S_2S_4\cos^2\theta \end{bmatrix} \begin{bmatrix} a_1 \\ b_3 \end{bmatrix} = \mathbf{T} \begin{bmatrix} a_3 \\ b_3 \end{bmatrix} . \quad (3.12b)$$

It can be easily verified that the representations in (3.12) correspond to a lossless two-port, i.e., $\mathbf{S}_*\mathbf{S} = \mathbf{I}$ where, for an allpass section S_i, we have $S_{i*} = 1/S_i$. It follows from Belevitch's representation (see (2.24)) that, for the representations in (3.12), the reflectance and transmittance are given by

$$\rho := \frac{h}{g} = \frac{S_4 \sin^2\theta}{1 - S_2S_4 \cos^2\theta} \quad , \quad \frac{f}{g} = \frac{(\cos\theta)(1 - S_2S_4)}{1 - S_2S_4 \cos^2\theta} . \quad (3.13a,b)$$

At a transmission zero we have from (3.13) that

$$S_2S_4 = 1 \quad \Rightarrow \quad \rho = S_4 \quad (3.14)$$

and

$$d = \left[\ln \frac{g}{h}\right]' = \frac{[\text{Arg } S_4]' + [\text{Arg } S_2]' \cos^2\theta}{-\sin^2\theta} \quad (3.15)$$

where we have used the fact that at $\psi = j\phi \leftrightarrow z = e^{j\omega T}$, $|S_2| = |S_4| = 1$.

We are now in position to derive all 1st-order reciprocal sections. As we have seen in the previous section, we can choose $S_4 = \pm 1$ to realize all 1st-order reciprocal sections . This choice is consistent with (3.14) since, for these cases, $\rho = \pm 1$ (see Property 6 eq. (2.32)). The possible locations of transmission zeros are $\psi = 0 \leftrightarrow z = 1$ or $\psi = \infty \leftrightarrow z = -1$. At these locations, a 1st-order allpass section S_2 selected from Fig. 2.9 has the value $S_2 = \pm 1$ – a value which can be made consistent with $S_2S_4 = 1$. However, for WD circuits, it is important to have the option, if possible, of making port 3 reflection-free. For this choice, the rules for terminating a matched 4-port adaptor to ensure computability require that ports 1 and 2 be terminated in reflection-free one-ports, i.e., we must choose $S_2 = \pm z^{-1}$. This choice is not restrictive because, in addition to the location of the transmission zero, only one degree of freedom is required to fix the location of the zero of g. This degree of freedom is provided by (3.15), i.e.,

$$S_2 = \pm z^{-1} \text{ and } S_4 = \pm 1 \quad \Rightarrow \quad d = \frac{2\cos^2\theta}{\sin^2\theta} = \frac{2n}{1-n} \text{ and } \delta = \frac{\cos^2\theta}{\sin^2\theta} = \frac{n}{1-n} \quad (3.16)$$

where δ was defined in (2.36) and has the same properties as d in the analog domain. Since the choice $S_2 = \pm z^{-1}$ corresponds to $R_1 = R_2$ (see Fig. 2.9), the reactive element value in the analog domain is equal to the reference at port 2, i.e., from (3.3) and (3.16) we have that

$$\frac{G_2}{G_1} = \frac{n}{1-n} = \frac{d}{2} \tag{3.17}$$

The canonic polynomials f, g and h are obtained from (3.13). The four different cases corresponding to $S_2 = \pm z^{-1}$ and $S_4 = \rho = \pm 1$, in both the analog and WD domains, are given in Tables 3.1-3.4.

By *Lemma* 2.1, d is real and positive. It is obvious from Tables 3.1-3.4 that for g to be real and Hurwitz, it is necessary and sufficient that d be real and positive. In addition to specifying the canonic polynomials, we also provide in Tables 3.1-3.4 two ideal transformer values n_1 and n_2 which, when combined with the main two-port, induce the reflection-free property at ports 1 and 2, respectively. In general, these can be obtained for both domains using

$$\cos\gamma_1 = \frac{h}{\sigma g_*} \quad , \quad \cos\gamma_2 = \frac{h_*}{\sigma g} \quad \text{at} \quad \psi = 1 \ \text{ or } \ z^{-1} = 0 \tag{3.18a,b}$$

and from (2.14b)

$$n_i = \tan^2\left(\frac{\gamma_i}{2}\right) \qquad i = 1, 2 \tag{3.19}$$

In deriving the above, we have used eqs. (2.14a), (2.39c,d), and the fact that a reflectance at a reflection-free port is zero at $\psi = 1 \leftrightarrow z^{-1} = 0$.

For the WD domain, the primitive polynomials in Tables 3.1-3.4 are obtained by substituting $\psi = (1 - z^{-1})/(1 + z^{-1})$ in the analog domain polynomials. The term primitive is used to designate polynomials whose coefficients are simple functions (usually linear) of the minimal characterization. The port 2 reflection-free polynomials are obtained from the primitive ones by absorbing a normalized 2-port adaptor with the parameter $\cos\gamma_2$. Note that port 2 referred to in Tables 3.3-3.6 is the output port, which is port 3 in the matched 4-port adaptor. As will be discussed in Chapter IV, a section defined by the primitive polynomials is extracted first, followed by an extraction of the chosen normalized 2-port adaptor (ideal transformer). This is done to make the synthesis more flexible, and for numerical reasons.

As remarked earlier, the choice $S_4 = \pm 1$ also allows the realization of two types of 2nd-order reciprocal sections that have port 2 terminated in one of the allpass sections from Fig. 2.11, i.e.,

$$S_2 = \frac{\pm\, z^{-1}(z^{-1} - \cos\omega_0 T)}{1 - z^{-1}\cos\omega_0 T} \ \leftrightarrow \ S_2 = \frac{\pm\,(1-\psi)(\phi_0^2 - \psi)}{(1+\psi)(\phi_0^2 + \psi)} \tag{3.20}$$

The transmission zeros are located at $\psi = j\phi_0 \leftrightarrow z = e^{j\omega_0 T}$ where $\phi_0 = \tan \omega_0 T/2$. As before, S_2 must be chosen reflection-free but, again, no degrees of freedom are lost. From (3.20) and (3.15) we have

$$d = \frac{4n}{(1-n)(1+\phi_0^2)} \quad \text{and} \quad \delta = \frac{d}{1+\cos\omega_0 T} = \frac{2n}{(1-n)} \tag{3.21}$$

In order to satisfy $S_2 S_4 = 1$ at $\psi = j\phi_0 \leftrightarrow z = e^{j\omega_0 T}$, it is necessary to associate the upper sign in (3.20) with $S_4 = -1$ and the lower sign with $S_4 = 1$. The resulting two 2nd-order reciprocal sections in both domains are given in Tables 3.5-3.6.

From Property 6 eq. (2.32), the reflectance of a general 2nd-order reciprocal section evaluated at a $\psi = j\phi_0 \leftrightarrow z = e^{j\omega_0 T}$ transmission zero is unimodular. It follows from (3.14) that

$$S_4 = e^{j\alpha} \quad \text{and} \quad S_2 = e^{-j\alpha} \quad \text{at} \quad \psi = j\phi_0 \leftrightarrow z = e^{j\omega_0 T} \text{ where } \phi_0 = \tan \omega_0 T/2 \tag{3.22}$$

Choosing Fig. 2.9a and b for S_4 and S_2, respectively, yields

$$\begin{aligned} S_4(j\phi_0) &= \frac{\frac{R_4}{R_1} - j\phi_0}{\frac{R_4}{R_1} + j\phi_0} = e^{j\alpha} \quad \Rightarrow \quad \frac{R_4}{R_1} = -\phi_0 \cot\frac{\alpha}{2} \\ S_4(e^{j\omega_0 T}) &= \frac{1-\gamma_4 e^{j\omega_0 T}}{e^{j\omega_0 T} - \gamma_4} = e^{j\alpha} \quad \Rightarrow \quad \gamma_4 = \frac{1-\frac{R_4}{R_1}}{1+\frac{R_4}{R_1}} = \frac{\sin\left(\frac{\alpha+\omega_0 T}{2}\right)}{\sin\left(\frac{\alpha-\omega_0 T}{2}\right)} \end{aligned} \tag{3.23}$$

$$\begin{aligned} S_2(j\phi_0) &= \frac{j\phi_0\frac{R_2}{R_1} - 1}{j\phi_0\frac{R_2}{R_1} + 1} = e^{-j\alpha} \quad \Rightarrow \quad \frac{R_2}{R_1} = -\frac{\cot\frac{\alpha}{2}}{\phi_0} \\ S_2(e^{j\omega_0 T}) &= -\frac{1+\gamma_2 e^{j\omega_0 T}}{e^{j\omega_0 T} + \gamma_2} = e^{-j\alpha} \quad \Rightarrow \quad \gamma_2 = \frac{1-\frac{R_2}{R_1}}{1+\frac{R_2}{R_1}} = -\frac{\cos\left(\frac{\alpha-\omega_0 T}{2}\right)}{\cos\left(\frac{\alpha+\omega_0 T}{2}\right)} \end{aligned} \tag{3.24}$$

From (3.15) we have

$$d = \frac{(1+\cos^2\theta)\sin\alpha}{-\phi_0 \sin^2\theta} \quad \text{and} \quad \delta = \frac{(1+\cos^2\theta)\sin\alpha}{-(\sin\omega_0 T)\sin^2\theta} \tag{3.25}$$

In order to ensure the necessary condition $d > 0 \Leftrightarrow \delta > 0$, it is necessary that $\alpha < 0$ in (3.25).

In general, however, $-\pi < \alpha < \pi$. To allow the possibility of $0 < \alpha < \pi$, we simply interchange the input and output ports by permuting the rows and columns in (3.12a). At a transmission zero, we still have $S_2 S_4 = 1$ which now implies

$$\rho = S_2 = e^{j\alpha} = e^{-j\alpha'} \qquad \text{where} \quad \alpha' := -\alpha \Rightarrow \alpha' < 0 \tag{3.26}$$

and (3.23)-(3.25) hold with α replaced with α'.

Another solution for the case $0 < \alpha < \pi$ is obtained by interchanging the types of terminations for S_4 and S_2, i.e., we choose Figs. 2.9b and a for S_4 and S_2, respectively. In this case we have

$$\begin{aligned}
S_4\left(j\phi_0\right) &= \frac{j\phi_0 \dfrac{R_4}{R_1} - 1}{j\phi_0 \dfrac{R_4}{R_1} + 1} = e^{j\alpha} \quad \Rightarrow \quad \frac{R_4}{R_1} = \frac{\cot\dfrac{\alpha}{2}}{\phi_0} \\
S_4\left(e^{j\omega_0 T}\right) &= -\frac{1 + \gamma_4 e^{j\omega_0 T}}{e^{j\omega_0 T} + \gamma_4} = e^{j\alpha} \quad \Rightarrow \quad \gamma_4 = \frac{1 - \dfrac{R_4}{R_1}}{1 + \dfrac{R_4}{R_1}} = -\frac{\cos\left(\dfrac{\alpha + \omega_0 T}{2}\right)}{\cos\left(\dfrac{\alpha - \omega_0 T}{2}\right)}
\end{aligned} \tag{3.27}$$

$$\begin{aligned}
S_2\left(j\phi_0\right) &= \frac{\dfrac{R_2}{R_1} - j\phi_0}{\dfrac{R_2}{R_1} + j\phi_0} = e^{-j\alpha} \quad \Rightarrow \quad \frac{R_2}{R_1} = \phi_0 \cot\frac{\alpha}{2} \\
S_2\left(e^{j\omega_0 T}\right) &= \frac{1 - \gamma_2 e^{j\omega_0 T}}{e^{j\omega_0 T} - \gamma_2} = e^{-j\alpha} \quad \Rightarrow \quad \gamma_2 = \frac{1 - \dfrac{R_2}{R_1}}{1 + \dfrac{R_2}{R_1}} = \frac{\sin\left(\dfrac{\alpha - \omega_0 T}{2}\right)}{\sin\left(\dfrac{\alpha + \omega_0 T}{2}\right)}
\end{aligned} \tag{3.28}$$

The first solution is more convenient since it does not require a change in the terminations. The canonic polynomials obtained from (3.13) for both domains are given in Table 3.7. According to the rules of terminating a matched 4-port adaptor, the WD circuit in Table 3.7 is uncomputable due to the delay-free loop created by the four 2-port adaptors. Computability, however, can be achieved by giving up one degree of freedom by setting either

$$\gamma_4 = 0 \Rightarrow \alpha = -\omega_0 T \text{ and } \gamma_2 = -\cos\omega_0 T \tag{3.30a}$$

or

$$\gamma_2 = 0 \Rightarrow \alpha = \omega_0 T + \pi \text{ and } \gamma_4 = \cos\omega_0 T \tag{3.30b}$$

Choosing (3.30a) or (3.30b) allows port 1 or port 3 to be reflection-free, respectively. The latter choice leads to the following set of canonic polynomials:

$$\begin{aligned}
f &= (\cos\theta)(z^2 - 2(\cos\omega_0 T)z + 1) \qquad g = z^2 - (\cos\omega_0 T)(1 + \cos^2\theta)z + \cos^2\theta \\
h &= (\sin^2\theta)z\,(-z\cos\omega_0 T + 1) \quad \Rightarrow \quad h_* = (\sin^2\theta)(z - \cos\omega_0 T)
\end{aligned} \tag{3.31}$$

A 2nd-order reciprocal WD section corresponding to (3.31) and realized using the WD circuit in Table 3.7 (with $\gamma_2 = 0$) has two important properties: 1) it retains losslessness with quantized multipliers, i.e., it's structurally lossless; 2) a single multiplier γ_4 controls the location of the transmission zero. However, with one degree of freedom less, the zeros of g cannot be chosen freely. Their location is given by an intersection of two circles which are defined in the following way: let $z = u + jv$

$$g(z) = 0 \;\Rightarrow\; \left(u - \frac{1}{\cos\,\omega_0 T}\right)^2 + v^2 = \tan^2\omega_0 T \quad \text{and} \quad u^2 + v^2 = \cos^2\theta \qquad (3.32)$$

A graphical representation of (3.32) is shown in Fig. 3.9.

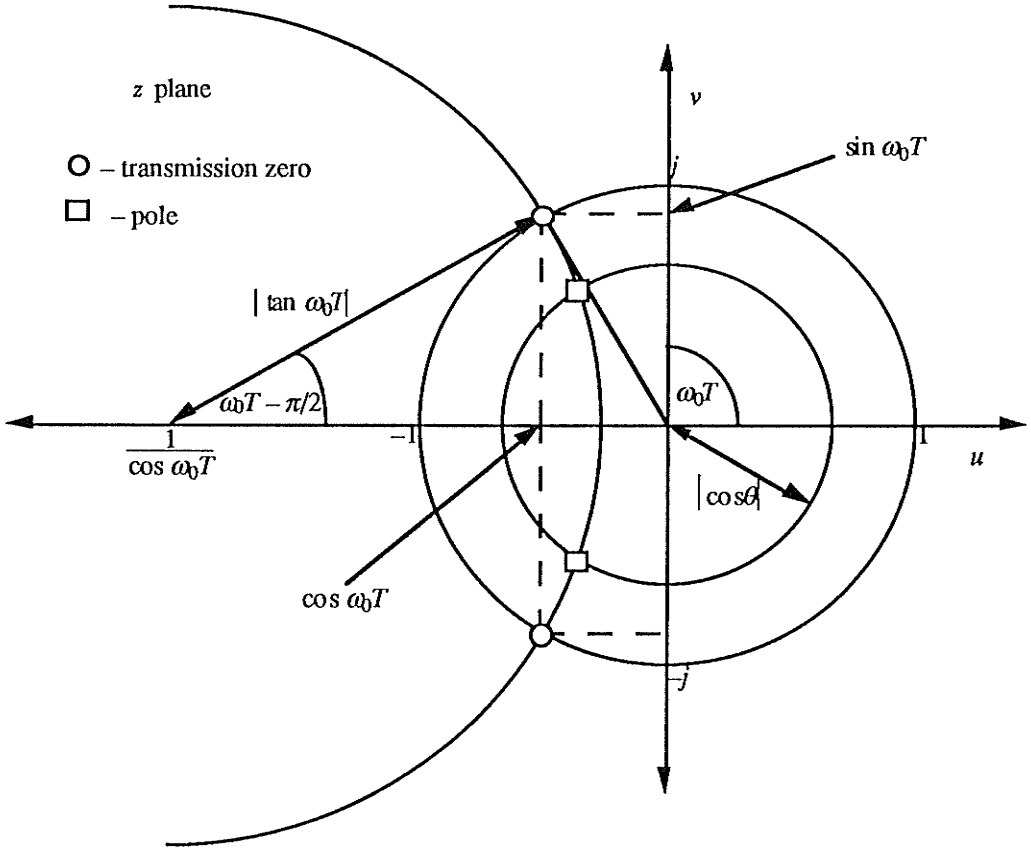

Fig. 3.9 Graphical representation of (3.32).

Choosing the constraint in (3.30a) results in the same situation except the roles of h and h_* in (3.31) are interchanged. Although the constraint in either case appears quite limiting, a design example is given in Chapter 5 where such sections are indeed used. Other examples can be found in [29],[58]. In practice, however, a nonlinear optimization of the canonic polynomials must be performed to determine if a filter, with each 2nd-order reciprocal section constrained according to (3.30), can still satisfy the given specifications.

Table 3.1 1st-order reciprocal section **1A**

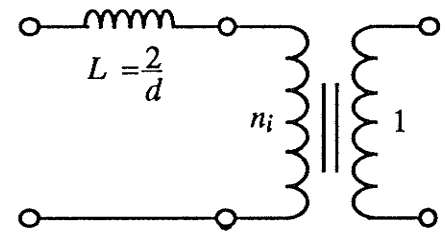

$\sigma = 1$ $\quad f = d$ $\quad g = \psi + d$ $\quad h = \psi$

$\rho(\infty) = 1$ $\quad d > 0$ $\quad n = \frac{d}{d+2}$

$n_1 = \sqrt{\frac{2n-1}{n}}$ $\quad n_2 = \frac{\pm 1}{\sqrt{n}}$

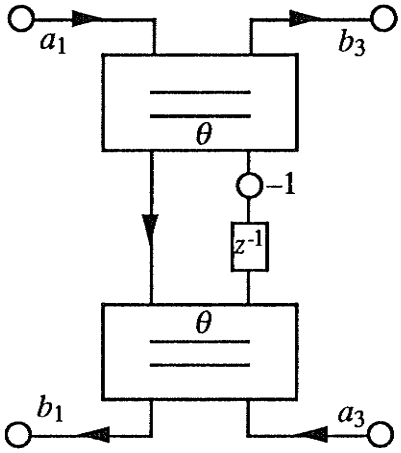

Port 2 Reflection-Free	Primitive Polynomials
$\sigma = 1$ $f = \sqrt{n}\,(z^{-1}+1)$ $g = n\,z^{-1}+1$ $h = 1-n$	$\sigma = 1$ $f = 2\delta(z^{-1}+1)$ $g = (2\delta-1)z^{-1}+2\delta+1$ $h = 1-z^{-1}$

$S_2 = -z^{-1}$ $\quad S_4 = 1$ $\quad \rho(-1) = 1$

$\delta = \frac{d}{2} > 0$ $\quad \cos\theta = \sqrt{n} = \sqrt{\frac{\delta}{\delta+1}}$

$\cos\gamma_1 = \frac{1}{2\delta-1}$ $\quad \cos\gamma_2 = \frac{-1}{2\delta+1}$

Table 3.2 1st-order reciprocal section **1B**

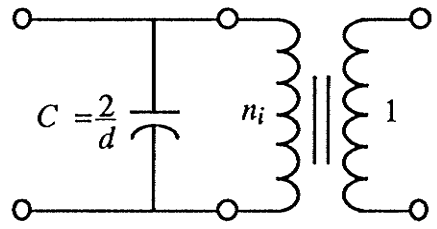

$\sigma = 1$ $\quad f = d$ $\quad g = \psi + d$ $\quad h = -\psi$

$\rho(\infty) = -1$ $\quad d > 0$ $\quad n = \frac{d}{d+2}$

$n_1 = \sqrt{\frac{n}{2n-1}}$ $\quad n_2 = \pm\sqrt{n}$

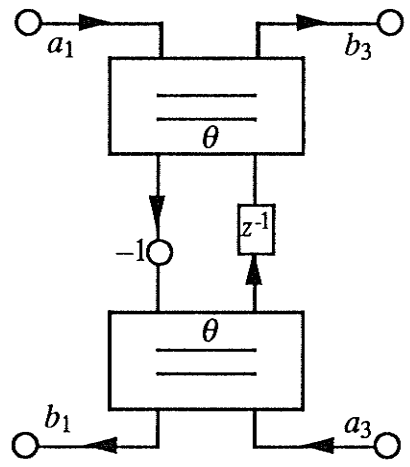

Port 2 Reflection-Free	Primitive Polynomials
$\sigma = 1$ $f = \sqrt{n}\,(z^{-1}+1)$ $g = n\,z^{-1}+1$ $h = n-1$	$\sigma = 1$ $f = 2\delta(z^{-1}+1)$ $g = (2\delta-1)z^{-1}+2\delta+1$ $h = z^{-1}-1$

$S_2 = z^{-1}$ $\quad S_4 = -1$ $\quad \rho(-1) = -1$

$\delta = \frac{d}{2} > 0$ $\quad \cos\theta = \sqrt{n} = \sqrt{\frac{\delta}{\delta+1}}$

$\cos\gamma_1 = \frac{-1}{2\delta-1}$ $\quad \cos\gamma_2 = \frac{1}{2\delta+1}$

Table 3.3 1st-order reciprocal section **1C**

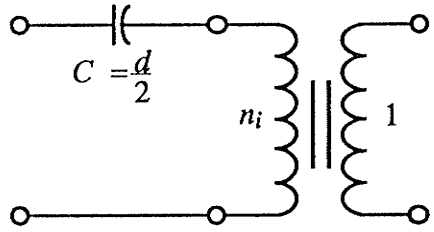

$\sigma = -1$ $\quad f = d\psi$ $\quad g = d\psi + 1$ $\quad h = +1$

$\rho(0) = 1$ $\quad d > 0$ $\quad n = \dfrac{d}{d+2}$

$n_1 = \sqrt{\dfrac{2n-1}{n}}$ $\quad n_2 = \dfrac{\pm 1}{\sqrt{n}}$

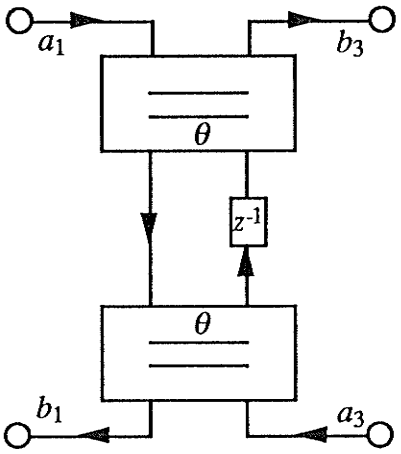

Port 2 Reflection-Free	Primitive Polynomials
$\sigma = -1$	$\sigma = -1$
$f = \sqrt{n}\,(z^{-1} - 1)$	$f = 2\delta(1 - z^{-1})$
$g = n\,z^{-1} - 1$	$g = (1 - 2\delta)z^{-1} + 2\delta + 1$
$h = n - 1$	$h = z^{-1} + 1$

$S_2 = z^{-1}$ $\quad S_4 = 1$ $\quad \rho(1) = 1$

$\delta = \dfrac{d}{2} > 0$ $\quad \cos\theta = \sqrt{n} = \sqrt{\dfrac{\delta}{\delta+1}}$

$\cos\gamma_1 = \dfrac{1}{2\delta - 1}$ $\quad \cos\gamma_2 = \dfrac{-1}{2\delta + 1}$

Table 3.4 1st-order reciprocal section **1D**

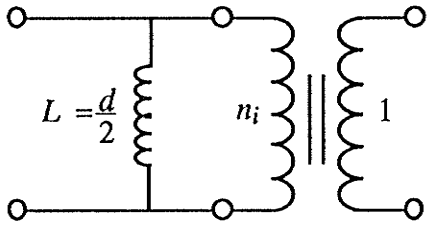

$\sigma = -1$ $\quad f = d\psi$ $\quad g = d\psi + 1$ $\quad h = -1$

$\rho(0) = -1$ $\quad d > 0$ $\quad n = \dfrac{d}{d+2}$

$n_1 = \sqrt{\dfrac{n}{2n-1}}$ $\quad n_2 = \pm\sqrt{n}$

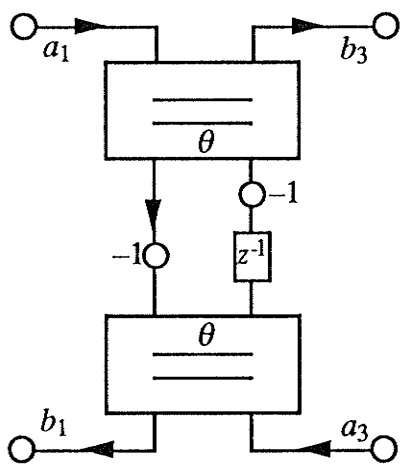

Port 2 Reflection-Free	Primitive Polynomials
$\sigma = -1$	$\sigma = -1$
$f = \sqrt{n}\,(z^{-1} - 1)$	$f = 2\delta(1 - z^{-1})$
$g = n\,z^{-1} - 1$	$g = (1 - 2\delta)z^{-1} + 2\delta + 1$
$h = 1 - n$	$h = -(z^{-1} + 1)$

$S_2 = -z^{-1}$ $\quad S_4 = -1$ $\quad \rho(1) = -1$

$\delta = \dfrac{d}{2} > 0$ $\quad \cos\theta = \sqrt{n} = \sqrt{\dfrac{\delta}{\delta+1}}$

$\cos\gamma_1 = \dfrac{-1}{2\delta - 1}$ $\quad \cos\gamma_2 = \dfrac{1}{2\delta + 1}$

Table 3.5 2nd-order reciprocal section **2A**

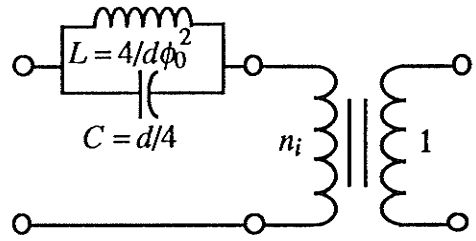

$\sigma = 1$

$f = \psi^2 + \phi_o^2$

$g = \psi^2 + \frac{2}{d}\psi + \phi_o^2$

$h = \frac{2}{d}\psi$

$\rho(j\phi_o) = 1$ $\quad n_1 = \sqrt{\frac{2n-1}{n}}$

$d > 0$ $\quad n_2 = \frac{\pm 1}{\sqrt{n}}$

$n = \frac{d(1+\phi_0^2)}{d(1+\phi_0^2)+4}$

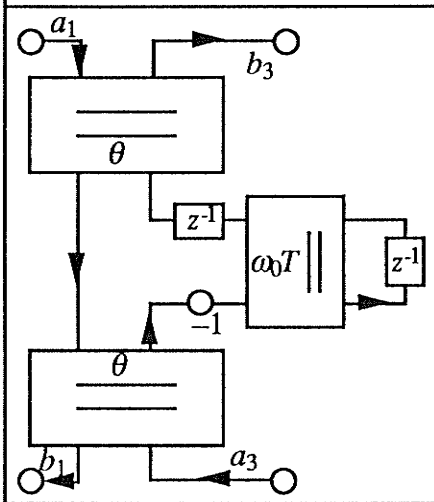

Port 2 Reflection-Free	Primitive Polynomials
$\sigma = 1$	$\sigma = 1$
$f = \sqrt{n}\ (z^{-2} - 2\varphi z^{-1} + 1)$	$f = \delta(z^{-2} - 2\varphi z^{-1} + 1)$
$g = nz^{-2} - \varphi(1+n)z^{-1} + 1)$	$g = (\delta - 1)z^{-2} - 2\delta\varphi z^{-1} + 1 + \delta$
$h = (n-1)(\varphi z^{-1} - 1)$	$h = 1 - z^{-2}$

$S_2 = \frac{z^{-1}(z^{-1} - \varphi)}{\varphi z^{-1} - 1}$ $\quad \varphi = \cos\omega_0 T = \frac{1-\phi_0^2}{1+\phi_0^2}$ $\quad \cos\gamma_1 = \frac{1}{\delta - 1}$

$S_4 = 1$ $\quad \cos\gamma_2 = \frac{-1}{1+\delta}$

$\rho(e^{j\omega_0 T}) = 1$ $\quad \cos\theta = \sqrt{n} = \sqrt{\frac{\delta}{\delta+2}}$ $\quad \delta = \frac{d}{1+\varphi} > 0$

Table 3.6 2nd-order reciprocal section **2B**

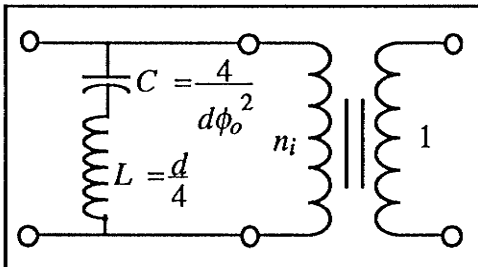

$\sigma = 1$

$f = \psi^2 + \phi_o^2$

$g = \psi^2 + \frac{2}{d}\psi + \phi_o^2$

$h = -\frac{2}{d}\psi$

$\rho(j\phi_o) = -1$

$d > 0$ $\quad n_1 = \sqrt{\frac{n}{2n-1}}$

$n = \frac{d(1+\phi_0^2)}{d(1+\phi_0^2)+4}$ $\quad n_2 = \pm\sqrt{n}$

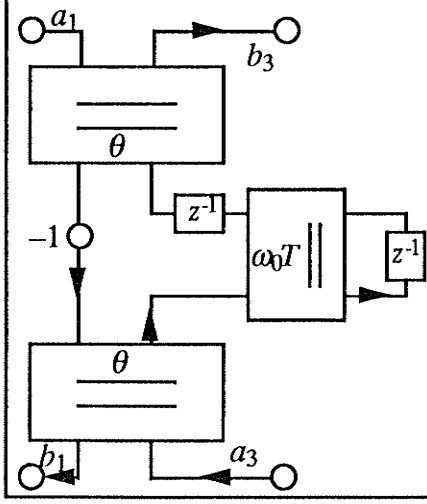

Port 2 Reflection-Free	Primitive Polynomials
$\sigma = 1$	$\sigma = 1$
$f = \sqrt{n}\ (z^{-2} - 2\varphi z^{-1} + 1)$	$f = \delta(z^{-2} - 2\varphi z^{-1} + 1)$
$g = nz^{-2} - \varphi(1+n)z^{-1} + 1)$	$g = (\delta - 1)z^{-2} - 2\delta\varphi z^{-1} + 1 + \delta$
$h = (1-n)(\varphi z^{-1} - 1)$	$h = z^{-2} - 1$

$S_2 = \frac{z^{-1}(\varphi - z^{-1})}{\varphi z^{-1} - 1}$ $\quad \varphi = \cos\omega_0 T = \frac{1-\phi_0^2}{1+\phi_0^2}$ $\quad \cos\gamma_1 = \frac{-1}{\delta - 1}$

$S_4 = 1$ $\quad \cos\gamma_2 = \frac{1}{1+\delta}$

$\rho(e^{j\omega_0 T}) = -1$ $\quad \cos\theta = \sqrt{n} = \sqrt{\frac{\delta}{\delta+2}}$

Table 3.7 2nd-order reciprocal (Brune) section.

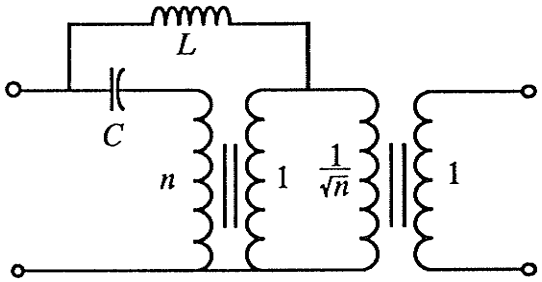

$$\sigma = 1$$

$$f = (\sin\gamma)(\psi^2 + \phi_0^2)$$

$$g = \psi^2 + \frac{2}{d}\psi + \phi_0^2$$

$$h = (\cos\gamma)\psi^2 + \frac{2\cos\alpha}{d}\psi - \phi_0^2\cos\gamma$$

$$= \cos\gamma\,(\psi + \phi_0\cot\frac{\alpha}{2})(\psi - \phi_0\tan\frac{\alpha}{2})$$

$$n = \cot^2\frac{\gamma}{2} \qquad L = \frac{n-1}{n\phi_o\tan\frac{\alpha}{2}} \qquad C = \frac{\tan\frac{\alpha}{2}}{\phi_o(n-1)}$$

$$\rho(j\phi_o) = e^{j\alpha} \quad , \quad d > 0$$

$$-1 < \cos\gamma = \frac{\sin\alpha}{d\,\phi_o} < 1$$

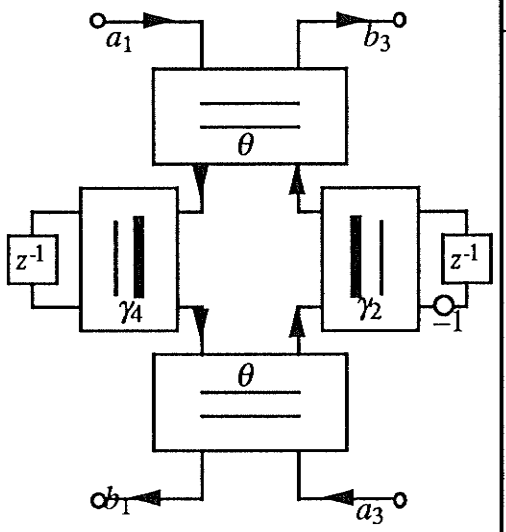

Primitive Polynomials

$$f = \delta(\sin\gamma)\left(z^{-2} - 2(\cos\omega_0 T)\,z^{-1} + 1\right) \qquad \sigma = 1$$

$$g = (\delta - 1)\,z^{-2} - 2\delta(\cos\omega_o T)\,z^{-1} + \delta + 1$$

$$h = \frac{z^{-2}\sin(\alpha - \omega_o T) - 2(\sin\alpha)\,z^{-1} + \sin(\alpha + \omega_o T)}{\sin\omega_o T}$$

$$= \frac{\left[z^{-1} - \frac{\sin\left(\frac{\alpha+\omega_0 T}{2}\right)}{\sin\left(\frac{\alpha-\omega_0 T}{2}\right)}\right]\left[z^{-1} - \frac{\cos\left(\frac{\alpha+\omega_0 T}{2}\right)}{\cos\left(\frac{\alpha-\omega_0 T}{2}\right)}\right]}{\frac{\sin\omega_0 T}{\sin(\alpha - \omega_0 T)}}$$

$$\rho(e^{j\omega_o T}) = e^{j\alpha} \qquad \delta = \frac{d}{1+\cos\omega_o T} > 0 \qquad -1 < \cos\gamma = \frac{\sin\alpha}{\delta\sin\omega_o T} < 1 \quad , \quad \phi_o = \tan\frac{\omega_o T}{2}$$

$$\gamma_2 = -\frac{\cos\left(\frac{\alpha-\omega_0 T}{2}\right)}{\cos\left(\frac{\alpha+\omega_0 T}{2}\right)} \qquad \gamma_4 = \frac{\sin\left(\frac{\alpha+\omega_0 T}{2}\right)}{\sin\left(\frac{\alpha-\omega_0 T}{2}\right)} \qquad \cos\theta = \sqrt{\frac{\delta\frac{\sin\omega_0 T}{\sin\alpha} + 1}{\delta\frac{\sin\omega_0 T}{\sin\alpha} - 1}}$$

3.3 1st- and 2nd-order Elementary Nonreciprocal Sections

A natural question arises with respect to the WD circuit in Fig. 3.8 as to what can be achieved when the two normalized 2-port adaptors are made independent of each other. The resulting circuit is shown in Fig. 3.10.

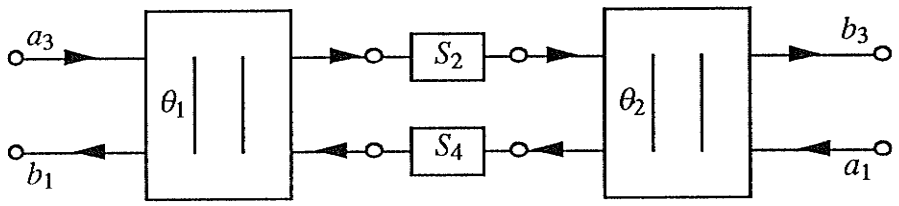

Fig. 3.10 A generalization of Fig. 3.8.

As for the reciprocal case, the grouping of wave variables in Fig. 3.10 corresponds to the hybrid representation:

$$\begin{aligned}\begin{bmatrix} b_1 \\ a_3 \end{bmatrix} &= \frac{1}{\sin\theta_1}\begin{bmatrix} 1 & -\cos\theta_1 \\ -\cos\theta_1 & 1 \end{bmatrix}\begin{bmatrix} S_4 & 0 \\ 0 & 1/S_2 \end{bmatrix}\frac{1}{\sin\theta_2}\begin{bmatrix} 1 & -\cos\theta_2 \\ -\cos\theta_2 & 1 \end{bmatrix}\begin{bmatrix} a_1 \\ b_3 \end{bmatrix} \\ &= \frac{1}{S_2\sin\theta_1\sin\theta_2}\begin{bmatrix} S_2S_4 + \cos\theta_1\cos\theta_2 & -\left(S_2S_4\cos\theta_2 + \cos\theta_1\right) \\ -\left(S_2S_4\cos\theta_1 + \cos\theta_2\right) & 1 + S_2S_4\cos\theta_1\cos\theta_2 \end{bmatrix}\begin{bmatrix} a_1 \\ b_3 \end{bmatrix} = \mathbf{H}\begin{bmatrix} a_1 \\ b_3 \end{bmatrix}\end{aligned} \tag{3.33}$$

Regrouping the wave variables according to (2.22a) and (2.22b) yields the scattering and transfer matrices:

$$\begin{bmatrix} b_1 \\ b_3 \end{bmatrix} = \frac{\begin{bmatrix} S_4\sin\theta_1\sin\theta_2 & -\left(S_2S_4\cos\theta_2 + \cos\theta_1\right) \\ S_2S_4\cos\theta_1 + \cos\theta_2 & S_2\sin\theta_1\sin\theta_2 \end{bmatrix}}{1 + S_2S_4\cos\theta_1\cos\theta_2}\begin{bmatrix} a_1 \\ a_3 \end{bmatrix} = \mathbf{S}\begin{bmatrix} a_1 \\ a_3 \end{bmatrix} \tag{3.34a}$$

$$\begin{bmatrix} b_1 \\ a_1 \end{bmatrix} = \frac{\begin{bmatrix} -\left(S_2S_4 + \cos\theta_1\cos\theta_2\right) & S_4\sin\theta_1\sin\theta_2 \\ -S_2\sin\theta_1\sin\theta_2 & 1 + S_2S_4\cos\theta_1\cos\theta_2 \end{bmatrix}}{S_2S_4\cos\theta_1 + \cos\theta_2}\begin{bmatrix} a_3 \\ b_3 \end{bmatrix} = \mathbf{T}\begin{bmatrix} a_3 \\ b_3 \end{bmatrix} \tag{3.34b}$$

It can be easily verified that the representations in (3.34) correspond to a lossless two-port, i.e., $\mathbf{S}_*\mathbf{S} = \mathbf{I}$ where, for an allpass section S_i, we have $S_{i*} = 1/S_i$. It follows from Belevitch's representation (see (2.24)) that, for the representations in (3.34), the reflectance and transmittance are given by

$$\rho := \frac{h}{g} = \frac{S_4 \sin\theta_1 \sin\theta_2}{1 + S_2 S_4 \cos\theta_1 \cos\theta_2} \quad , \quad \frac{f}{g} = \frac{S_2 S_4 \cos\theta_1 + \cos\theta_2}{1 + S_2 S_4 \cos\theta_1 \cos\theta_2} \quad . \quad (3.35a,b)$$

At a transmission zero the following holds:

$$S_2 S_4 = -\frac{\cos\theta_2}{\cos\theta_1} \quad \Rightarrow \quad \rho = S_4 \frac{\sin\theta_1}{\sin\theta_2} \quad . \quad (3.36)$$

It follows from Property 6 eq. (2.33) that the reflectance of a 1st-order nonreciprocal section is real and $|\rho| \neq 1$ when evaluated at a $\psi = -r \leftrightarrow z^{-1} = -\varphi$ transmission zero. In the analog domain, there are four possible circuits that can realize a section with $f = \psi + r$. However, all four circuits are equivalent to within a gyrator [4], i.e., after absorbing an appropriate ideal transformer, they differ at most by the value of σ. In the WD domain, this value can be easily changed by absorbing a two-port defined by $b_2 = a_1$ and $b_1 = -a_2$, which corresponds to the simplest case of a gyrator with a gyration ratio of $n = 1$ (see Fig. 2.8). It follows that a single prototype is sufficient. (Note: in the analog domain, it may be of interest to have available two types of 1st-order nonreciprocal sections because reciprocal sections change to their duals when being commuted with a gyrator – a feature which may not be desirable.) One such prototype that is consistent with (3.36) can be obtained by letting $S_4 = 1$ and $S_2 = -z^{-1}$, where S_2 is again chosen to satisfy the termination rules of the matched 4-port adaptor. (Note that by allowing the two non-zero off-diagonal blocks in $\widehat{S}_4$ in Fig. 3.6 to be independent, the matching conditions at each port are still satisfied.) The above choices yield

$$\varphi = \frac{r+1}{r-1} = \frac{\cos\theta_2}{\cos\theta_1} \quad \text{and} \quad \rho = \frac{\sin\theta_1}{\sin\theta_2} \quad (3.37)$$

from which we can solve for θ_1 and θ_2. Since only two degrees of freedom are available, we may arbitrarily choose $\cos\theta_1 > 0$ and $\sin\theta_2 > 0$. The canonic polynomials for the 1st-order nonreciprocal section are obtained from (3.35), and are given for both domains in Table 3.8. Note that the solution is unconstrained. Two important special cases of this section are also given in Table 3.8. These correspond to an ideal transformer cascaded with a QUARL (see Fig. 2.3).

The f polynomial for the general 2nd-order case is given by

$$f = \psi^2 - 2r\,(\cos\phi_0)\psi + r^2 \quad \leftrightarrow \quad f = z^{-2} - 2k\,(\cos\omega_0 T)z^{-1} + k^2 \quad (3.38a)$$

where

$$k\cos\omega_0 T + jk\sin\omega_0 T = \frac{1 - r^2 + j\ 2r\sin\phi_0}{1 + r^2 + 2r\cos\phi_0} \quad . \quad (3.38b)$$

For this case, the reflectance is a general complex number, i.e., $\rho\left(re^{j\phi_0}\right)=\rho\left(ke^{j\omega_0 T}\right)=\beta e^{j\alpha}$. As in the reciprocal case, we choose Figs. 2.9a and b for S_4 and S_2, respectively. A solution obtained from (3.36) and (3.38) is given by

$$S_4\left(re^{j\phi_0}\right)=\frac{\frac{R_4}{R_1}-re^{j\phi_0}}{\frac{R_4}{R_1}+re^{j\phi_0}}=\beta e^{j\alpha}\frac{\sin\theta_2}{\sin\theta_1}\quad\Rightarrow\quad\frac{R_4}{R_1}=\frac{r}{\tan\alpha}\left(-\sin\phi_0\pm\sqrt{\sin^2\phi_0+\tan^2\alpha}\right)$$

$$S_4\left(ke^{j\omega_0 T}\right)=\frac{1-\gamma_4 ke^{j\omega_0 T}}{ke^{j\omega_0 T}-\gamma_4}=\beta e^{j\alpha}\frac{\sin\theta_2}{\sin\theta_1}\quad\Rightarrow\quad\gamma_4=\frac{1-\frac{R_4}{R_1}}{1+\frac{R_4}{R_1}} \tag{3.39a}$$

$$S_2\left(re^{j\phi_0}\right)=\frac{re^{j\phi_0}-\frac{R_1}{R_2}}{re^{j\phi_0}+\frac{R_1}{R_2}}=-\frac{1}{\beta}e^{-j\alpha}\frac{\tan\theta_1}{\tan\theta_2}\quad\Rightarrow\quad\frac{R_1}{R_2}=\frac{r}{\tan\alpha}\left(\sin\phi_0\pm\sqrt{\sin^2\phi_0+\tan^2\alpha}\right)$$

$$S_2\left(ke^{j\omega_0 T}\right)=-\frac{1+\gamma_2 ke^{j\omega_0 T}}{ke^{j\omega_0 T}+\gamma_2}=-\frac{1}{\beta}e^{-j\alpha}\frac{\tan\theta_1}{\tan\theta_2}\quad\Rightarrow\quad\gamma_2=\frac{1-\frac{R_2}{R_1}}{1+\frac{R_2}{R_1}} \tag{3.39b}$$

$$\cos\theta_1=\sqrt{\frac{\beta^2\frac{\cos\theta_1}{\cos\theta_2}+1}{\beta^2\frac{\cos\theta_2}{\cos\theta_1}+1}}\qquad\text{where}\qquad\frac{\cos\theta_2}{\cos\theta_1}=\frac{2r\cos\phi_0-\frac{R_4}{R_1}-\frac{R_1}{R_2}}{2r\cos\phi_0+\frac{R_4}{R_1}+\frac{R_1}{R_2}} \tag{3.39c}$$

where $R_4/R_2=r^2$ and the signs in (3.39a,b) are chosen such that the resistance ratios are positive. Substituting (3.39) into (3.35) yields the canonic polynomials with coefficients as functions of the minimal parameter set $\{r,\ \phi_0,\ \beta,\ \alpha\}$ in the analog domain and $\{k,\ \omega_0 T,\ \beta,\ \alpha\}$ in the WD domain. These are given in Table 3.9 along with realizability conditions which ensure that g is Hurwitz and the overall two-port is real. Note that these constraints are obtained with relative ease once the canonic forms of f, g and h in Table 3.9 are given.

As in the 2nd-order reciprocal case, the WD circuit in Fig. 3.10 is not computable unless either S_2 or S_4 is made reflection-free. This can only be accomplished by giving up one degree of freedom. Letting $\gamma_2=0\Leftrightarrow S_2=-z^{-1}$ satisfies the termination restriction and, together with (3.39b), implies that $\alpha=\omega_0 T$. Substituting this constraint into (3.39) yields:

$$\frac{R_4}{R_1}=r^2\quad\Leftrightarrow\quad\gamma_4=\frac{R_1-R_4}{R_1+R_4}=\frac{2k\cos\omega_0 T}{1+k^2}\ ,\ \frac{\cos\theta_2}{\cos\theta_1}=-k^2\ ,\ \cos\theta_1=\sqrt{\frac{\beta^2/k^2-1}{\beta^2k^2-1}} \tag{3.40}$$

The WD circuit corresponding to this solution is shown in Table 3.9. However, unlike the reciprocal case, the four ports of the analog circuit do not all correspond to the WD circuit ports. The equivalence merely holds for the two-port characterization given by (3.34).

The zeros of g are constrained in the same way as for the reciprocal case (see Fig. 3.9) except that now the transmission zeros can move off the unit circle and $\cos^2\theta$ is replaced with $-\cos\theta_1 \cos\theta_2$.

Table 3.8 1st- order nonreciprocal section **1E**

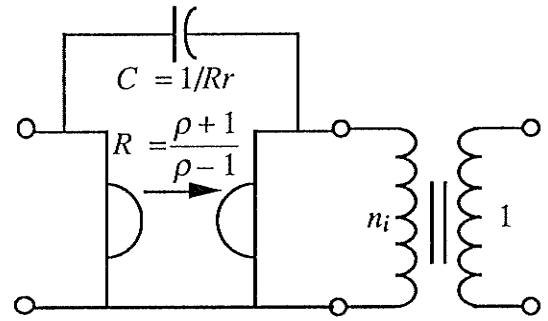

$$\sigma = -1 \qquad \frac{h}{g}(-r) = \rho$$

$$f = \psi + r$$

$$g = \psi + \frac{r(\rho^2+1)}{\rho^2-1}$$

$$h = \frac{2r\rho}{\rho^2-1} \qquad r \gtrless 0 \quad \Leftrightarrow \quad \rho^2 \gtrless 1$$

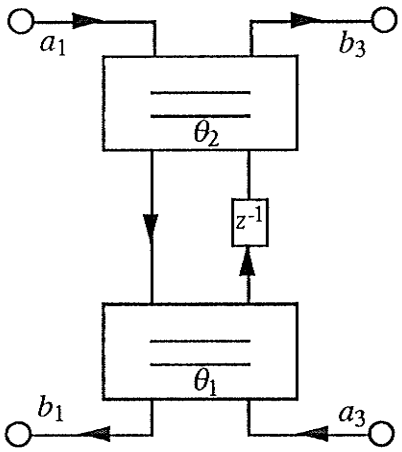

Port 2 Reflection-Free	Primitive Polynomials
$\sigma = -1$	$\sigma = -1$
$f = (\cos\theta_1)\, z^{-1} + \cos\theta_2$	$f = (\rho^2-1)(z^{-1}+\varphi)$
$g = (\cos\theta_1)(\cos\theta_2)\, z^{-1} + 1$	$g = (\rho^2+\varphi)\, z^{-1} + 1 + \rho^2\varphi$
$h = (\sin\theta_1)(\sin\theta_2)$	$h = \rho(1+\varphi)(z^{-1}+1)$

$$\cos\theta_1 = \sqrt{\frac{1-\rho^2}{1-\varphi^2\rho^2}} \qquad \cos\theta_2 = \varphi\cos\theta_1 \qquad \varphi = \frac{r+1}{r-1}$$

$$\sin\theta_1 = \rho\sin\theta_2 \qquad \sin\theta_2 = \sqrt{\frac{1-\varphi^2}{1-\varphi^2\rho^2}} \qquad \frac{h}{g}(-\varphi) = \rho$$

$$\cos\gamma_2 = \frac{-\rho(1+\varphi)}{1+\rho^2\varphi} \qquad |\varphi| \gtrless 1 \quad \Leftrightarrow \quad \rho^2 \gtrless 1$$

Special case: $\cos\theta_1 = 0$

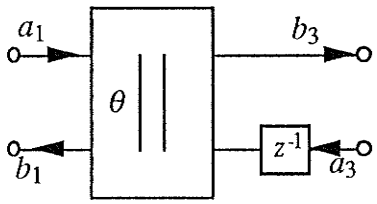

$\sigma = 1 \quad f = \sin\theta = \cos\theta_2$

$g = 1 \quad h = -\cos\theta = \sin\theta_2$

Special case: $\cos\theta_2 = 0$

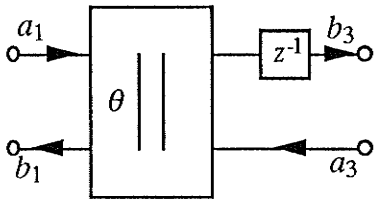

$\sigma = 1 \quad f = z^{-1}\sin\theta = z^{-1}\cos\theta_1$

$g = 1 \quad h = -\cos\theta = \sin\theta_1$

Table 3.9 2nd-order nonreciprocal analog section

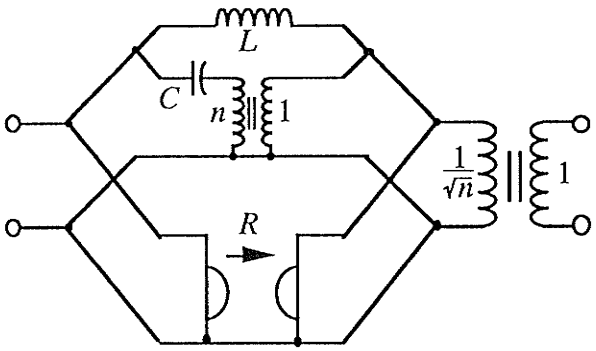

$$f = (\sin\gamma)\,(\psi^2 - 2r\,(\cos\phi_o)\,\psi + r^2)$$

$$g = \psi^2 + \frac{2r\,(\cos\phi_o)\,(1+\beta^2)}{1-\beta^2}\psi + r^2$$

$$h = (\cos\gamma)\left(\psi^2 + \frac{2r\,(\sin\phi_o)}{\tan\alpha}\psi - r^2\right)$$

$$\sigma = 1 \qquad \rho\,(re^{j\phi_o}) = \beta e^{j\alpha}$$

$$\cos\phi_o \gtrless 0 \quad \Leftrightarrow \quad \beta^2 \lessgtr 1$$

$$G_1 + H_1 = \frac{2r\,(\cos\phi_o)}{1-\beta^2}\,(\beta^2 + 2\beta\cos\alpha + 1)$$

$$-1 < \cos\gamma = \frac{2\beta\sin\alpha}{(1-\beta^2)\tan\phi_o} < 1$$

$$n = \cot^2\frac{\gamma}{2} \qquad R = \frac{G_1 + H_1}{-2r\,(1+\cos\gamma)\cos\phi_o} \qquad C = \frac{1-\cos\gamma}{G_1 + H_1} \qquad L = \frac{G_1 + H_1}{r^2\,(1+\cos\gamma)}$$

Constrained ($\alpha = \omega_0 T$) WD solution

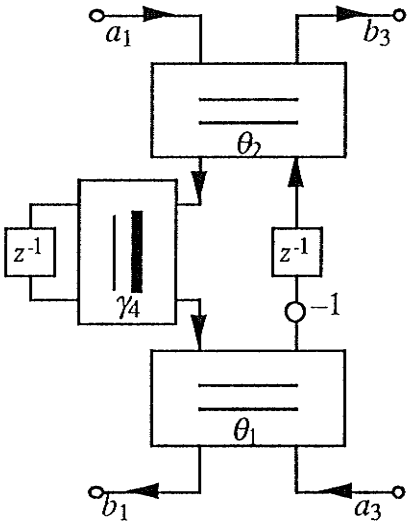

Primitive polynomials and realizability conditions

$$f = (\sin\gamma)\,(z^{-2} - 2k\,(\cos\omega_o T)\,z^{-1} + k^2) \qquad \sigma = 1$$

$$g = \frac{k^2-\beta^2}{1-\beta^2}\,z^{-2} - 2k\,(\cos\omega_o T)\,z^{-1} + \frac{1-\beta^2 k^2}{1-\beta^2}$$

$$h = (\cos\gamma)\left(\frac{k\sin(\alpha-\omega_0 T)}{\sin\alpha}z^{-2} - (1+k^2)z^{-1} + \frac{k\sin(\alpha+\omega_0 T)}{\sin\alpha}\right)$$

$$\rho\,(ke^{-j\omega_o T}) = \beta e^{j\alpha} \qquad k \gtrless 1 \quad \Leftrightarrow \quad \beta^2 \gtrless 1$$

$$-1 < \cos\gamma = \frac{\beta(1-k^2)\sin\alpha}{k(1-\beta^2)\sin\omega_0 T} < 1$$

$$\gamma_4 = \frac{2k\cos\omega_0 T}{1+k^2} \qquad \frac{\cos\theta_2}{\cos\theta_1} = -k^2 \qquad \cos\theta_1 = \sqrt{\frac{\beta^2/k^2 - 1}{\beta^2 k^2 - 1}}$$

3.4 Derivation of a General Unconstrained 2nd-order Section

The constraints given by (3.30), which ensure computability for 2nd-order reciprocal and nonreciprocal sections, may not always be imposed without violating the filter specifications. It is therefore necessary to have available unconstrained sections. In this Section, we derive a computable, unconstrained WD section which can realize all 1st- and 2nd-order reciprocal and nonreciprocal sections. There are many solutions possible [14],[15],[17],[30] due to the nonuniqueness of factoring an orthogonal scattering matrix into a product of basic Givens rotations, which are essentially equivalent to normalized 2-port adaptors. The resulting WD circuits are comprised of only normalized 2-port adaptors and delays. However, the number of these adaptors for the reciprocal case is usually greater than the number of degrees of freedom, with the extra adaptors being dependent on the minimal set. It is in the nature of this dependence that the many equivalent circuits can be distinquished – a dependence of a linear nature being the most desirable. One such solution involves the matched 4-port adaptor where ports 2 and 4, instead of being decoupled as in Fig. 3.10, now form a coupling network, as shown in Fig. 3.11.

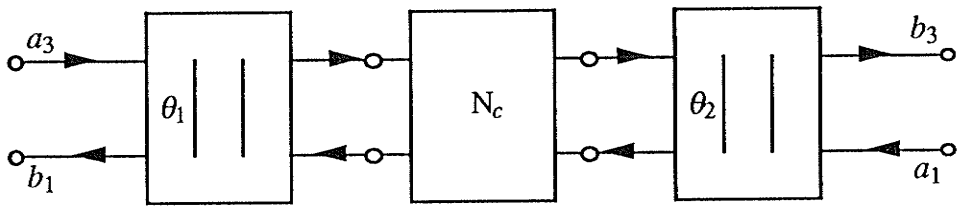

Fig. 3.11 An alternative termination of the matched 4-port adaptor.

In order to show that there indeed exists a lossless two-port N_c such that the circuit in Fig. 3.11 realizes a general 2nd-order section, we first rewrite the scattering matrix equation in (2.24a) in the following way:

$$\begin{aligned}\begin{bmatrix} b_1 \\ b_2 \end{bmatrix} &= \frac{1}{g}\begin{bmatrix} h & \sigma f_* \\ f & -\sigma h_* \end{bmatrix}\begin{bmatrix} a_1 \\ a_2 \end{bmatrix} = \frac{1}{g}\begin{bmatrix} \sigma f_* & h \\ -\sigma h_* & f \end{bmatrix}\begin{bmatrix} 0 & 1 \\ 1 & 0 \end{bmatrix}\begin{bmatrix} a_1 \\ a_2 \end{bmatrix} \\ &= \mathbf{S}\begin{bmatrix} a_1 \\ a_2 \end{bmatrix} = \mathbf{S}_2\mathbf{S}_1\begin{bmatrix} a_1 \\ a_2 \end{bmatrix}\end{aligned} \tag{3.42}$$

The transfer matrix corresponding to $\mathbf{S}_2$ is obtained using (2.11b) and it turns out to be equal to the hybrid matrix $\mathbf{H}$ of the original two-port, i.e.

$$\mathbf{T}_2 = \frac{1}{f_2}\begin{bmatrix} \sigma_2 g_{2*} & h_2 \\ \sigma_2 h_{2*} & g_2 \end{bmatrix} = \frac{1}{-\sigma h_*}\begin{bmatrix} -\sigma g_* & \sigma f_* \\ -f & g \end{bmatrix} = \mathbf{H} \tag{3.43}$$

where $$\sigma_2 = -\sigma \quad , \quad f_2 = -\sigma h_* \quad , \quad h_2 = \sigma f_* \quad , \quad g_2 = g \tag{3.44}$$

Eqs. (3.42)-(3.44) describe a network equivalence which is illustrated for both domains in Fig. 3.12.

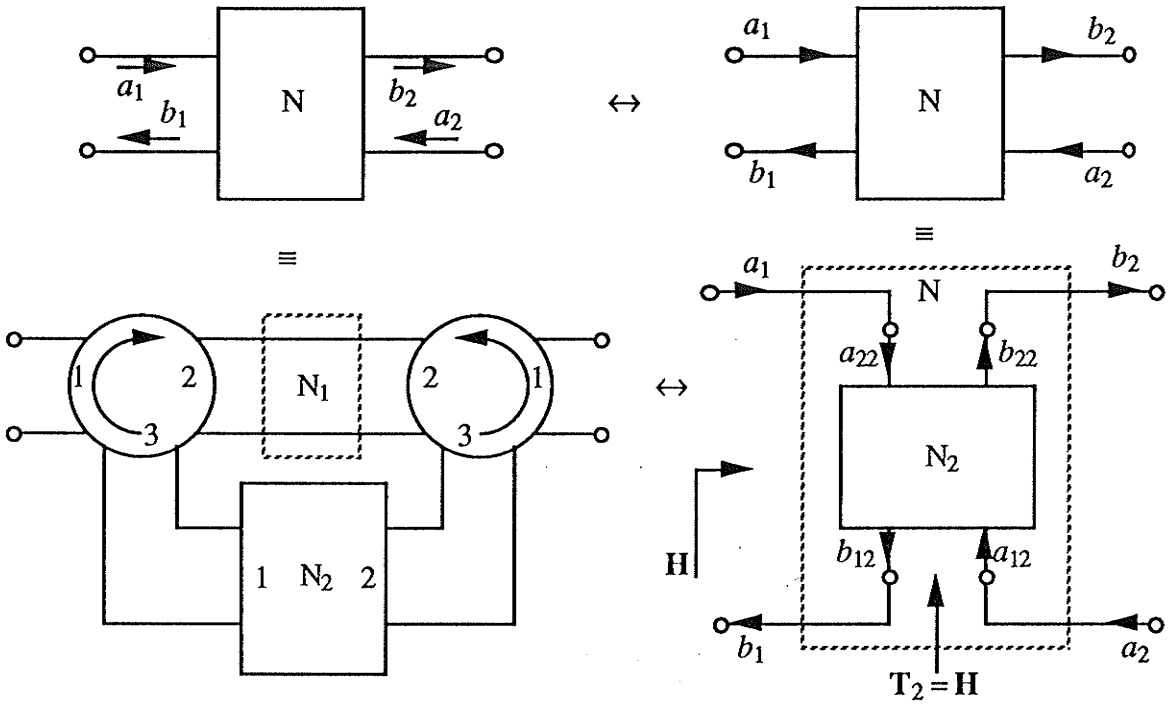

Fig. 3.12 A network equivalence that allows the problem of factoring the hybrid matrix **H** to be equivalent to factoring the transfer matrix of a related two-port network.

The 3-port analog circulators in Fig. 3.12 are defined by $b_2 = a_1$, $b_3 = a_2$, $b_1 = a_3$. The transfer matrix that corresponds to $\mathbf{S}_1$ is a unity, i.e., it characterizes a direct connection of two ports, as shown by N_1 in Fig. 3.12. The above equivalence was used in generating the various normalized 2-port adaptor equivalences in Fig. 3.5.

Although the network equivalence in Fig. 3.12 is of limited use in the analog domain, it has great practical utility in the WD domain. From the point of view of network synthesis, the main feature of the above equivalence is the fact that $f_2 = -\sigma h_*$, i.e., the transmission zeros of N_2 (zeros of f_2) are the zeros of $-\sigma h_*$. At the outset, however, one can always induce a desired factor in $-\sigma h_*$ by absorbing an appropriate normalized 2-port adaptor (ideal transformer). For the 2nd-order cases in Tables 3.7 and 3.9, the primitive h polynomials, and consequently $-\sigma h_*$ as well, have two real factors; and for the port 2 reflection-free case, one of the factors becomes $\psi - 1 \leftrightarrow z^{-1}$. These factors now become the transmission zeros of N_2, and it follows that N_2 can be realized as a cascade connection of two 1st-order

nonreciprocal sections, with the section realizing $\psi - 1 \leftrightarrow z^{-1}$ being a special case (see Table 3.8) of section **1E**. Therefore, the problem of deriving WD circuits for 2nd-order sections reduces to deriving WD circuits for 1st-order nonreciprocal sections – a problem whose solution is known.

The procedure of equating $\mathbf{T}_2 = \mathbf{H}$ can also be applied in generating WD circuits for 1st-order sections in Tables 3.1-3.4 and 3.8. These are now built-up from a zeroth-order section (2-port adaptor) and the simplest 1st-order section shown in Fig. 2.3. In general, the problem of generating higher-order canonic sections reduces, via the network equivalence in Fig. 3.12, to a lower order problem. In fact, entire filters can be designed by using the following iteration: induce a reflection-free factor ($\psi - 1 \leftrightarrow z^{-1}$) in h_*; apply Fig. 3.12; extract a special case of the 1st-order nonreciprocal section; repeat [15],[17]. The resulting structures, however, do not have a cascade topology.

For the general 2nd-order section with a reflection-free port 2, we have $f_2 = -\sigma h_* = cz^{-1}(z^{-1} + \varphi_1)$. A cascade two-port network with a corresponding f polynomial is shown in Fig. 3.13.

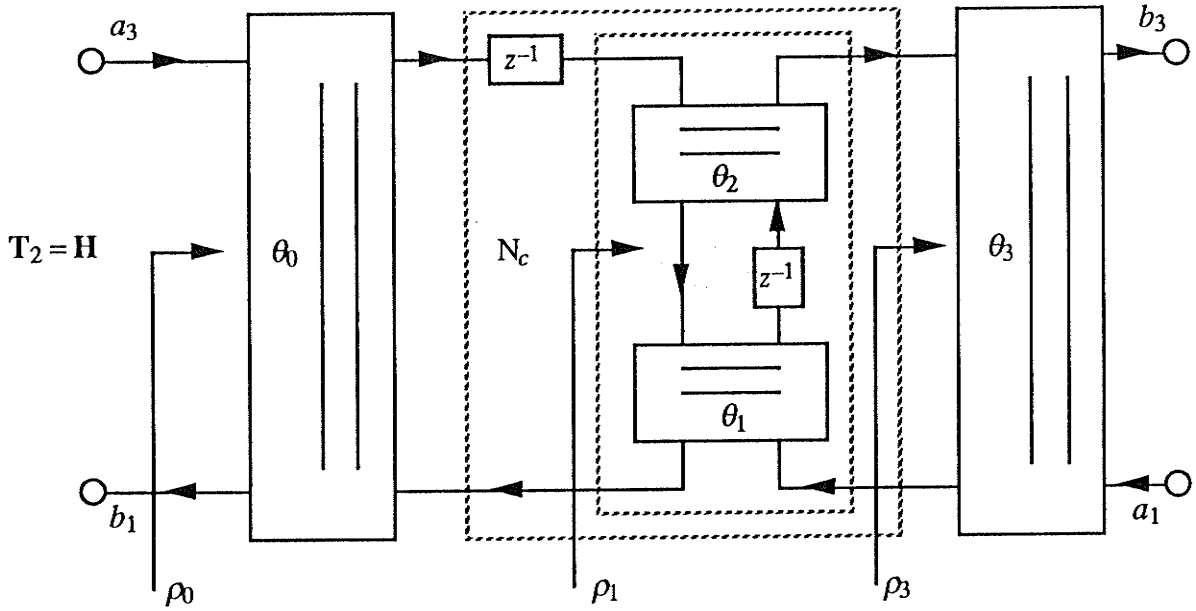

Fig. 3.13 A matched 4-port adaptor that realizes the required $f_2 = -\sigma h_* = cz^{-1}(z^{-1} + \varphi_1)$.

Note that the circuit in Fig. 3.13 is a matched 4-port adaptor with a coupling network N_c (see Fig. 3.11) that realizes both 1st-order factors of f_2. The transfer matrix $\mathbf{T}_2$ is given by

$$\mathbf{T}_2 = \mathbf{T}_{\theta_0} \frac{\begin{bmatrix} z^{-1} & 0 \\ 0 & 1 \end{bmatrix} \begin{bmatrix} -(z^{-1}+\cos\theta_1\cos\theta_2) & \sin\theta_1\sin\theta_2 \\ -z^{-1}\sin\theta_1\sin\theta_2 & \cos\theta_1\cos\theta_2 z^{-1}+1 \end{bmatrix}}{z^{-1}} \mathbf{T}_{\theta_3} \qquad (3.44)$$
$$\cos\theta_1 z^{-1} + \cos\theta_2$$

where the transfer matrices for the 1st-order nonreciprocal sections are obtained from Table 3.8 and $\mathbf{T}_{\theta_i}$ from (2.14a). The set of canonic polynomials is obtained from $\mathbf{T}_2 = \mathbf{H}$, i.e.,

$$\begin{aligned} f &= -(\cos\theta_0)z^{-2} + \frac{(a-b)}{2}z^{-1} + \cos\theta_3 \qquad & \sigma &= 1 \\ g &= -(\cos\theta_0)(\cos\theta_3)z^{-2} + \frac{(a+b)}{2}z^{-1} + 1 \qquad & a &= (1-\cos\theta_0)(1+\cos\theta_3)\cos(\theta_1-\theta_2) \\ h &= -(\sin\theta_0)(\sin\theta_3)(z^{-1}\cos\theta_2 + \cos\theta_1) \qquad & b &= (1+\cos\theta_0)(1-\cos\theta_3)\cos(\theta_1+\theta_2) \end{aligned} \tag{3.45}$$

By *Lemma* 2.2, the reflectance value ρ_0 of the 1st section in Fig. 3.13 can be obtained by evaluating the overall reflectance $\frac{h_2}{g_2} = \frac{\sigma f_*}{g}$ at the transmission zero of the 1st section, which is located at $z^{-1} = 0$. The canonic polynomial set $\{\sigma, f, g, h\}$, with port 2 reflection-free, can be obtained by combining the primitive set $\{\sigma_0, f_0, g_0, h_0\}$ from Table 3.7 or 3.9 with a normalized 2-port adaptor obtained from (3.18b), i.e.,

$$\sigma = 1 \quad , \quad f = \sin\gamma_2 f_0 \quad , \quad g = g_0 - \cos\gamma_2 \sigma h_{0*} \quad , \quad h = h_0 - \cos\gamma_2 \sigma g_{0*} \tag{3.46a}$$

where
$$\cos\gamma_2 = \frac{\sigma h_{0*}}{g_0}(0) \tag{3.46b}$$

Substituting (3.46) into the overall reflectance at $z^{-1} = 0$ yields

$$\rho_0 = \frac{h_2}{g_2}(0) = \frac{\sigma f_*}{g}(0) = \frac{\sin\gamma_2 f_{0*}(0)}{g_0(0) - \cos\gamma_2 \sigma h_{0*}(0)} = \frac{f_{0*}(0)}{\sin\gamma_2 g_0(0)} \tag{3.47}$$

From the special case ($\cos\theta_2 = 0$) in Table 3.8 we have

$$\cos\theta_0 = -\rho_0 \tag{3.48}$$

Comparing f from (3.45) with the forms given in (3.38) yields

$$\cos\theta_3 = -k^2\cos\theta_0 = k^2\rho_0 \quad \text{and} \quad \cos\theta_3 = -\cos\theta_0 = \rho_0 \tag{3.49a,b}$$

for the nonreciprocal and reciprocal cases, respectively. Finally, the middle section in Fig. 3.13 is characterized by $\rho_1 = \frac{\sin\theta_1}{\sin\theta_2}$ and $\varphi_1 = \frac{\cos\theta_2}{\cos\theta_1}$ where $f_2(-\varphi_1) = h_*(-\varphi_1) = 0$. To obtain ρ_1, consider the circuit in Fig. 3.14, which was obtained from Fig. 3.13 by letting $z^{-1} = -\varphi_1$ and using the decoupling property of lossless two-ports when evaluated at their transmission zeros. It follows from Fig. 3.14 and the transfer matrix of the normalized 2-port adaptor from (2.14a) that

$$\rho_1 = \frac{\frac{h_2}{g_2}(-\varphi_1) - \rho_0}{-\varphi_1\left(1 - \rho_0 \frac{h_2}{g_2}(-\varphi_1)\right)} \qquad \text{where} \quad \frac{h_2}{g_2}(-\varphi_1) = \frac{f_{0*}(-\varphi_1)}{(\sin\gamma_2)\, g_0(-\varphi_1)} \tag{3.50}$$

The result in (3.50) holds for both reciprocal and nonreciprocal cases.

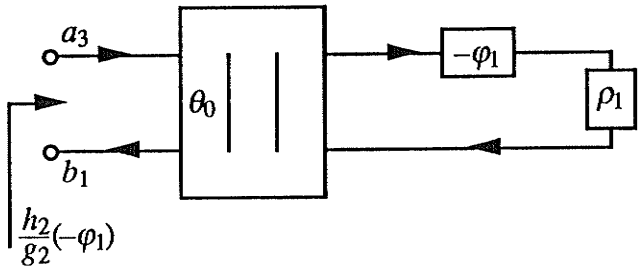

Fig. 3.14 Circuit derived from Fig. 3.13 by letting $z^{-1} = -\varphi_1$.

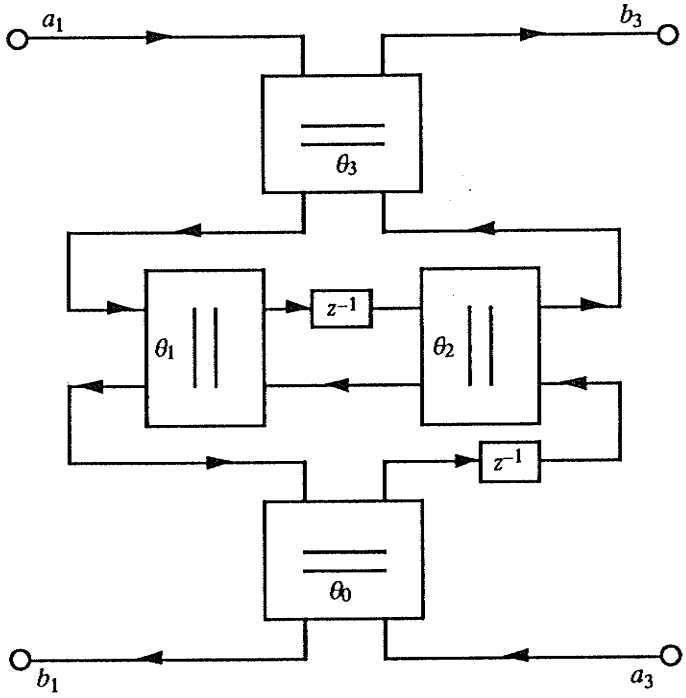

$$f = -(\cos\theta_0)z^{-2} + \frac{(a-b)}{2}z^{-1} + \cos\theta_3 \qquad \sigma = 1$$

$$g = -(\cos\theta_0)(\cos\theta_3)z^{-2} + \frac{(a+b)}{2}z^{-1} + 1 \qquad a = (1-\cos\theta_0)(1+\cos\theta_3)\cos(\theta_1 - \theta_2)$$

$$h = -(\sin\theta_0)(\sin\theta_3)(z^{-1}\cos\theta_2 + \cos\theta_1) \qquad b = (1+\cos\theta_0)(1-\cos\theta_3)\cos(\theta_1 + \theta_2)$$

Fig. 3.15 WD circuit of a general 2nd-order section with port 2 reflection-free. For a reciprocal realization set $\theta_0 = \pi - \theta_3$.

Given the primitive polynomials from Table 3.7 and 3.9, the circuit in Fig. 3.13 is now fully specified. We have redrawn it in Fig. 3.15 with the input and output ports in standard locations. By applying Fig. 3.6 to Fig. 3.15, an equivalent circuit is derived, as shown in Fig. 3.16. This circuit has appeared elsewhere in an unnormalized form and without the solutions for the multipliers of the 2-port adaptors in terms of the known input parameters [11, p.307]. The conlusions reached in Section 3.1 regarding the equivalence between Fig. 3.4b and 3.6 apply here as well.

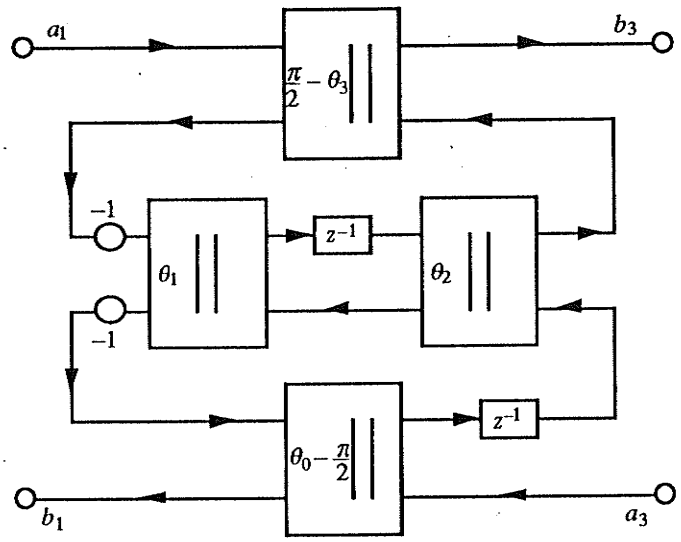

Fig 3.16 A WD circuit equivalent to Fig. 3.15.

The solutions for θ_i in terms of the minimal characterization for the three different cases (two reciprocal and one nonreciprocal) of a 2nd-order section are given in Table 3.10. These were obtained from eqs. (3.46)-(3.50) and the primitive polynomials in Tables 3.7 and 3.9. The section designated by **2C** realizes a pair of inverse real zeros and is therefore equivalent to a cascade of two 1st-order nonreciprocal (**1E**) sections. The corresponding situation in the analog domain is shown in Table 3.11, where the 2nd-order section is referred to as the C-section [2]. In the WD domain, a realization of the C-section using the circuit in Fig. 3.15 is preferable to the cascade of two 1E sections because, for the latter, quantization of the four multipliers to binary fractions cannot always be achieved such that $\varphi = \frac{\cos\theta_2}{\cos\theta_1} = \frac{\cos\theta_3}{\cos\theta_4}$ is satisfied exactly, and the resulting cascade becomes nonreciprocal. Reciprocity, however, can be approached with greater ease using the circuit in Fig. 3.15.

The circuit in Fig. 3.15 is truly general in a sense that, for appropriately chosen θ_i, it can be made equivalent to all the WD circuits in Tables 3.1-3.9. The required θ_i are given in Table 3.12. The fact that one circuit realizes all is of interest from the VLSI implementation point of view.

Table 3.10 Solutions for three types of a 2nd-order section.
(The sign of cos θ_1 is set equal to –sgn (θ_{1D})).

section	2C	2D	2E
f	$(\varphi z^{-1} - 1)(z^{-1} - \varphi)$	$z^{-2} - 2(\cos\omega_o T)z^{-1} + 1$	$z^{-2} - 2k(\cos\omega_o T)z^{-1} + k^2$
ρ	$\rho(\varphi) := \rho$	$\rho(e^{-j\omega_0 T}) = e^{j\alpha}$	$\rho(ke^{-j\omega_0 T}) = \beta e^{j\alpha}$
δ	$\varphi[\ln\rho]'$	$e^{-j\omega_0 T}[\ln\rho]'$	
$\varphi_1 = \frac{\varphi_{1N}}{\varphi_{1D}}$	$\frac{\frac{2\varphi\cos\gamma_2}{1+\varphi^2} - \cos\gamma}{\frac{2\varphi\cos\gamma}{1+\varphi^2} - \cos\gamma_2}$	$\frac{-\cos\gamma - \cos(\alpha - \omega_0 T)}{\cos\alpha + \cos\gamma\cos(\omega_0 T)}$	$\frac{\cos\gamma - \frac{2k\cos(\omega_0 T)\cos\gamma_2}{1+k^2}}{\cos\gamma_2 - \frac{2k\cos(\omega_0 T)\cos\gamma}{1+k^2}}$
$\cos\gamma$	$\frac{\rho(1-\varphi^2)\delta}{(\rho^2-1)\varphi}$	$\frac{\sin\alpha}{\delta\sin\omega_0 T}$	$\frac{\beta(1-k^2)\sin\alpha}{k(1-\beta^2)\sin\omega_0 T}$
$\cos\gamma_2$	$\frac{\rho(1-\varphi^2)(\delta+1)}{\varphi^2\rho^2-1}$	$\frac{\sin(\alpha-\omega_0 T)}{(\delta+1)\sin\omega_0 T}$	$\frac{\beta(1-k^2)\sin(\alpha-\omega_0 T)}{(1-k^2\beta^2)\sin\omega_0 T}$
ρ_0	$\frac{-\delta\tan\gamma}{(\delta+1)\tan\gamma_2}$	$\frac{\delta\sin\gamma}{(\delta+1)\sin\gamma_2}$	$\frac{(1-\beta^2)\sin\gamma}{(1-k^2\beta^2)\sin\gamma_2}$
ρ_1	$\frac{\sin\gamma_2}{\sin\gamma}$	$-\frac{\tan\gamma_2}{\tan\gamma}$	$-\frac{\tan\gamma_2}{\tan\gamma}$
$\cos\theta_0$ $\sin\theta_0$	$-\rho_0 \quad , \quad \sqrt{1-\rho_0^2}$	$-\rho_0 \quad , \quad \sqrt{1-\rho_0^2}$	$-\rho_0 \quad , \quad \sqrt{1-\rho_0^2}$
$\cos\theta_1$ $\sin\theta_1$	$\pm\sqrt{\frac{1-\rho_1^2}{1-\rho_1^2\varphi_1^2}} \quad \rho_1\sin\theta_2$	$\pm\sqrt{\frac{1-\rho_1^2}{1-\rho_1^2\varphi_1^2}} \quad \rho_1\sin\theta_2$	$\pm\sqrt{\frac{1-\rho_1^2}{1-\rho_1^2\varphi_1^2}} \quad \rho_1\sin\theta_2$
$\cos\theta_2$ $\sin\theta_2$	$\varphi_1\cos\theta_1 \quad \sqrt{\frac{1-\varphi_1^2}{1-\rho_1^2\varphi_1^2}}$	$\varphi_1\cos\theta_1 \quad \sqrt{\frac{1-\varphi_1^2}{1-\rho_1^2\varphi_1^2}}$	$\varphi_1\cos\theta_1 \quad \sqrt{\frac{1-\varphi_1^2}{1-\rho_1^2\varphi_1^2}}$
$\cos\theta_3$ $\sin\theta_3$	$\rho_0 \quad , \quad \sqrt{1-\rho_0^2}$	$\rho_0 \quad , \quad \sqrt{1-\rho_0^2}$	$k^2\rho_0 \quad , \quad \sqrt{1-k^4\rho_0^2}$

Table 3.11 2nd-order reciprocal C-section

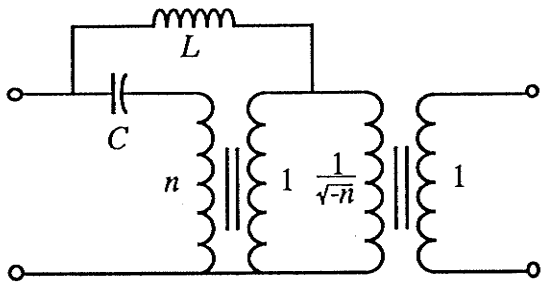

$$f = -(\sin\gamma)(\psi^2 - r^2) \qquad \sigma = 1$$

$$g = \psi^2 + \frac{2r(1+\rho^2)}{1-\rho^2}\psi + r^2 = (\psi+\psi_0)(\psi+\psi_1)$$

$$h = (\cos\gamma)(\psi^2 - \frac{2}{d}\psi - r^2)$$

$$\psi_0 = r\frac{1+\rho}{1-\rho} \qquad \psi_1 = r\frac{1-\rho}{1+\rho} \qquad n = -\cot^2\frac{\gamma}{2} \qquad L = \frac{2\psi_o}{r^2(1+\cos\gamma)} \qquad C = \frac{1-\cos\gamma}{2\psi_o}$$

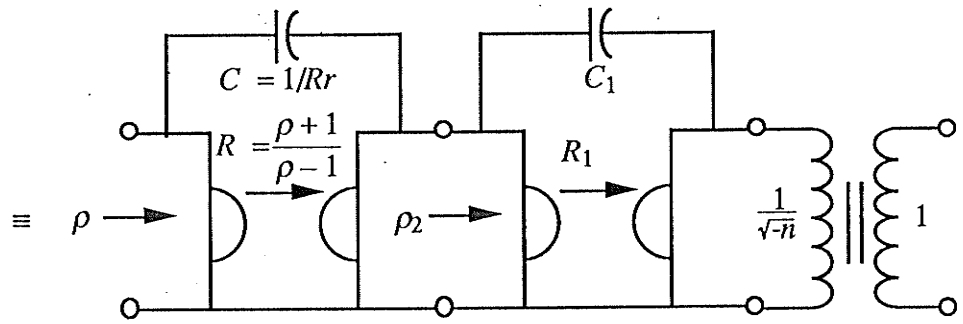

$$-1 < \cos\gamma = \frac{2r\rho d}{\rho^2 - 1} < 1 \qquad \frac{h}{g}(r) = \rho\,, \quad r \gtrless 0 \Leftrightarrow \rho^2 \lessgtr 1 \qquad \rho_2 = \frac{1+\rho\cos\gamma}{\cos\gamma+\rho}$$

$$f = -(\sin\gamma)(z^{-2} - (\varphi + 1/\varphi)z^{-1} + 1) \qquad \frac{h}{g}(\varphi) = \rho \qquad |\varphi| \gtrless 1 \Leftrightarrow \rho^2 \gtrless 1$$

$$g = \left[\frac{\varphi - \rho^2/\varphi}{1-\rho^2}\right] z^{-2} - 2z^{-1} + \frac{1/\varphi - \rho^2\varphi}{1-\rho^2} \qquad -1 < \cos\gamma = \frac{\rho(1-\varphi^2)\,\delta}{(\rho^2-1)\,\varphi} < 1$$

$$h = (\cos\gamma)((1+1/\delta)z^{-2} - (\varphi + 1/\varphi)z^{-1} + 1 - 1/\delta) \qquad \delta = \frac{2\varphi d}{(1+\varphi)^2} \qquad \varphi = \frac{1-r}{1+r}$$

Table 3.12 Values of θ_i that reduce Fig. 3.15 to those in Tables 3.1-3.9.

section	1A	1B	1C	1D	2A	2B	2D $\alpha = \omega_0 T + \pi$	1E	2E $\alpha = \omega_0 T$
θ_0	$\pi - \theta$	$\pi - \theta$	$\pi - \theta$	$\pi - \theta$	$\pi - \theta$	$\pi - \theta$	$\pi - \theta$	θ_1	θ_1
θ_1	π	0	π	0	π	0	$\omega_0 T$	π	$\cos^{-1}\frac{2k\cos\omega_0 T}{1+k^2}$
θ_2	π	0	0	π	$\omega_0 T$	$\pi - \omega_0 T$	π	0	π
θ_3	θ	θ	θ	θ	θ	θ	θ	θ_2	θ_2

3.5 Analysis of Fig. 3.15 with Quantized Multipliers

As discussed in Section 2.2, two independent quantizations of $\alpha \cong \cos\theta$ and $\beta \cong \sin\theta$ are required for each normalized 2-port adaptor to ensure realizability. Since $\alpha^2 + \beta^2 = 1$ cannot be satisfied with binary fractions, it follows that losslessness cannot be achieved for quantized normalized 2-port adaptors. Consequently, WD circuits comprised of them can only be made passive, which means that nominally reciprocal sections no longer have transmission zeros on the unit circle. Losslessness, however, is important because it leads to lower sensitivity of the filter response to parameter variations. It is well known that at a frequency for which the filter is exactly lossless, the derivative (1st-order sensitivity) of the response with respect to any parameter must be zero because the filter transfer function (scattering parameter) is passive and, therefore, it must decrease in amplitude as any of the parameters – including the frequency variable – change from the value at which exact losslessness was achieved [11],[43]. This argument does not hold for strictly passive transfer functions.

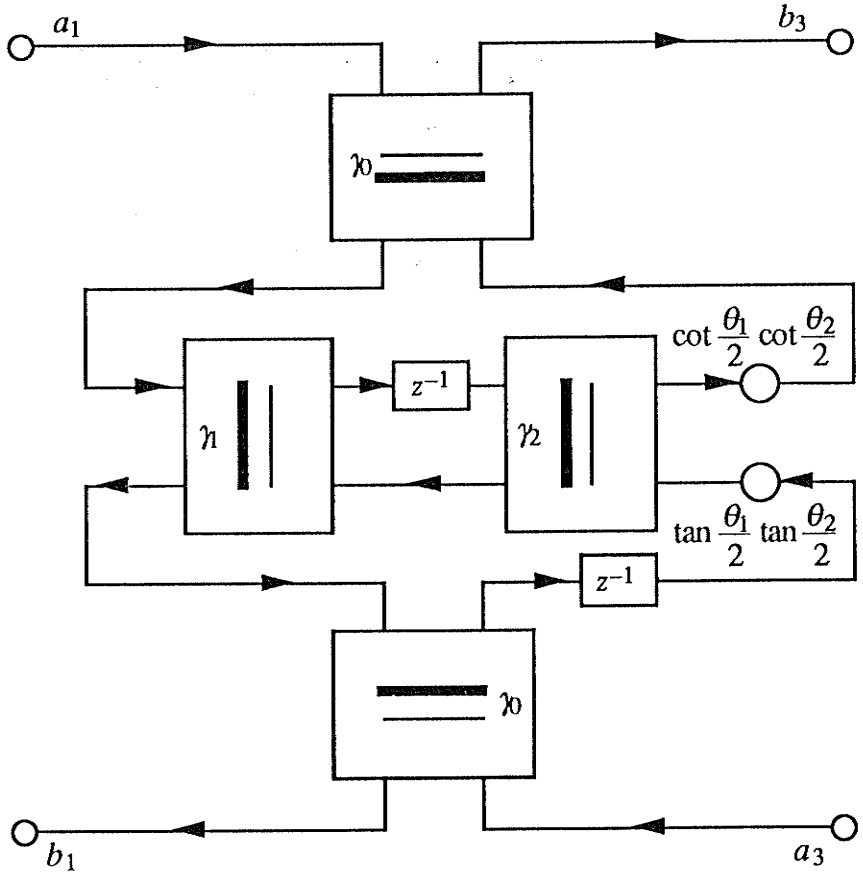

Fig. 3.17 Voltage wave equivalent circuit of Fig. 3.15

The amount by which the transmission zeros move off the unit circle depends on the number of sources of passivity that the sections realizing those transmission zeros possess. In Fig. 3.15 we have four sources of passivity. This number can be reduced substantially by converting each normalized 2-port adaptor to its voltage wave equivalent by using Fig. 2.7a, followed by shifting the resulting pairs of inverse multipliers out of the structure. Applying this process to Fig. 3.15 yields, for the reciprocal case, a WD circuit shown in Fig. 3.17. Note that not all inverse pairs of multipliers can be shifted out of the structure. The pairs associated with $\theta_0 = \pi - \theta_3$ and θ_3 cancel each other out, which is one of the reasons for choosing the structure in Fig. 3.15. The pairs associated with θ_1 and θ_2 can be grouped together at one location, as shown in Fig. 3.17. This pair is given by

$$\cot\frac{\theta_1}{2}\cot\frac{\theta_2}{2} = \pm\sqrt{\frac{(1+\gamma_1)(1+\gamma_2)}{(1-\gamma_1)(1-\gamma_2)}} \cong \frac{m}{2^x} \quad , \quad \tan\frac{\theta_1}{2}\tan\frac{\theta_2}{2} = \pm\sqrt{\frac{(1-\gamma_1)(1-\gamma_2)}{(1+\gamma_1)(1+\gamma_2)}} \cong \frac{k}{2^x} \tag{3.51}$$

and, in general, must be quantized independently. For convenience, we have assumed the same exponent x for both multipliers. In practice, the sign of γ_1 is chosen such that the magnitude of the multipliers in (3.51) is as close to one as possible. This is accomplished by correctly labeling port 1 (by placing the heavy bar on the corresponding side) of the corresponding 2-port adaptor in Fig. 3.17.

The extra quantization must be performed in a passive way so that the overall section remains passive and, consequently, the suppression schemes for nonlinear oscillations can be applied. The passivity condition for the pair of quantized multipliers can be derived by examining the circuit in Fig. 3.18.

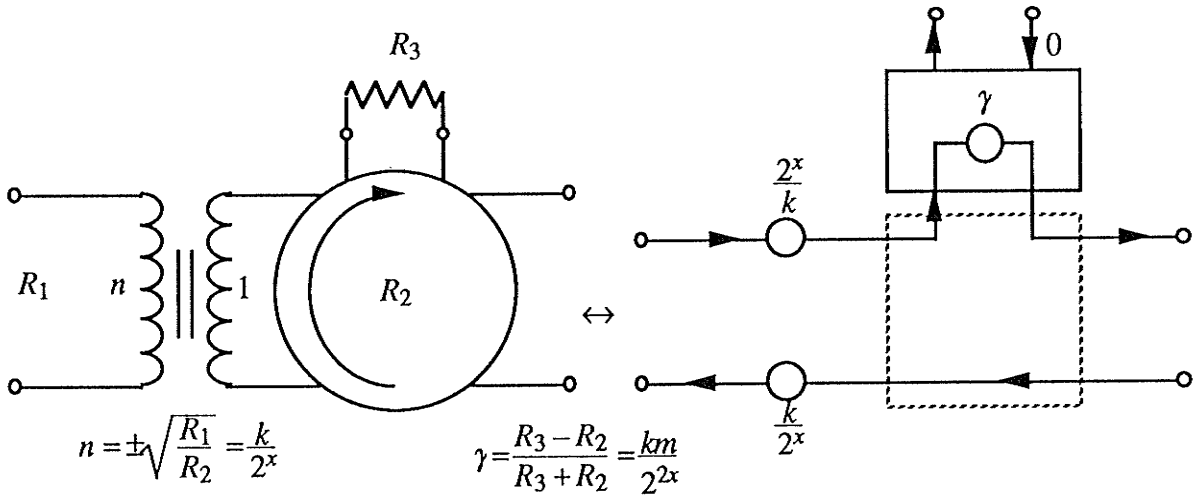

Fig. 3.18 Passive quantization of a pair of multipliers $\frac{k}{2^x}$ and $\frac{m}{2^x}$.

The pair of inverse multipliers in Fig. 3.18 corresponds to a voltage wave ideal transformer, which is known to be lossless. For a passive realization we must have $R_3 > 0$, which implies that

$$|\gamma| < 1 \quad \Leftrightarrow \quad |km| < 2^{2x} \tag{3.52}$$

Expression (3.52) is the required condition. Note that if R_3 in Fig. 3.18 corresponds to an open- or a short-circuit, then $|\gamma| = 1 \quad \Leftrightarrow \quad |km| = 2^{2x}$, which can only be satisfied nontrivially if $k = \pm 1$ and $m = \pm 2^{2x}$, or vice versa. This is the only case for which the section in Fig. 3.17 remains ideally lossless.

The f polynomial corresponding to Fig. 3.17 with the quantizations from (3.51) is given by

$$f = z^2 + z\left(\gamma_1\gamma_2\left(1 + \frac{km}{2^{2x}}\right) + \frac{m\,(1-\gamma_1)(1-\gamma_2)}{2^x\gamma_0} + \frac{k\gamma_0\,(1+\gamma_1)(1+\gamma_2)}{2^x}\right) + \frac{km}{2^{2x}} \tag{3.53}$$

Clearly, the transmission zeros have moved off the unit circle. The movement is minimized if the integer k or m with the lower absolute value is obtained first, and the other is chosen such that the product km is as close to 2^{2x} as possible without violating (3.52).

For the quantized power wave structure in Fig. 3.15, the constant term for the monic f polynomial is given by

$$F_0 = \left(\alpha_0^2 + \beta_0^2\right)\left(\alpha_1^2 + \beta_1^2\right)\left(\alpha_2^2 + \beta_2^2\right) \tag{3.54}$$

To ensure passivity, each factor in (3.54) must be less than one, thereby making the shift away from the unit circle much greater than in (3.53). In Section V, a design example is presented with both types of adaptors which clearly illustrates the relative advantage of using voltage wave over power wave adaptors.

3.6 Quasi-Lattice Termination of the Matched 4-Port Adaptor

In Sections 3.2 and 3.3, we examined the possibility of realizing elementary sections using the matched 4-port adaptor with ports 2 and 4 terminated in allpass sections. In this section, we investigate an alternative termination possibility; namely, ports 3 and 4 are terminated in allpass sections, i.e.,

$$a_3 = S_3 b_3 \qquad \text{and} \qquad a_4 = S_4 b_4 \ . \tag{3.55}$$

The resulting structures for both domains, obtained from Fig. 3.1, Fig. 3.4b and the port references from (3.3), are shown in Fig. 3.19.

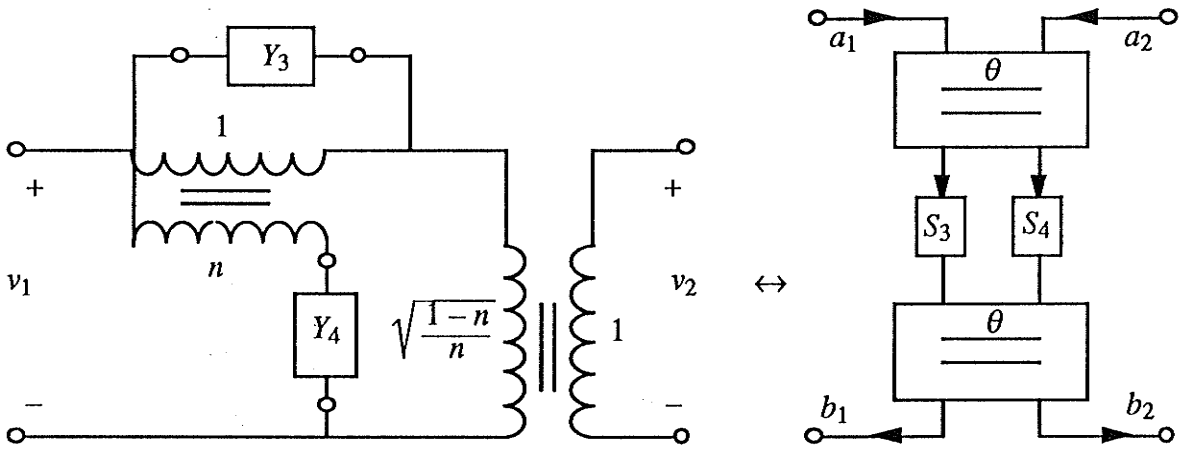

$$S_3 = \frac{n - Y_3}{n + Y_3} \qquad S_4 = \frac{1 - (1-n)Y_3}{1 + (1-n)Y_3} \qquad \cos\theta = \sqrt{n} \qquad \sin\theta = \sqrt{1-n}$$

Fig. 3.19 Matched 4-port adaptor with ports 3 and 4 terminated in allpass sections.

Again, the WD circuit in Fig. 3.19 illustrates that a particular two-port characterization factors in a natural way, i.e.,

$$\begin{aligned}\begin{bmatrix} b_1 \\ b_2 \end{bmatrix} &= \begin{bmatrix} -\sqrt{n} & \sqrt{1-n} \\ \sqrt{1-n} & \sqrt{n} \end{bmatrix} \begin{bmatrix} S_3 & 0 \\ 0 & S_4 \end{bmatrix} \begin{bmatrix} -\sqrt{n} & \sqrt{1-n} \\ \sqrt{1-n} & \sqrt{n} \end{bmatrix} \begin{bmatrix} a_1 \\ a_2 \end{bmatrix} \\ &= \begin{bmatrix} nS_3 + (1-n)S_4 & -\sqrt{n(1-n)}\,(S_3 - S_4) \\ -\sqrt{n(1-n)}\,(S_3 - S_4) & nS_4 + (1-n)S_3 \end{bmatrix} \begin{bmatrix} a_1 \\ a_2 \end{bmatrix} = \mathbf{S} \begin{bmatrix} a_1 \\ a_2 \end{bmatrix}\end{aligned} \ . \tag{3.56}$$

The grouping of wave variables in (3.56) corresponds to the scattering matrix representation (see eq. (2.22a)). The corresponding transfer matrix obtained from (2.11b) is given by

$$\begin{bmatrix} b_1 \\ a_1 \end{bmatrix} = \frac{1}{\sqrt{n\,(1-n)}\,(S_3 - S_4)} \begin{bmatrix} S_3 S_4 & -nS_3 - (1-n)S_4 \\ nS_4 + (1-n)S_3 & -1 \end{bmatrix} \begin{bmatrix} a_2 \\ b_2 \end{bmatrix} = \mathbf{T} \begin{bmatrix} a_2 \\ b_2 \end{bmatrix} \quad . \tag{3.57}$$

It can be easily verified that eqs. (3.56), (3.57) correspond to a lossless two-port, i.e., $\mathbf{S}_* \mathbf{S} = \mathbf{I}$ where, for an allpass section S_i, we have $S_{i*} = 1/S_i$. It follows from Belevitch's representation (see (2.24)) that the corresponding reflectance and transmittance are given by

$$\rho := \frac{h}{g} = n\,S_3 + (1-n)S_4 \qquad , \qquad \frac{f}{g} = -\sqrt{n\,(1-n)}\,(S_3 - S_4) \quad . \tag{3.58a,b}$$

At a transmission zero, we have from (3.57) that

$$S_3 = S_4 \qquad \Rightarrow \qquad \rho = S_3 = S_4 \tag{3.59}$$

and

$$d = \left[\ln \frac{g}{h}\right]' = -n\,[\text{Arg}\ S_3]' - (1-n)\,[\text{Arg}\ S_4]' \tag{3.60}$$

where we have used the fact that at $\psi = j\phi \leftrightarrow z = e^{j\omega T}$, $|S_3| = |S_4| = 1$.

The main feature of the WD circuit in Fig. 3.19 is that it is structurally lossless, i.e., once all the normalized 2-port adaptors have been converted to voltage wave adaptors, the number of remaining multipliers that need to be quantized is minimal and, consequently, a one-to-one mapping to a lossless analog circuit always exists. On the other hand, the WD circuit in Fig. 3.19 can only be made reflection-free, say at port 2, if both S_3 and S_4 contain delays in series (factors of z^{-1}). This is because the set of all directed paths from a_2 to b_2 includes both allpass sections – in contrast to the paths between a_3 and b_3 in Fig. 3.8. Consequently, 1st-order sections, where either S_3 or S_4 has degree one, cannot be made reflection-free in a computable fashion, i.e., it is possible to induce the reflection-free property numerically through cancellations, but the resulting circuit still lacks the required delay in series for every directed path between a_2 and b_2. For sections of degree 2 and higher, imposing the reflection-free property would mean inducing a factor of z^{-1} in both the f and h polynomials (see (3.58)), which compromises the ability of choosing desired transmission zeros and is therefore unacceptable. We conclude that the circuit in Fig. 3.19 cannot simultaneously satisfy the requirements of the reflection-free property and an independent selection of transmission zeros.

Forgoing the reflection-free property, the WD circuit in Fig. 3.19 can realize all 1st-order reciprocal sections by letting $S_4 = \pm 1$ and selecting S_3 from Figs. 3.9a and b. For example, letting

$$S_4 = 1 \qquad \text{and} \qquad S_3 = \frac{z^{-1} - \gamma_3}{1 - \gamma_3\, z^{-1}} \tag{3.61a}$$

results in the following scattering coefficients obtained from (3.58):

$$\frac{f}{g} = \frac{\sqrt{n\,(1-n)}\,(1+\gamma_3)\,(z^{-1}-1)}{1-\gamma_3 z^{-1}} \quad \text{and} \quad \frac{h}{g} = \frac{z^{-1}(n-\gamma_3(1-n))+1-n-\gamma_3 n}{1-\gamma_3 z^{-1}} \tag{3.61b}$$

The degree of freedom provided by γ_3 is required for fixing the location of the pole (zero of g). It would appear that the degree of freedom provided by n could be used to induce a reflection-free port 2 by simply letting

(3.62)

$$n = \frac{\gamma_3}{1+\gamma_3} \;\Rightarrow\; f = \sqrt{\gamma_3}\,(z^{-1}-1) \;,\; g = 1-\gamma_3 z^{-1} \;,\; h = 1-\gamma_3 \;,\; h_* = (1-\gamma_3)z^{-1}$$

Comparing (3.62) to port 2 reflection-free polynomials in Table 3.3, it is clear that for $\gamma_3 = \frac{\delta}{1+\delta}$ the two circuits are equivalent, as shown in Fig. 3.20. However, the WD circuit in Fig. 3.20a has a structural reflection-free port, i.e., every path from a_3 to b_3 must pass through a delay; whereas the circuit in Fig. 3.20b creates a factor of z^{-1} in h_* numerically, not structurally. Consequently, the former circuit is preferable.

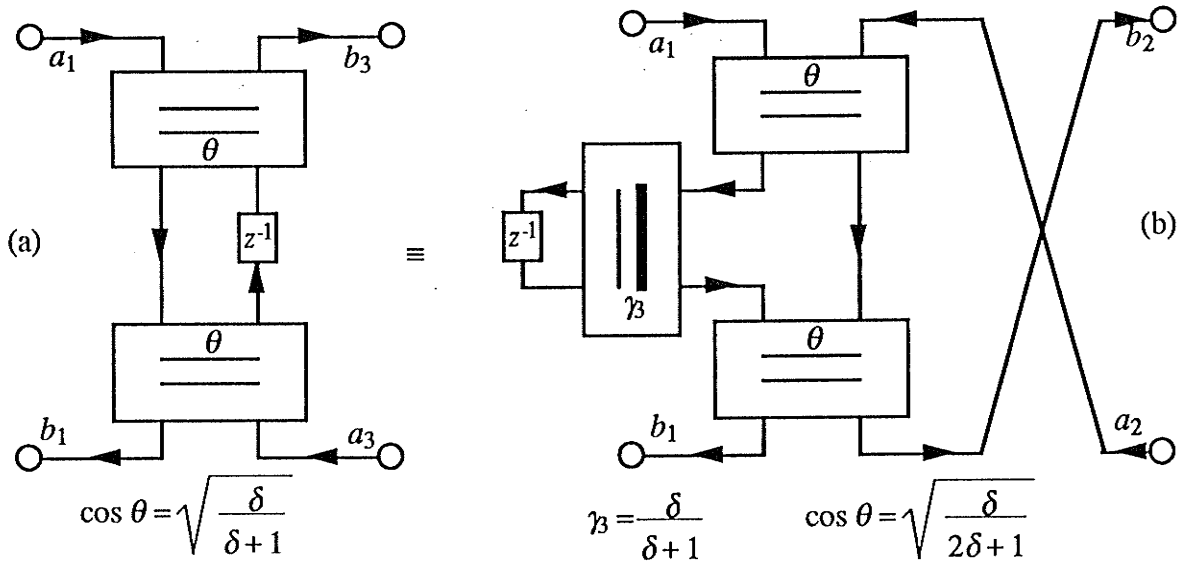

Fig. 3.20 (a) WD circuit from Table 3.3 and (b) its equivalent.

By making the remaining selections for S_3 and S_4, circuits that are equivalent to those in Tables 3.1, 3.2 and 3.4 can be derived. If S_3 is chosen to be a 2nd-degree allpass section from Fig. 2.11, equivalent circuits for Tables 3.5 and 3.6 can be derived. In all cases, however, the conclusions made with regards to Fig. 3.20 hold.

Another type of 2nd-order section that can be realized with the structure in Fig. 3.19 is obtained by letting

$$S_3 = \frac{\gamma_3 - z^{-1}}{1 - \gamma_3 z^{-1}} \leftrightarrow S_3 = \frac{\psi - \psi_3}{\psi + \psi_3} \quad , \quad S_4 = \frac{z^{-1} - \gamma_4}{1 - \gamma_4 z^{-1}} \leftrightarrow S_4 = \frac{-\psi + \psi_4}{\psi + \psi_4} \tag{3.63}$$

which are allpass sections obtained from Figs. 2.9a and b, respectively. Substituting (3.63) into (3.58) yields the following canonic polynomials:

$$\begin{aligned} f &= -2\sqrt{n\,(1-n)}\;(\psi^2 - \psi_3\psi_4) \qquad g = (\psi + \psi_3)\,(\psi + \psi_4) \\ h &= (2n-1)\,(\psi^2 - \frac{\psi_3 - \psi_4}{2n-1}\,\psi - \psi_3\psi_4) \end{aligned} \tag{3.64}$$

To ensure stable realization, the conditions $\psi_3 > 0$ and $\psi_4 > 0$ must hold, which means that a section described by (3.64) realizes a pair of transmission zeros on the real axis (see the f polynomial in (3.64)), i.e., a C-section from Table 3.11. An equivalence can be established between (3.64) and the primitive polynomials in Table 3.11 by setting

$$\psi_3 = r\frac{1-\rho}{1+\rho} \leftrightarrow \gamma_3 = \frac{\varphi + \rho}{1 + \rho\varphi} \quad , \quad \psi_4 = r\frac{1+\rho}{1-\rho} \leftrightarrow \gamma_3 = \frac{\varphi - \rho}{1 - \rho\varphi} \tag{3.65a}$$

and

$$\cos\,\theta = \sqrt{n} = \cos\frac{\gamma}{2} \tag{3.65b}$$

The solution given by (3.65) can be derived independently by solving (3.59) and (3.60). It follows that, as an alternative to the WD circuit in Fig. 3.15, section 2C without a reflection-free port can also be realized using the circuit shown in Table. 3.13. Note that the canonic polynomials for this case are the primitive polynomials from Table 3.11.

For $n = 1/2$, the scattering matrix in (3.56) reduces to

$$\mathbf{S} = \frac{1}{2}\begin{bmatrix} S_3 + S_4 & S_4 - S_3 \\ S_4 - S_3 & S_3 + S_4 \end{bmatrix} \tag{3.66}$$

which characterizes a symmetric lattice filter [11], which was shown in Fig. 2.12. It is common practice to set $n = 1/2$ when an entire filter is realized using the structure in Fig. 2.12. However, when the structure in Fig. 3.19 is used to realize a particular section, or a group of sections, which is part of a chain connection, the degree of freedom associated with n is fixed by the particular filter being implemented and, in general, is not equal to 1/2. For example, the turns-ratio for the 2nd-order section in Table 3.13 is not a free parameter. It is for this reason that we refer to the structure in Fig. 3.19 as quasi-lattice.

Table 3.13 Quasi-lattice realization of non reflection-free section **2C**

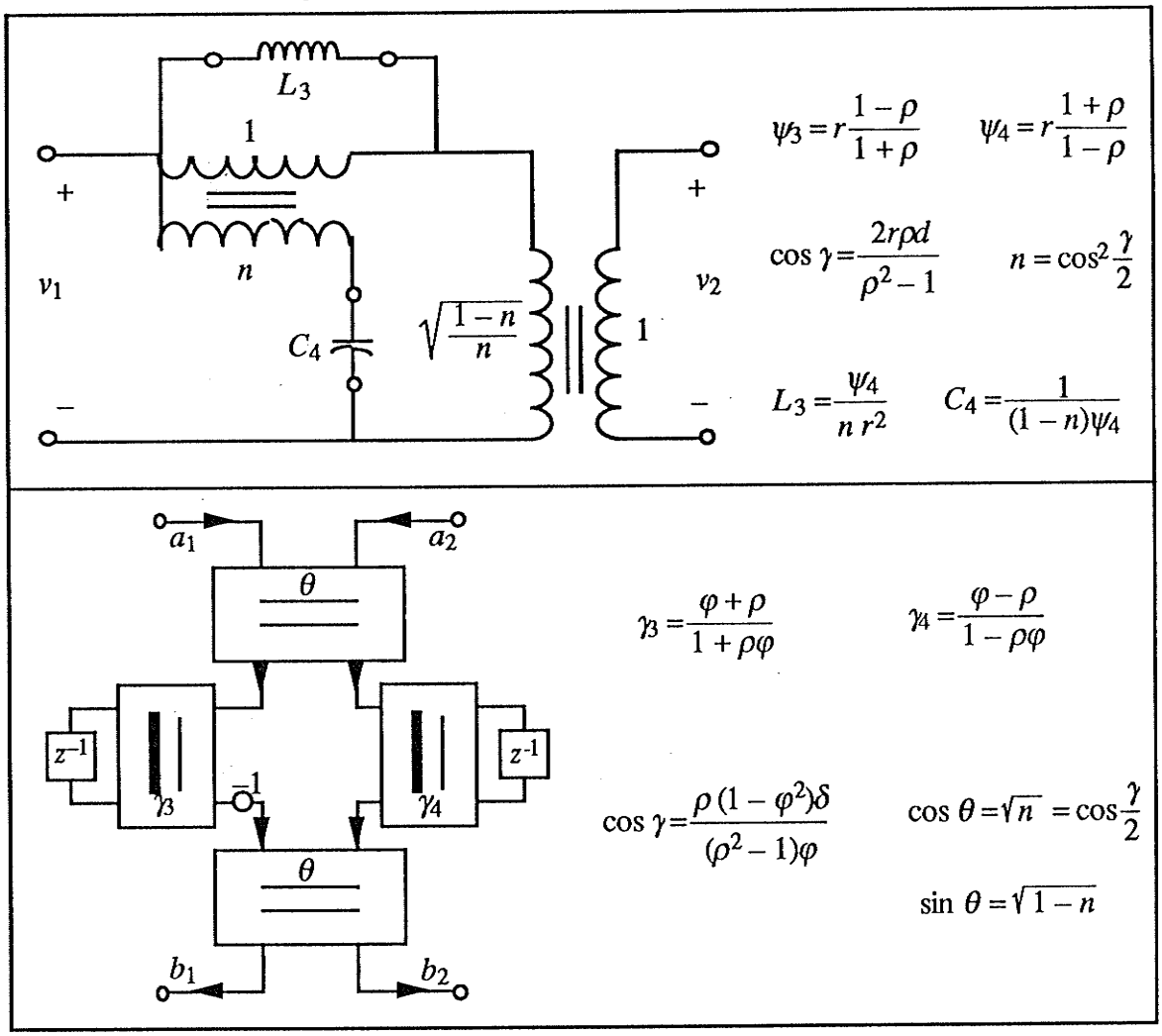

As mentioned in Section 2.3, in addition to structural losslessness, WD lattice filters are in many ways the most efficient WD structures available [11]. They can realize odd-order Butterworth, Chebychev and Cauer (elliptic) responses [2],[5] with only as many 2-port adaptors as the degree of the filter. They can also be used to realize a chain of elementary sections more efficiently. For example, consider a chain connection of two elementary sections shown in Fig 3.21a. By applying basic network equivalences [53], the circuit in Fig. 3.21a can be converted to its equivalent shown in Fig. 3.21b. A match can be established between Fig. 3.21b and Fig. 3.19 if the former circuit is cascaded with an ideal transformer with the turns-ratio given by

$$\sqrt{\frac{1-m}{m}} = \sqrt{\frac{(1-n)C_1}{C_2 - n\,(1-n)C_1}} \quad \leftrightarrow \quad \cos\theta = 2m-1 \tag{3.67}$$

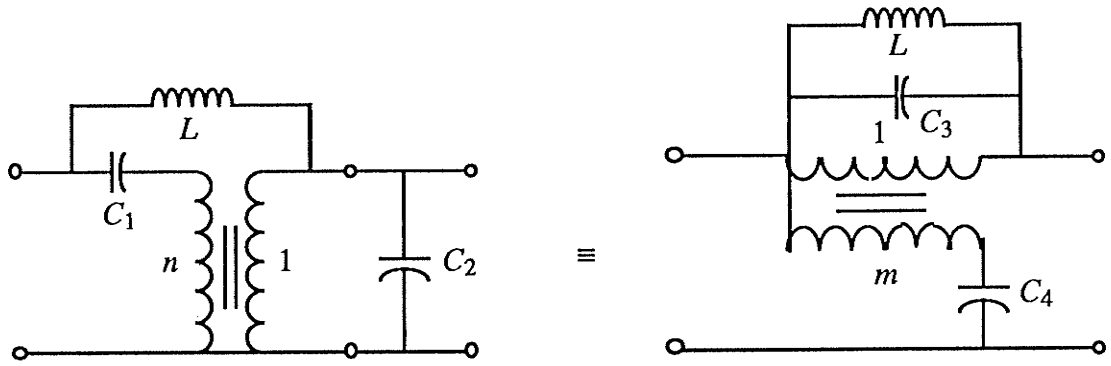

$$m = \frac{C_2 - n(1-n)C_1}{C_2 + (1-n)^2 C_1} \qquad C_3 = \frac{C_1 C_2}{C_2 + (1-n)^2 C_1} \qquad C_4 = C_2 + (1-n)^2 C_1$$

Fig. 3.21 (a) A cascade of two elementary sections and (b) an equivalent circuit that corresponds to the quasi-lattice structure in Fig. 3.19.

It follows that in the WD domain, a chain connection of non-reflection-free sections **2D** and **1B** and a 2-port adaptor defined by (3.67), can be replaced with a WD circuit in Fig. 3.19 with S_3 and S_4 from Figs. 2.11a and 2.9a, respectively. The resulting structure, as shown in Fig. 3.22, requires one fewer 2-port adaptor than the cascade realization and is structurally lossless. However, to ensure computability, it must be terminated on both sides by sections with reflection-free ports.

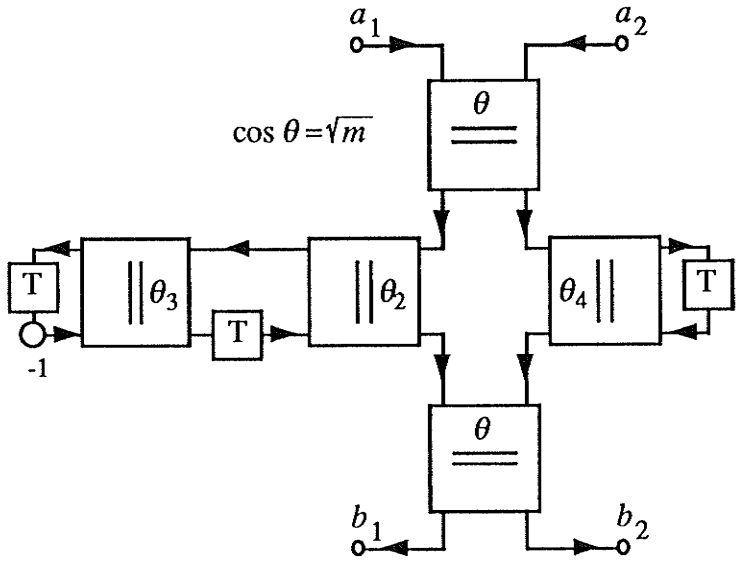

Fig. 3.22 Quasi-lattice WD circuit of a 3rd-order section.

IV. SYNTHESIS ALGORITHM

In this Chapter, we present a synthesis algorithm that, given a set of canonic polynomials $\{f, g, h\}$ with f given in factored form with a chosen order, provides sets of values $\{\psi_i, \rho_i, d_i\}$ in the ψ-domain or $\{z_i, \rho_i, \delta_i\}$ in the z-domain, with each set characterizing an elementary section whose chain connection realizes the given $\{f, g, h\}$. Having obtained these characterizations, it is then possible to derive the realization circuits. This step, however, is completely independent of the cascade decomposition process.

Two cases are examined: 1) all the transmission zeros are distinct and 2) at least two zeros share the same location. It is shown that the multiple-zero subset requires a slightly different characterization – referred to as the sample characterization – from the distinct zeros. Finally, several methods of extracting the last constant section (an ideal transformer $\leftrightarrow$ 2-port adaptor) are presented.

4.1 Cascade Synthesis of Lossless Two-Ports with Distinct Transmission Zeros

The class of filters with distinct transmission zeros includes transfer functions with optimum selectivity. Included in this class are Cauer (elliptic) responses which are known to have the optimum selectivity, and are therefore of great interest.

We are given three polynomials f, g, and h that satisfy $gg_* = hh_* + ff_*$ and the other Properties 1-7 from Section 2.4. For the distinct transmission zero case, the number of transmission zeros always equals $m = \deg g$, with one transmission zero possibly at infinity. The complex transmission zeros are grouped with their complex conjugates, which must always exist since f is real, to form real factors. The polynomial f is given in factored form

$$f = \prod_{i=1}^{L} f_i \tag{4.1}$$

and the order of the L real factors specifies the desired sequence of transmission zeros in the final realization. Common factors between g and h are allowed as long as $m = \deg g$ is determined with the common factors included.

The first two steps of the algorithm convert the input polynomials into a set of numbers which, in effect, forms a different but equivalent characterization of the lossless two-port network. The algorithm is presented for the ψ- and z-domains in tandem because the differences that do exist are minor.

Step 1. For the set of transmission zeros $\{\psi_i : f_i(\psi_i) = 0\} \leftrightarrow \{z_i^{-1} : f_i(z_i^{-1}) = 0\}$ compute the reflectance values

$$\rho_i \equiv \rho_i(\psi_i) = \frac{h}{g}(\psi_i) \qquad i = 1(1)L \tag{4.2}$$

For each transmission zero located at $\psi_i = j\,\phi_i \leftrightarrow z_i^{-1} = e^{-j\omega_i T}$ where $\phi_i = \tan\left(\frac{\omega_i T}{2}\right)$, it follows from Property 6 (p.25) that it is sufficient to retain the argument of ρ_i, i.e.

$$\rho_i = e^{j\alpha_i} \tag{4.3}$$

As will be shown shortly, the unimodularity of the reflectance cannot change during the decomposition process – a property important for numerical reasons.

For the z^{-1}-domain, we use (4.2) and (4.3) with ψ_i replaced with z_i^{-1}. Due to Properties 1-3 (p.11-12), the reflectance values for the two domains are the same.

Step 2. For each factor f_i that corresponds to a reciprocal section, i.e., $f_i = \sigma_i f_{i*}$, compute the value of the delay:

$$d_i \equiv d_i(\psi_i) = \frac{g'}{g}(\psi_i) - \frac{h'}{h}(\psi_i) \qquad \leftrightarrow \qquad d_i(z_i^{-1}) = \frac{g'}{g}(z_i^{-1}) - \frac{h'}{h}(z_i^{-1}) \tag{4.4a,b}$$

As was shown in Section 2.4 eqs. (2.35), (2.36), it is convenient in the z^{-1}-domain to multiply the $d_i(z_i^{-1})$ by $-z_i^{-1}$, i.e. we define

$$\delta_i \equiv -z_i^{-1}\, d_i(z_i^{-1}) \tag{4.5}$$

For $\psi_i = j\,\phi_i \leftrightarrow z_i^{-1} = e^{-j\omega_i T}$, we have from eq. (2.36) that

$$\delta_i = \frac{d_i}{2\cos^2\left(\frac{\omega_i T}{2}\right)} \tag{4.6}$$

As $\phi_i \to \infty$, $\omega_i T \to \pi$, and it can be shown that $\delta_i = \frac{d_i}{2}$. Again, the delay values for both domains are simply related.

Theorem 4.1: The set of values $\{\psi_i, \rho_i, d_i : i = 1(1)L\} \leftrightarrow \{z_i^{-1}, \rho_i, \delta_i : i = 1(1)L\}$ is sufficient to complete the cascade decomposition of a lossless two-port to within a constant section. Moreover, these values are sufficient for any chosen order of the transmission zeros.

Proof: First note that the $d_i \leftrightarrow \delta_i$ for nonreciprocal factors of f are not needed and are included above and below for ease of presentation.

From *Lemma* 2.2 we have that the reflectance and delay values for the first member of a

cascade are given by ρ_1 and $d_1\,(\delta_1)$. In Chapter III, it was shown that the set $\{\psi_1\,,\,\rho_1\,,\,d_1\}$ $\leftrightarrow \{z_1^{-1}\,,\,\rho_1\,,\,\delta_1\}$ forms a minimal characterization of every 1st and 2nd-order elementary section. From this set, one obtains via Tables 3.1-3.13 the canonic polynomial set $\{\sigma_1\,,f_1\,,\,g_1\,,\,h_1\}$. To add flexibility to the decomposition process, the set $\{\sigma_1\,,f_1\,,\,g_1\,,\,h_1\}$ is usually chosen to be the primitive set. We return to this point later. Note also that the choice of f_1, and hence the first section, is completely arbitrary, and is initially specified by the user.

The next two steps of the algorithm, which are developed here as part of the proof of *Theorem* 4.1, involve the recomputation of the remaining values $\{\psi_i\,,\,\rho_i\,,\,d_i : i = 2(1)L\} \leftrightarrow$ $\{z_i^{-1}\,,\,\rho_i\,,\,\delta_i : i = 2(1)L\}$ such that the new set characterizes a lossless two-port network with $f_b = \prod_{i=2}^{L} f_i$ and of degree $m - m_1$, where m_1 is the degree of section 1. The extraction and recomputation steps are depicted in Fig. 4.1.

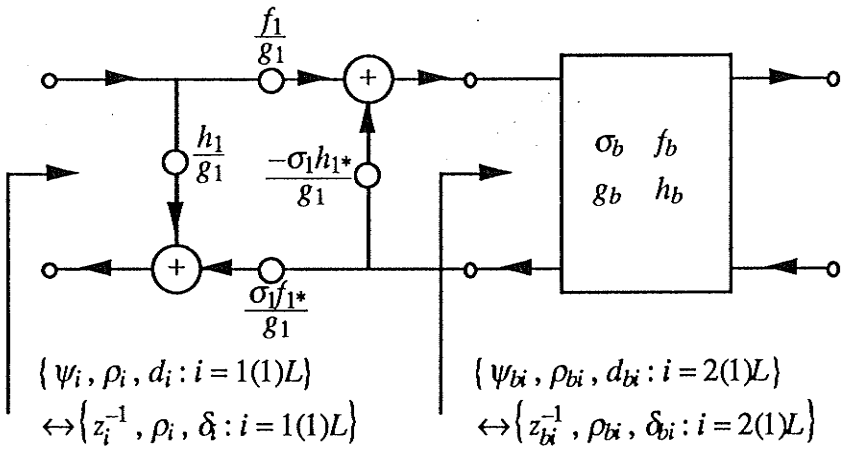

Fig. 4.1 Flowgraph representation of the basic extraction step.

At this stage, most other synthesis algorithms simply attempt to obtain, through various means, the remainder polynomials $\{\sigma_b, f_b, g_b, h_b\}$. From (2.46), these are given by

$$\left\{\sigma_b = \frac{\sigma}{\sigma_1}\;,\; f_b = \frac{f}{f_1}\;,\; g_b = \frac{g_{1*}g - h_{1*}h}{f_1 f_{1*}}\;,\; h_b = \frac{g_1 h - h_1 g}{\sigma_1 f_1 f_{1*}}\right\} \tag{4.7a}$$

and were simply obtained from $\mathbf{T_b} = \mathbf{T}_1^{-1}\mathbf{T}$. Fettweis has shown [3],[4] that a realizable (Hurwitz) polynomial g_b of degree $m - m_1$ can always be found. This is equivalent to stating that there can always be found $\{\sigma_1\,,f_1\,,\,g_1\,,\,h_1\}$ such that the numerator of g_b in (4.7a) contains the factor $f_1 f_{1*}$, and once this common factor has been cancelled, the remaining

polynomial is strictly Hurwitz, i.e., all the zeros are strictly in the left-hand plane $\leftrightarrow$ inside the unit circle (z-plane). In other words, the factor $f_1 f_{1*}$ is a removable singularity. Forcing the factor $f_1 f_{1*}$ to appear in the numerator of g_b in (4.7a), also induces the same factor to appear in the numerator h_b in (4.7a) [3],[4]. Most synthesis algorithms can be distinquished from the practical point of view by the method they employ in effectively removing this common factor.

However, to be able to extract the next elementary section, it is sufficient to know $\{\psi_2, \rho_b(\psi_2), d_b(\psi_2)\} \leftrightarrow \{z_2^{-1}, \rho_b(z_2^{-1}), d_b(z_2^{-1})\}$, from which one again obtains via Tables 3.1-3.13 the canonic polynomial set $\{\sigma_2, f_2, g_2, h_2\}$. An explicit knowledge of $\{\sigma_b, f_b, g_b, h_b\}$ is therefore not required in order to continue with the extraction process. We now show how to obtain $\{\psi_{bi}, \rho_{bi}, d_{bi} : i = 2(1)L\}$ from the knowledge of $\{\psi_i, \rho_i, d_i : i = 2(1)L\}$ and $\{\sigma_1, f_1, g_1, h_1\}$, and similarly for the z-domain.

From (4.7a) we have

$$\rho_b := \frac{h_b}{g_b} = \frac{g_1 h - h_1 g}{\sigma_1 (g_{1*} g - h_{1*} h)} = \frac{g_1 \frac{h}{g} - h_1}{\sigma_1 \left(g_{1*} - h_{1*} \frac{h}{g}\right)} \quad . \tag{4.7b}$$

It follows from (4.7b) that at the remaining transmission zeros

$$\rho_{bi}(\psi_i) = \left[\frac{g_1 \rho_i - h_1}{\sigma_1 (g_{1*} - h_{1*} \rho_i)}\right]_{\psi = \psi_i} \leftrightarrow \rho_{bi}(z_i^{-1}) = \left[\frac{g_1 \rho_i - h_1}{\sigma_1 (g_{1*} - h_{1*} \rho_i)}\right]_{z^{-1} = z_i^{-1}} \quad i = 2(1)L \ . \tag{4.8}$$

For a lossless two-port $\rho_{bi}(\psi_i) \neq 0$ or ∞, i.e., if the numerator in (4.8) becomes zero, then so must the denominator. For this to occur , we must have $\frac{h_1}{g_1} = \frac{g_{1*}}{h_{1*}} = \rho_i$ which, when substituted into $1 = \frac{h_1 h_{1*}}{g_1 g_{1*}} + \frac{f_1 f_{1*}}{g_1 g_{1*}}$, yields $\frac{f_1 f_{1*}}{g_1 g_{1*}}(\psi_i) = 0$. This contradicts our original assumption that all the transmission zeros are distinct. Thus, eq. (4.8) poses no arithmetical difficulties.

Lemma 4.1: Unimodularity of the reflectance is preserved during an extraction step described by (4.7b), i.e., if $\rho_i = e^{j\alpha_i}$ then $\rho_{bi} = e^{j\alpha_{bi}}$.

Proof: A reflectance can only be modular at $\psi = j\phi \leftrightarrow z^{-1} = e^{-j\omega T}$. Evaluating (4.8) at $\psi_i = j\,\phi_i \leftrightarrow z_i^{-1} = e^{-j\omega_i T}$ yields

$$\begin{aligned} \rho_{bi}(j\phi_i) &= \frac{\rho_i \left(g_1 - h_1 \rho_i^*\right)}{\sigma_1 (g_{1*} - h_{1*} \rho_i)} = \frac{\rho_i \left(g_1 - h_1 \rho_i^*\right)}{\sigma_1 \left(g_1^* - h_1^* \rho_i\right)} \\ &= \frac{\rho_i \left(g_1 - h_1 \rho_i^*\right)}{\sigma_1 \left(g_1 - h_1 \rho_i^*\right)^*} = \frac{\rho_i}{\sigma_i} \exp\left[2j \operatorname{Arg} (g_1 - h_1 \rho_i^*)\right] \end{aligned} \quad . \tag{4.9}$$

In deriving (4.9) we have used the fact that $g_{1*}(j\phi_i) = g_1(-j\phi_i) = g_1^*(j\phi_i)$, and similarly for h_{1*}. From (4.9), it follows easily that

$$\alpha_{bi} = \alpha_i + 2\text{Arg}\left(g_1 - h_1\rho_i^*\right) - \text{Arg}\,(\sigma_1) \tag{4.10}$$

In the z-domain, we have $g_{1*} = z^{-m_1}g_1(z)$ and $h_{1*} = z^{-m_1}h_1(z)$ where m_1 is the degree of section 1. The term z^{-m_1} induces an additional factor in (4.10), i.e.,

$$\alpha_{bi} = \alpha_i + 2\text{Arg}\left(g_1 - h_1\rho_i^*\right) - \text{Arg}\,(\sigma_1) - m_1\omega_i T \tag{4.11}$$

In summary, eq. (4.8) is used to recompute the reflectance values associated with transmission zeros located off the $j\phi$-axis $\leftrightarrow$ unit circle, and eqs.(4.10)-(4.11) are used to recompute the arguments of unimodular reflectances.

To complete the *proof* of *Theorem* 4.1, we must also show how to obtain the delay values of the remainder network. The delay function is defined by $d := \left[\ln\frac{g}{h}\right]'$. From (4.7b), we have in the ψ-domain

$$\begin{aligned} d_b &= \left[\ln\left(\sigma_1\frac{g}{h}\frac{g_{1*} - h_{1*}\frac{h}{g}}{g_1 - h_1\frac{g}{h}}\right)\right]' \\ &= d + \frac{(g_{1*})' - \left(h_{1*}\frac{h}{g}\right)'}{g_{1*} - h_{1*}\frac{h}{g}} - \frac{(g_1)' - \left(h_1\frac{g}{h}\right)'}{g_1 - h_1\frac{g}{h}} \\ &= d + \frac{-\left(g_1'\right)_* + \frac{h}{g}\left(\left(h_1'\right)_* + d\,h_{1*}\right)}{g_{1*} - h_{1*}\frac{h}{g}} - \frac{g_1' - \frac{g}{h}\left(h_1' + d\,h_1\right)}{g_1 - h_1\frac{g}{h}} \\ &= d + \frac{h_1' + d\,h_1 - g_1'\frac{h}{g}}{g_1\frac{h}{g} - h_1} + \left[\frac{h_1' + d_*\,h_1 - g_1'\frac{g_*}{h_*}}{g_1\frac{g_*}{h_*} - h_1}\right]_* \end{aligned} \tag{4.12}$$

where we have used $(g_{1*})' = (g_1(-\psi))' = -\left(g_1'(\psi)\right)_*$ and similarly for h_{1*}. At $\psi = \psi_i$, we have from $gg_* = hh_* + ff_*$ that $\frac{h}{g}(\psi_i) = \frac{g_*}{h_*}(\psi_i)$ and $d\,(\psi_i) = d_*(\psi_i)$, where the latter fact was shown in the proof of *Lemma* 2.1.Substituting these results into the last line of (4.12) yields

$$d_{bi} = d_i + \Delta(\psi_i) + \Delta(-\psi_i) \qquad \text{where} \quad \Delta(\psi_i) := \left[\frac{h_1' + d_i h_1 - \rho_i g_1'}{\rho_i g_1 - h_1} \right]_{\psi = \psi_i} \tag{4.13}$$

For $\psi_i = j\,\phi_i$, eq. (4.13) simplifies to

$$d_{bi} = d_i + 2\,\mathrm{Re}\left\{\Delta\left(j\phi_i\right)\right\} \tag{4.14}$$

Note that the denominator of $\Delta(\psi_i)$ cannot vanish for the same reason as for eq. (4.8).

In the z^{-1}-domain, we have $(g_{1*})' = \left(z^{-m_1} g_1(z)\right)' = m_1 z\, g_{1*} - z^2 \left(g_1'\right)_*$, and similarly for h_{1*}. Substituting these into (4.12) and (4.13) yields

$$d_{bi} = d_i + \Delta\left(z_i^{-1}\right) + z_i^2\, \Delta(z_i) + z_i\, m_1 \qquad \text{where} \quad \Delta\left(z_i^{-1}\right) \equiv \left[\frac{h_1' + d_i h_1 - \rho_i g_1'}{\rho_i g_1 - h_1} \right]_{z^{-1} = z_i^{-1}} \tag{4.15}$$

For $z_i^{-1} = e^{-j\omega_i T}$, eq. (4.15) multiplied by $-z_i^{-1}$ simplifies to

$$\delta_{bi} = \delta_i - 2\,\mathrm{Re}\left\{\Delta\left(e^{-j\omega_i T}\right) e^{-j\omega_i T}\right\} - m_1 \tag{4.16}$$

Having obtained $\left\{\psi_{bi},\, \rho_{bi},\, d_{bi} : i = 2(1)L\right\} \leftrightarrow \left\{z_{bi}^{-1},\, \rho_{bi},\, \delta_{bi} : i = 2(1)L\right\}$, it is now possible to continue on with the extraction process, i.e., subscript b in the above is dropped and the next transmission zero is selected. This completes the *proof* of *Theorem* 4.1.

Summarizing the recursive part of the algorithm:

Step 3. Select transmission zero j. From the set of values $\left\{\psi_j,\, \rho_j,\, d_j\right\} \leftrightarrow \left\{z_j^{-1},\, \rho_j,\, \delta_j\right\}$ obtain from Tables 3.1-3.13 the corresponding primitive polynomial set $\left\{\sigma_j, f_j, g_j, h_j\right\}$. If desired, circuit parameters that realize this section may also be computed.

Step 4. Recompute the $d_i \leftrightarrow \delta_i$ for the remaining transmission zeros using the formulae (4.13)-(4.16) with subscript 1 replaced by j.

Step 5. Recompute the ρ_i at the remaining transmission zeros using the formulae (4.9)-(4.11) with subscript 1 replaced by j. When recomputing for a transmission zero at infinity, the mapping $\psi \to 1/\psi \leftrightarrow z^{-1} \to z$ must be applied to h_j and g_j, regardless of the type of section j. For all 1st-order sections j, this mapping also induces $\sigma_j \to -\sigma_j$.

Step 6. Drop subscript b and return to step 3 until all the transmission zeros are extracted.

Step 7. Extract the final constant section (see Section 4.4).

4.2 Recomputation Step Using an Ideal Transformer ↔ 2-port Adaptor

In practice, it is desirable to have the option of extracting three kinds of canonic sections: port 1 reflection-free, port 2 reflection-free, and a feed-through at some frequency. The simplest way of achieving this flexibility is to extract a section described by the primitive polynomials first, followed by the extraction of an ideal transformer ↔ 2-port adaptor that induces the desired property. The canonic polynomial set resulting from absorbing an ideal transformer ↔ 2-port adaptor is given in Fig. 4.2a, where for port 1 and port 2 reflection-free sections, $\cos\theta = \frac{h_P}{\sigma_P\, g_{P*}}$ and $\cos\theta = \frac{h_{P*}}{\sigma_P\, g_P}$ at $\psi = 1$ $\left(z^{-1} = 0\right)$, respectively. In the analog domain, the ideal transformer is usually chosen such that it eliminates the ideal transformer that was induced by the primitive polynomials themselves (see for example Table 3.7). This is in keeping with the usual criterion for analog circuit design, i.e., minimization of the number of ideal transformers. Although an extraction of these zeroth-order sections is an explicit step in the synthesis algorithm, they are usually absorbed in such a way that they do not explicitly appear in the final realization.

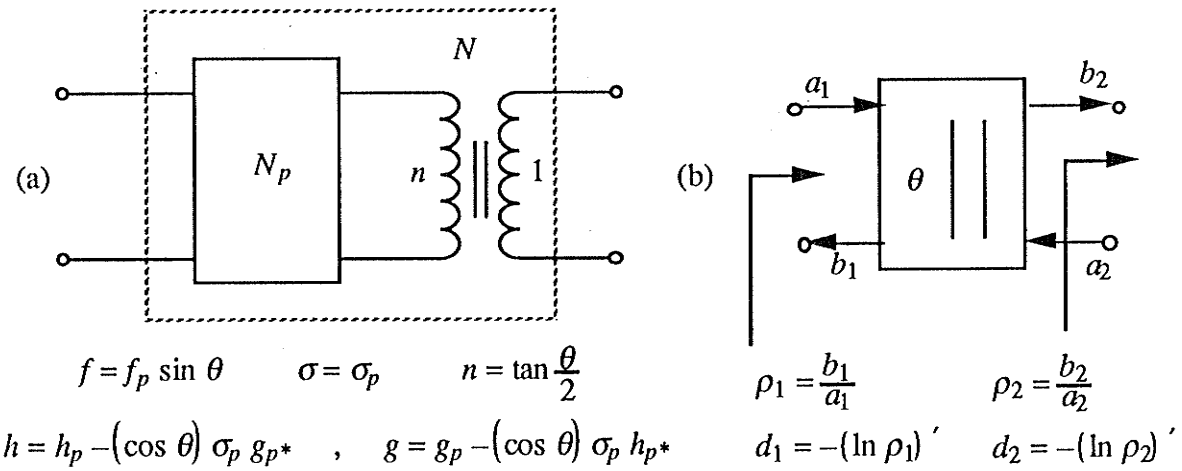

Fig. 4.2 (a) Absorption of an ideal transformer. (b) Recomputation step using a 2-port adaptor.

To complete the extraction step, the reflectance and delay values must be recomputed, as shown in Fig. 4.2b. From Fig. 4.2b and eq. (2.14), it follows that

$$\rho_2 = \frac{\rho_1 + \cos\theta}{1 + \rho_1 \cos\theta} \quad \Rightarrow \quad \rho_2 = \rho_1 \quad \text{for} \quad \rho_1 = \pm 1 \tag{4.17}$$

For $\rho_1 = e^{j\alpha_1}$, eq.(4.17) reduces, using *Lemma* 4.1, to

$$\tan\frac{\alpha_2}{2} = \tan^2\frac{\theta}{2}\tan\frac{\alpha_1}{2} \tag{4.18}$$

For the delay values, it follows from (4.13, (4.15) and (2.14) that

$$\begin{aligned}\frac{d_2}{d_1} \equiv \frac{\delta_2}{\delta_1} &= \frac{\sin^2\theta}{1+\cos^2\theta+(\rho_1+1/\rho_1)\cos\theta} \\ &= \frac{\sin\alpha_2}{\sin\alpha_1} \qquad \text{for} \quad \rho_1 = e^{j\alpha_1} \\ &= \left[\tan^2\frac{\theta}{2}\right]^{\rho_1} \qquad \text{for} \quad \rho_1 = \pm 1\end{aligned} \tag{4.19a,b,c}$$

It has been observed experimentally that the two-stage recomputation process, in addition to the flexibility that it offers, produces less roundoff error than the process that extracts sections with the ideal transformer $\leftrightarrow$ 2-port adaptor already absorbed. This is mainly due to the fact that the coefficients of primitive polynomials can be obtained from the minimal set $\{\psi_j\,,\,\rho_j\,,\,d_j\} \leftrightarrow \left\{z_j^{-1}\,,\,\rho_j\,,\,\delta_j\right\}$ with high accuracy because of the simple nature of the algebraic expressions involved; and the recomputation step using the ideal transformer $\leftrightarrow$ 2-port adaptor via (4.17)-(4.19) is also of a simple nature.

Illustrative Design Example

To illustrate some of the results in this and the previous section, a simple example has been constructed, as shown in Fig. 4.3. The canonic polynomials are obtained by combining the three canonic sections using (2.39):

$$\begin{aligned} f &= 16\sqrt{2}\,\psi(\psi^2+1) & f &= 2\sqrt{2}\,(z^{-1}-1)(z^{-1}+1)(z^{-2}+1) \\ g &= 4\psi^4+28\psi^3+36\psi^2+44\psi+16 \;\leftrightarrow & g &= z^{-4}-z^{-3}-3z^{-2}-5z^{-1}-8 \\ h &= -4\psi^4-4\psi^3-4\psi^2+12\psi+16 & h &= -3z^{-3}-5z^{-2}-7z^{-1}-1 \end{aligned} \tag{4.20}$$

and $\sigma = -1$. The first two steps of the algorithm involve evaluating the reflectance and delay functions at all the transmission zeros, i.e.,

$$\begin{bmatrix} \psi_1=0 & \alpha_1=0 & d_1=2 \\ \psi_2=\infty & \alpha_2=\pi & d_2=6 \\ \psi_3=j & \alpha_3=-\pi/2 & d_3=2 \end{bmatrix} \leftrightarrow \begin{bmatrix} z_1^{-1}=1 & \alpha_1=0 & \delta_1=1 \\ z_2^{-1}=-1 & \alpha_2=\pi & \delta_2=3 \\ z_3^{-1}=-j & \alpha_3=-\pi/2 & \delta_3=2 \end{bmatrix} \tag{4.21}$$

Applying step 3: the first row in (4.21) characterizes Section **1C** from Table 3.3, as shown for both domains in Fig. 4.3.

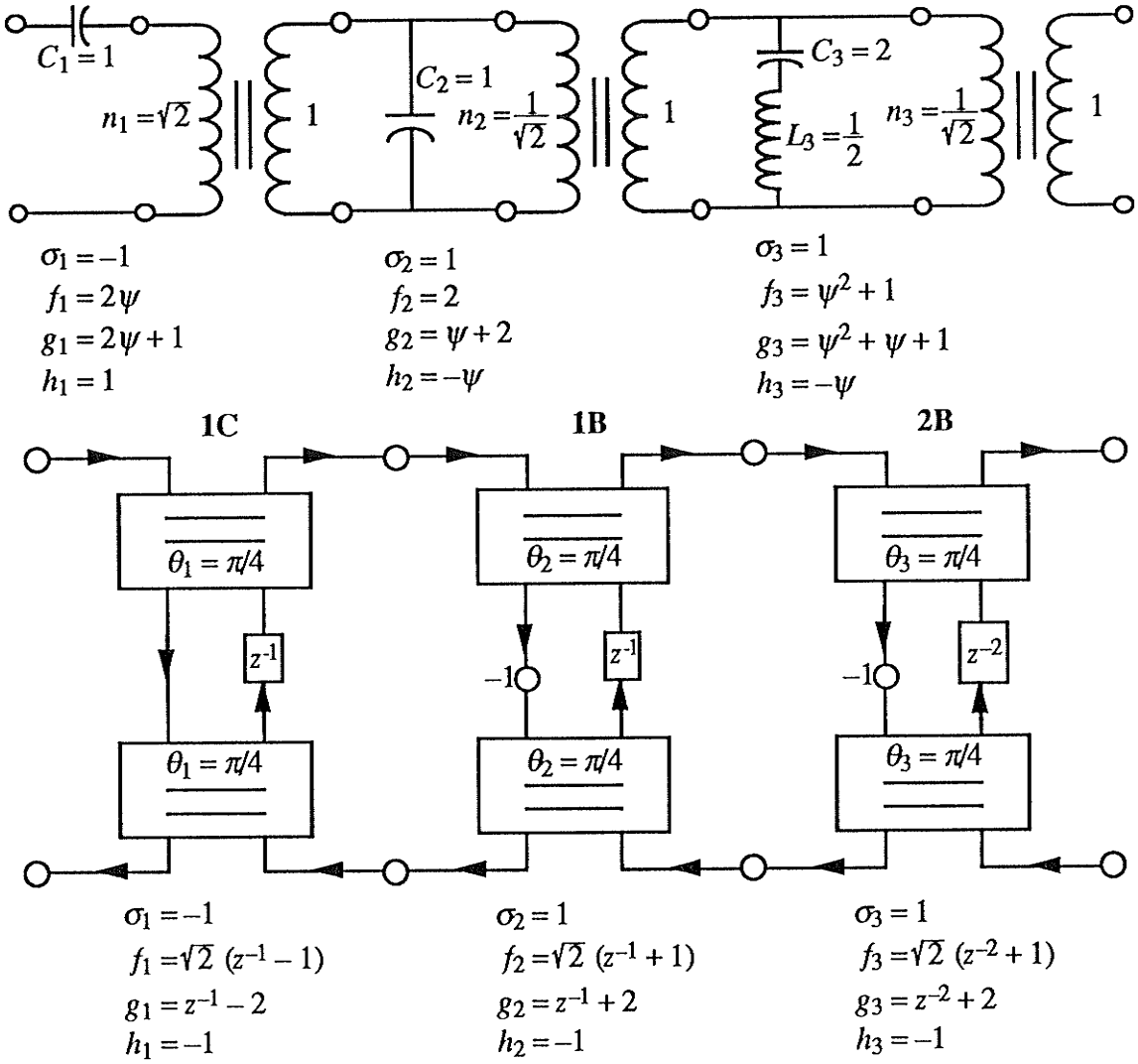

Fig 4.3 Design example of a 4th-order filter.

Steps 4 and 5 of the algorithm involve recomputing the remaining two rows in (4.21) using the primitive polynomials for section **1C** from Table 3.3, with the results given by

$$\begin{bmatrix} \psi_2 = \infty & \alpha_2 = \pi & d_2 = 4 \\ \psi_3 = j & \alpha_3 = \pi & d_3 = 2 \end{bmatrix} \leftrightarrow \begin{bmatrix} z_2^{-1} = -1 & \alpha_2 = \pi & \delta_2 = 2 \\ z_3^{-1} = -j & \alpha_3 = \pi & \delta_3 = 2 \end{bmatrix} \tag{4.22}$$

The second stage of the extraction step involves choosing the zeroth-order section parameter

that, for the example under consideration, makes port 2 of section 1 reflection-free. From Table 3.3, we have $\cos\theta = -1/3$. Recomputing (4.22) using (4.17) and (4.19c) yields

$$\begin{bmatrix} \psi_2 = \infty & \alpha_2 = \pi & d_2 = 2 \\ \psi_3 = j & \alpha_3 = \pi & d_3 = 1 \end{bmatrix} \leftrightarrow \begin{bmatrix} z_2^{-1} = -1 & \alpha_2 = \pi & \delta_2 = 1 \\ z_3^{-1} = -j & \alpha_3 = \pi & \delta_3 = 1 \end{bmatrix} \tag{4.23}$$

The recursive part of the algorithm is now repeated. Row 1 in (4.23) corresponds to section **1B** from Table 3.2. Recomputing the last row of (4.23) using the primitive polynomials for section **1B** from Table 3.2 yields

$$\begin{bmatrix} \psi_3 = j & \alpha_3 = \pi & d_3 = 1 \end{bmatrix} \leftrightarrow \begin{bmatrix} z_3^{-1} = -j & \alpha_3 = \pi & \delta_3 = 1 \end{bmatrix} \tag{4.24}$$

The reflection-free port 2 inducing parameter is given by $\cos\theta = 1/3$. Recomputing (4.24) yields

$$\begin{bmatrix} \psi_3 = j & \alpha_3 = \pi & d_3 = 2 \end{bmatrix} \leftrightarrow \begin{bmatrix} z_3^{-1} = -j & \alpha_3 = \pi & \delta_3 = 2 \end{bmatrix} \tag{4.25}$$

Finally, (4.25) corresponds to section **2B** in Table 3.6. The reflection-free port 2 inducing parameter is given by $\cos\theta = 1/3$. At this stage, the last constant section is extracted – a step which is presented in Section 4.4.

4.3 Sample Characterization of Multiple Transmission-Zero Subnetworks

When at least two elementary sections share the same transmission zero location $\psi_j \leftrightarrow z_j^{-1}$, it is not possible to obtain for the second and the following members of the multiple set the required $\{\rho_j\,,\,d_j\} \leftrightarrow \{\rho_j\,,\,\delta_j\}$ from the overall $\{f\,,\,g\,,\,h\}$ evaluated at $\psi_j \leftrightarrow z_j^{-1}$. This is because, at $\psi = \psi_j \leftrightarrow z^{-1} = z_j^{-1}$, the 1st member of the multiple set effectively decouples the remainder network, including the remaining members of the multiple set.

A solution to this problem , within the framework of reflectance values, has been advanced by Martens [54]. Instead of the usual characterization $\{\psi_j\ ,\ \rho_j\ ,\ d_j\} \leftrightarrow \{z_j^{-1}\ ,\ \rho_j\ ,\ \delta_j\}$ for each transmission zero of a multiple subset, a single characterization is used for the entire subset of multiple zeros. Since insufficient information is available from ρ evaluated at $\psi = \psi_j \leftrightarrow z^{-1} = z_j^{-1}$ without computing higher-order derivatives, the proposed characterization takes the form of $N = m+1$ samples of polynomials h and g taken on a circle with radius r centered at the location of the multiple zero, i.e. we compute for a multiple zero ψ_j

$$\{h_{jn}:\ h_{jn} = h(\psi_j + r\,W^n)\,,\ n = 0(1)N-1\} \tag{4.26a}$$

$$\{g_{jn}:\ g_{jn} = g(\psi_j + r\,W^n)\,,\ n = 0(1)N-1\} \tag{4.26b}$$

where $W \equiv e^{\,j\,2\pi/N}$, $N\ =\ m+1$, and $m\ =$ deg g. We refer to (4.26) as the sample characterization.

The values ρ_j and d_j can be obtained from $\{h_{jn}\}$ and $\{g_{jn}\}$ by using the following method. First note that it is always possible to express polynomials h and g as

$$h(\psi) = \sum_{i=0}^{N-1} a_i(\psi - \psi_j)^i \quad , \quad g(\psi) = \sum_{i=0}^{N-1} b_i(\psi - \psi_j)^i \tag{4.27a,b}$$

where $\{a_i\}$ and $\{b_i\}$ are coefficients of the Taylor series expansion about $\psi = \psi_j$. Evaluating h and g in (4.27) at $\psi = \psi_j + r\,W^n$ yields

$$h_{jn} = \sum_{i=0}^{N-1} a_i\,r^i W^{in} \quad , \quad g_{jn} = \sum_{i=0}^{N-1} b_i\,r^i W^{in} \tag{4.28}$$

Expressions in (4.28) have the form of the discrete Fourier transform (DFT) generalized to radius r [33]. It follows that ($\{a_i\}$ and $\{h_{jn}\}$) and ($\{b_i\}$ and $\{g_{jn}\}$) form DFT pairs

generalized to radius r. This also follows from an observation that a set of polynomial coefficients can be thought of as representing one period of a periodic discrete-time signal which, in turn, can be represented equivalently using its DFT coefficients. From computational considerations during the cascade synthesis of lossless two-ports, it is much easier, when completing the extraction step, to recompute the DFT coefficient set than the corresponding Taylor series coefficient set, even though only the first two Taylor series coefficients are needed to characterize any elementary section.

It follows from (4.27) and (4.28) that

$$h(\psi_j) = a_0 = \frac{1}{N}\sum_{n=0}^{N-1} h_{jn} \quad , \quad g(\psi_j) = b_0 = \frac{1}{N}\sum_{n=0}^{N-1} g_{jn} \tag{4.29a,b}$$

$$h'(\psi_j) = a_1 = \frac{1}{rN}\sum_{n=0}^{N-1} h_{jn}\, W^{-n} \quad , \quad g'(\psi_j) = b_1 = \frac{1}{rN}\sum_{n=0}^{N-1} g_{jn}\, W^{-n} \tag{4.29c,d}$$

and

$$\rho_j = \frac{h(\psi_j)}{g(\psi_j)} \quad , \quad d_j = \frac{g'(\psi_j)}{g(\psi_j)} - \frac{h'(\psi_j)}{h(\psi_j)} \tag{4.30a,b}$$

During the ith extraction step, the sets $\{h_{jn}\}$ and $\{g_{jn}\}$ where $j > i$, are recomputed in the ψ-domain using (4.7a) with subscript 1 replaced with i, i.e.

$$h_{bjn} = \left[\frac{h_{jn}\, g_i - g_{jn}\, h_i}{\sigma_i\, f_i\, f_{i*}}\right]_{\psi=\psi_{jn}} \quad , \quad g_{bjn} = \left[\frac{g_{jn}\, g_{i*} - h_{jn}\, h_{i*}}{f_i\, f_{i*}}\right]_{\psi=\psi_{jn}} \qquad n = 0(1)N\text{–}1 \tag{4.31a,b}$$

where

$$\psi_{jn} = \psi_j + r\, W^n \quad , \quad n = 0(1)N\text{–}1 \tag{4.32}$$

Note that the section being extracted (section i) could be the one that realizes one of the multiple zeros ψ_j. When recomputing using an ideal transformer $\leftrightarrow$ 2-port adaptor with $n = \tan \theta/2$, eqs. (4.31) reduce to

$$h_{bjn} = \frac{h_{jn} + g_{jn} \cos\theta}{\sin^2\theta} \quad , \quad g_{bjn} = \frac{g_{jn} + h_{jn} \cos\theta}{\sin^2\theta} \qquad n = 0(1)N\text{–}1 \tag{4.33}$$

Note also that the sample characterization requires an independent processing of polynomials h and g from which one obtains the same characterization of section i.

In the z^{-1}-domain, the multiple transmission zero at $z^{-1} = z_j^{-1}$ case is handled in exactly the same way as in the ψ-domain. The same equations (4.26)-(4.33) are used with ψ_j replaced with z_j^{-1} and ψ_{jn} with

$$z_{jn}^{-1} = z_j^{-1} + r_z W^n \quad , \quad n = 0(1)N-1 \tag{4.34}$$

For both domains, to extract the ith section that realizes one of the multiple transmission zeros, the ρ_i and possibly d_i (δ_i) are needed which are obtained using (4.29)-(4.30). The remaining members of the multiple zero subset are characterized using $\{h_{bjn}\}$ and $\{g_{bjn}\}$. As in step 6 of the main algorithm, subscript b is dropped and the next transmission zero is selected.

Remarks:

1. The radius r (r_z) is chosen to be 1/5 of the Euclidean distance between the multiple zero ψ_j (z_j^{-1}) and the next nearest transmission zero. The values r and r_z are usually different and both are much less than one. This choice has been determined experimentally and has been found to work well in practice.

2. It has been observed through numerous examples that the expressions in (4.29) tend to average out errors that might have accumulated in $\{h_{jn}\}$ and $\{g_{jn}\}$.

3. The sample characterization is not restricted to the multiple zero case. It can be applied to characterize distinct zeros as well. For the distinct plus multiple zero case, using the sample characterization for all transmission zeros simplifies the logical structure of the overall program, at the cost of substantially increasing the total number of polynomial evaluations. It has been observed that the accuracy of both approaches is comparable.

4. At the outset, the size of the sample sets characterizing the subnetwork that realizes the multiple-zero subset could be limited to the degree plus one of that subnetwork. Also, after each extraction step, the size of both $\{h_{jn}\}$ and $\{g_{jn}\}$ could be decreased by m_i to reflect order reduction. However, it has been found more convenient, from the point of view of programming, to keep the size invariant. Also, the averaging-out-of-error effect is more pronounced with the larger sized sets.

Illustrative Example

Consider a cascade of three elementary sections with a multiple zero of order three located at $\psi = 0$, as shown in Fig. 4.4. The canonic polynomials for each individual section can be obtained from Tables 3.3 and 3.4. The overall canonic polynomials for the circuit in Fig. 4.4 are given by

$$\sigma = -1 \quad , \quad f = \psi^3 \quad , \quad g = \psi^3 + 3\psi^2 + 4\psi + 4 \quad , \quad h = \psi^2 + 4 \tag{4.35}$$

Evaluating h and g at $\psi = e^{j n \pi/2}$, $n = 0(1)3$ sample points, yields the sample characterization which is given by the first row of numbers in (4.36):

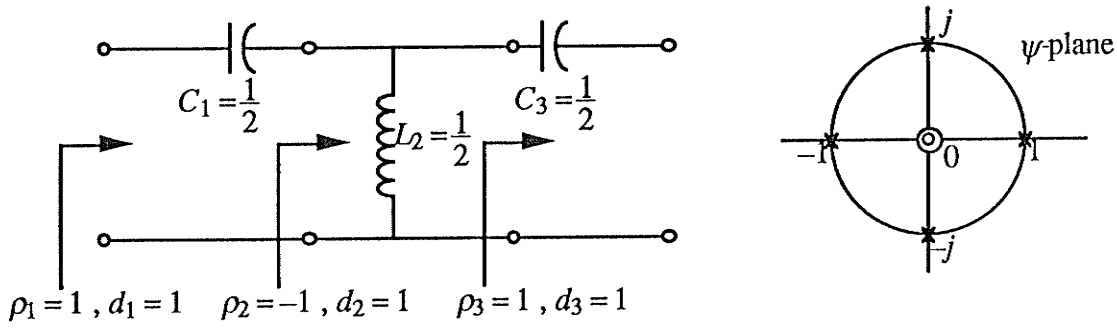

Fig. 4.4 Example of a circuit with a triple transmission zero at $\psi = 0$ and the sample locations in the ψ-domain..

	h_{j1}	h_{j2}	h_{j3}	h_{j4}	g_{j1}	g_{j2}	g_{j3}	g_{j4}		ρ_j	d_j
$j=1$	5	3	5	3	12	$1+3j$	2	$1-3j$	$\rightarrow$	1	1
$j=2$	–2	–2	–2	–2	5	$1+2j$	1	$1-2j$	$\rightarrow$	–1	1
$j=3$	1	1	1	1	2	$1+j$	0	$1-j$	$\rightarrow$	1	1

(4.36)

ρ_1 and d_1 are obtained from row 1 in (4.36) and eqs.(4.29) and (4.30). Rows 2 and 3 are obtained using the recomputation formulae (4.31) with rows 1 and 2 as input, respectively.

The problem of the decoupling property masking-out sections that follow the first member is not limited to multiple zeros. It also applies for the case where $f = \Pi f_i$ contains factors, say f_j and f_k, that are Hurwitz conjugates of each other, i.e., $f_k = \pm f_{j*}$. For real f, this can happen in two cases:

$$f_C = f_j f_k = (\psi - r)\,(\psi + r) = \psi^2 - r^2 \tag{4.37a}$$

$$f_D = f_j f_k = (\psi^2 - 2r\cos\phi\ \psi + r^2)\,(\psi^2 + 2r\cos\phi\ \psi + r^2) = \psi^4 - 2r^2\cos 2\phi\ \psi^2 + r^4 \tag{4.37b}$$

Note that f_C in (4.37a) corresponds to polynomial f of section **2C** (see Table 3.11) and, therefore, could be realized with that section. In the analog domain, f_D from (4.37b) is usually realized with the Darlington D-section. Here, however, we are interested in realizing f_C and f_D with a cascade of two elementary sections which do not necessarily have to follow each other in the overall cascade. For both cases, the overall $\{f, g, h\}$ evaluated at $\psi = \psi_j = -\psi_k$ (i.e., the zero of f_j) yields

$$1 = \frac{h}{g}(\psi_j) = \frac{h_*}{g_*}(\psi_j) = \frac{h}{g}(\psi_j)\,\frac{h}{g}(-\psi_j) = \rho_j\,\rho_k \tag{4.38}$$

Since, in general, ρ_k and ρ_j are independent, eq. (4.38) implies that ρ_k cannot be obtained from the overall $\{f, g, h\}$ due to the decoupling property.

To obtain ρ_k from the overall $\{f, g, h\}$, first note that the f_C and f_D in (4.37) correspond to reciprocal subnetworks. By *Lemma* 2.2, $d_C(\psi_k) = d(\psi_k)$ and $d_D(\psi_k) = d(\psi_k)$. The polynomials h_C and g_C can be obtained by combining the two elementary sections that realize f_j and f_k. From (2.39) with a and b replaced with j and k respectively, we have

$$\begin{aligned} d_C := \left[\ln \frac{g_C}{h_C}\right]' &= \left[\ln \frac{g_j + \sigma_j h_{j*} \dfrac{h_k}{g_k}}{h_j + \sigma_j g_{j*} \dfrac{h_k}{g_k}}\right]' \\ &= \frac{g_j' + \sigma_j \dfrac{h_k}{g_k}\left((h_{j*})' - d_k h_{j*}\right)}{g_j + \sigma_j h_{j*} \dfrac{h_k}{g_k}} - \frac{h_j' + \sigma_j \dfrac{h_k}{g_k}\left((g_{j*})' - d_k g_{j*}\right)}{h_j + \sigma_j g_{j*} \dfrac{h_k}{g_k}} \end{aligned} \quad . \tag{4.39}$$

At $\psi = \psi_k = -\psi_j$, it follows from (4.38) that $\dfrac{h_{j*}}{g_j}(\psi_k) = \dfrac{g_{j*}}{h_j}(\psi_k)$. Substituting this result into (4.39) and solving for ρ_k yields

$$\rho_k = \frac{h_k}{g_k}(\psi_k) = \left(\frac{d_j(\psi_k) - d(\psi_k)}{d(\psi_k) - d_j(-\psi_k)}\right) \frac{g_j}{\sigma_j h_{j*}}(\psi_k) \quad . \tag{4.40}$$

For the z^{-1}-domain, replace ψ_k with z_k^{-1} and $d_j(-\psi_k)$ with $z_k^{-2} d_j(z_k)$ in (4.40). Note that eq. (4.40) cannot be used for the multiple-zero case because then, $\psi_j = \psi_k$, which implies that section j is reciprocal and, consequently, $d_j(\psi_k) = d_j(-\psi_k) = d(\psi_k)$.

Eq. (4.40) was used in obtaining ρ_2 for the C-section in Table 3.11. The Darlington D-section with f_D from (4.37b) can be realized with a cascade of two **2E** sections from Table 3.10 and Fig. 3.15, where the reflectances $\beta_j e^{j\alpha_j}$ and $\beta_k e^{j\alpha_k}$ are obtained from the overall $\{f, g, h\}$ and eq. (4.40), respectively. The reflectance for section k is computed after section j has been extracted.

4.4 Extraction of the Last Ideal Transformer ↔ 2-Port Adaptor

The degree reduction that is effectively induced during the extraction step ensures that, after all the factors of f have been exhausted, the remainder polynomials, if these were computed, correspond to a zeroth-order section. In general, the remainder polynomials are nontrivial (i.e. $h_R \neq 0$) because the extracted sections are chosen with a desired property and, together, they comprise a network with canonic polynomials that may differ from the given ones by at most a zeroth-order section. It follows that an ideal transformer ↔ 2-port adaptor must be extracted to complete the synthesis, as shown in Fig. 4.5a.

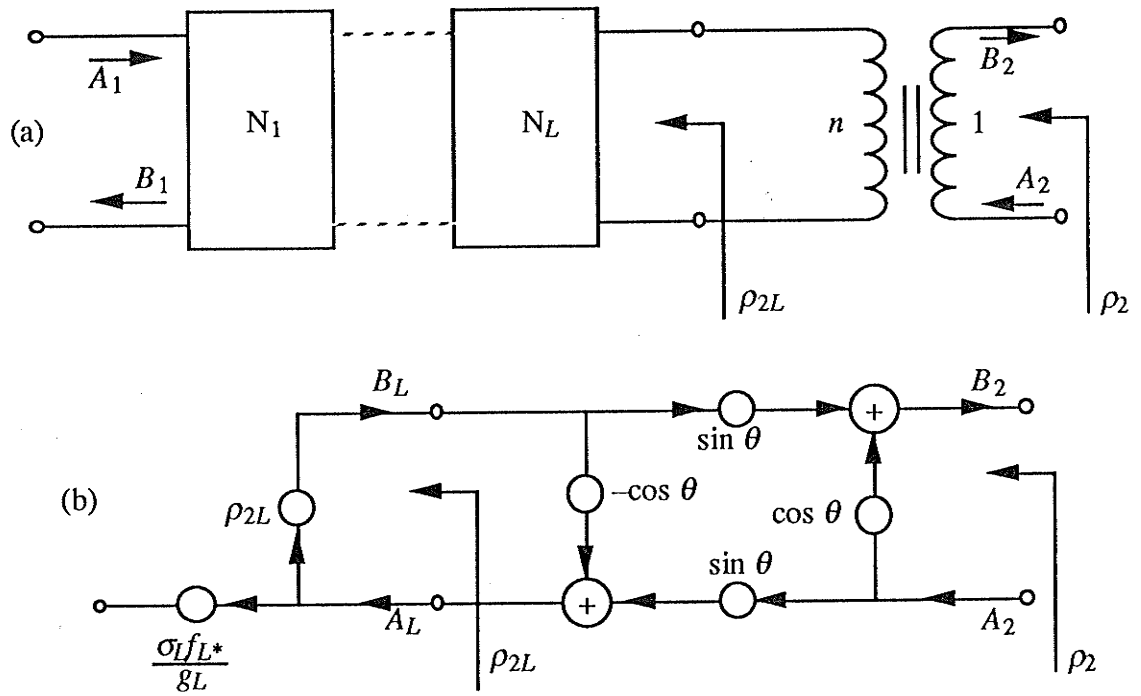

Fig. 4.5 (a) Extraction of the last ideal transformer and (b) its wave flowgraph equivalent when section L is evaluated at $\psi = \psi_L \leftrightarrow z^{-1} = z_L^{-1}$.

There are several ways of performing this step of which two are described here. The first method is based on the decoupling property of an elementary section N_L when evaluated at the location of its transmission zero $\psi = \psi_L \leftrightarrow z^{-1} = z_L^{-1}$. This is shown for the WD domain in Fig. 4.5b with an actual flowgraph of a normalized 2-port adaptor. To simplify the presentation, we define the following: let

$$\rho_{2L} := -\sigma_L \frac{h_{L*}}{g_L} \quad , \quad \rho_2 := -\sigma \frac{h_*}{g} \qquad \text{evaluated at } \psi = \psi_L \leftrightarrow z^{-1} = z_L^{-1} \tag{4.41}$$

where subscript L pertains to the last section. The situation is essentially the same as for the recomputation step using an ideal transformer $\leftrightarrow$ 2-port adaptor (see Fig. 4.2b) except that now it is the parameter $n \leftrightarrow \theta$ that is the unknown. It follows that eqs. (4.17)-(4.19) can be also be used here with ρ_2 and ρ_1 replaced with ρ_{2L} and ρ_2 respectively, i.e.,

$$n^2 = \tan^2\left(\frac{\theta}{2}\right) = \left[\frac{1+\rho_{2L}}{1-\rho_{2L}}\right]\left[\frac{1-\rho_2}{1+\rho_2}\right] \qquad \Leftrightarrow \qquad \cos\theta = \frac{1-n^2}{1+n^2} = \frac{\rho_{2L}-\rho_2}{\rho_{2L}\,\rho_2 - 1} \tag{4.42}$$

For $\rho_{2L} = e^{j\alpha_{2L}}$, it follows from (4.18) that $\rho_2 = e^{j\alpha_2}$, and eq. (4.42) can expressed as

$$n^2 = \tan^2\left(\frac{\theta}{2}\right) = \frac{\tan \alpha_{2L}/2}{\tan \alpha_2/2} \tag{4.43}$$

If $\rho_{2L} = \pm 1$, then also $\rho_2 = \pm 1$ (see (4.17)) and (4.42) is indeterminate. For this case, one can use (4.19c), i.e.,

$$n^2 = \tan^2\left(\frac{\theta}{2}\right) = \left[\frac{d_{2L}}{d_2}\right]^{\rho_{2L}} = \left[\frac{\delta_{2L}}{\delta_2}\right]^{\rho_{2L}} \tag{4.44}$$

where the delays are obtained in the usual manner. For the Example in Section 4.2, we have $\rho_{2L} = \frac{-\sigma_3 h_{3*}}{g_3}(-j) = -1$ and $\rho_2 = \frac{-\sigma h_*}{g}(-j) = -1$. We, therefore, must use (4.44) from which it follows that $n^2 = \tan^2\theta/2 = (4/4)^1 = 1$.

The sign of n cannot be obtained by using this method without additional considerations. However, the sign of n is usually of little importance since its only effect is to change the sign of the transmittance. If required, it can be obtained by evaluating the transmittance at any passband frequency.

The second method is based on using the sample characterization $\{h_{Ln}\}$, $\{g_{Ln}\}$ for the last section, regardless of the multiplicity of the last transmission zero. After the last section has been extracted, its sample sets $\{h_{Ln}\}$, $\{g_{Ln}\}$ are recomputed once again using (4.31) with $\{\sigma_i\ ,\ g_i\ ,\ h_i\}$ set equal to $\{\sigma_L\ ,\ g_L\ ,\ h_L\}$. This recomputation step induces degree reduction since section L completely removes the last transmission zero, from which it follows that the sets $\{h_{bLn}\}$, $\{g_{bLn}\}$ characterize a zeroth-order network. From (4.29a,b) and the definition of a normalized 2-port adaptor in (2.14), we have

$$g_\theta = \frac{1}{N}\sum_{n=0}^{N-1} g_{bLn} = \frac{1}{\sin\theta} = \frac{1+n^2}{2n} \quad , \quad h_\theta = \frac{1}{N}\sum_{n=0}^{N-1} h_{bLn} = \frac{-\cos\theta}{\sin\theta} = \frac{n^2-1}{2n} \tag{4.45}$$

and $$n = g_\theta + h_\theta = \frac{1}{g_\theta - h_\theta} \leftrightarrow \cos\theta = \frac{1-n^2}{1+n^2} = \frac{-h_\theta}{g_\theta} \quad , \quad \sin\theta = \frac{2n}{1+n^2} = \frac{1}{g_\theta} \tag{4.46}$$

For the Example in Section 4.3, we have $h_{b3n} = \{0, 0, 0, 0\}$ and $g_{b3n} = \{1, 1, 1, 1\}$, which yields $g_\theta = 1$, $h_\theta = 0 \Rightarrow n = 1$. Since the sample characterizations of polynomials h and g are processed separately, this method also provides the correct sign of n.

One case that deserves special mention involves a circuit where all the elementary sections are chosen with port 2 reflection-free. In this case, $\rho_{2i} = 0 \ \forall i$ at $z^{-1} = 0$, which, with reference to Fig. 4.5b, implies that the signal B_L is independent of A_2 and, therefore, the reflectance at port 2 evaluated at $z^{-1} = 0$ only depends on the last transformer $\leftrightarrow$ 2-port adaptor. It can be obtained from

$$\frac{B_2}{A_2} = -\sigma\frac{h_*}{g} = \cos\theta = \frac{1-n^2}{1+n^2} \qquad \text{evaluated at} \quad \psi = 1 \leftrightarrow z^{-1}=0 \tag{4.47}$$

For the case under discussion, eq. (4.47) is by far the most accurate method of obtaining n as its computation only uses the input data. It also provides an obvious means of investigating roundoff error accumulation since the value obtained from (4.47) can be assumed to be correct, and values obtained using the other two methods must be comparable to it. It has been determined this way that the other two methods are comparable in accuracy but highly sensitive to any errors in the solution of $gg_* = hh_* + ff_*$, i.e., the input data must represent a lossless two-port, otherwise the three methods of obtaining the last transformer provide different answers. Also, it has been observed for the examples so far examined, that no discernible differences exist between the same filters synthesized in both the ψ- and z^{-1}- domains.

V. DESIGN EXAMPLES

In this chapter, we present three design examples with the aim of demonstrating: 1) numerical robustness and relative immunity to roundoff error accumulation of the synthesis algorithm; 2) the effect of interchanging the reflectance and transmittance and using voltage versus power wave 2-port adaptors on the sensitivity of the filter response to parameter quantizations; 3) the possibility of deriving simplified filter structures by imposing a constraint from (3.30) on every general 2nd-order section and using the quasi-lattice structure from Fig. 3.22.

Synthesis algorithms that use the primary data only once and thereafter employ some sort of recomputation at each extraction step, generate roundoff error that tends to accumulate with each step. The amount of roundoff error that is generated depends mainly on the accuracy with which the extraction step is performed. For the algorithm described in Chapter IV, the only sources of roundoff error during the extraction step, assuming that ρ_i and d_i (δ_i) are computed in steps 1 and 2 with maximum precision, are the recomputation formulae (4.8)-(4.16). If care is taken in evaluating these expressions, the propagation of error can be kept to a minimum. For example, it has been found experimentally that for highly selective filters, dividing each term in (4.13) and (4.15) by g_i reduces roundoff error.

5.1 Example of a 14th-order Bandpass Filter [22]

The first design example serves to demonstrate the numerical robustness and relative immunity to roundoff error accumulation of the synthesis algorithm. An extremely narrow band 14th-order bandpass filter [22] with a relative bandwidth of 0.025% has been selected for synthesis in the ψ-domain. The zeros of the canonic polynomials $\{f, g, h\}$ are given in Table 5.1.

Table 5.1 Canonic polynomials for the filter from [22]

Transmission zeros	Zeros of g	Zeros of h
$\pm j$ 8.992424181e-1	-1.1552342827076e-5 $\pm j$ 8.9977021150841e-1	$\pm$ 8.998624919e-1
$\pm j$ 9.004825819e-1	-1.9199339335190e-5 $\pm j$ 8.9982635148176e-1	$\pm j$ 8.997450966e-1
$\pm j$ 8.996210097e-1	-1.9199339335362e-5 $\pm j$ 8.9989864851824e-1	$\pm j$ 8.997714358e-1
$\pm j$ 9.001039903e-1	-1.1552342827346e-5 $\pm j$ 8.9995478849159e-1	$\pm j$ 8.998270474e-1
$\pm j$ 8.996751863e-1	-3.4936618244783e-6 $\pm j$ 8.9998092104884e-1	$\pm j$ 8.998979526e-1
$\pm j$ 9.000498137e-1	-3.4936618243715e-6 $\pm j$ 8.9974407895116e-1	$\pm j$ 8.999535642e-1
0.000000000e+0	-8.9969779610465e-1	$\pm j$ 8.999799034e-1
	-9.0002721784407e-1	

The transmission zeros are all distinct and are located at $\psi = j\phi$, thus permitting a reciprocal realization where each section is characterized by a transmission zero ϕ_i, a unimodular reflectance value, and a positive delay. Note that all finite transmission zeros in

Table 5.1 are indistinguishable to three significant digits. Both g and h polynomials are monic and the constant factor of f is 3.29421739e-4. The sequence of transmission zeros that is specified in Table 5.1 is realized with a chain connection of six **2D** (Brune) sections followed by sections **1C** ($\psi = 0$) and **1B** ($\psi = \infty$) – eight sections in all followed by a constant section.

For comparison, minimal characterizations $\{\phi_i , \alpha_i , d_i : i = 1(1)8\}$ for the final realization were obtained using two independent methods: 1) from the element values in the final realization given by Göttlicher [22] by using the analog element formulae in Table 3.7, with the results given in Table 5.2. The synthesis algorithm developed in [22] operates on the driving point impedance and requires an accurate zero-finding routine; 2) The filter was synthesized using an algorithm developed by Williamson [31] which is based on rational interpolation and performs two factorizations to extract each section – a method which at each step uses only the primary data. Williamson's results agreed with Göttlicher's to six decimal places in the worst case, but the program was executed with only a 14 decimal precision.

Table 5.2 Reflectance and delay value comparisons for Example 5.1.

α obtained from [22]	α synthesized	d obtained from [22]	d synthesized
-1.681979729e+0	-1.681979729e+0	1.863999613e+2	1.863999613e+2
-1.556678547e+0	-1.556678547e+0	3.778343342e+0	3.778343342e+0
-9.890250576e-1	-9.890250576e-1	1.278142565e+0	1.278142566e+0
-1.703290746e-1	-1.703290747e-1	2.230086653e-1	2.230086655e-1
-1.440055120e-2	-1.440055121e-2	2.204588942e-2	2.204588948e-2
-2.285924135e-3	-2.285924149e-3	3.750590767e-3	3.750590906e-3
0.000000000e+0	0.000000000e+0	4.890808654e-4	4.890809058e-4
3.141592654e+0	3.141592654e+0	1.245308063e+0	1.245307860e+0

The synthesis was performed using the two-stage extraction step as described in Section 4.2. The resulting $\{\phi_i , \alpha_i , d_i : i = 1(1)8\}$ are given in Table 5.2. A comparison with Göttlicher's results clearly shows a slow accumulation of roundoff error, with the worst case for d_8 accurate to 7 significant digits. Such a slow rate is acceptable and, for common filter specifications that are normally much less stringent, the roundoff error is completely negligible. When the filter was synthesized using a one-stage extraction step, where the ideal transformer is absorbed by the primitive section before the recomputation step, three additional digits of accuracy were lost in the final section.

The final transformer value from [22] is given by $n = 0.8317997714$, and the values obtained using the two methods described in Section 4.4 are given by: from (4.44) $n = 0.831799704$, and from (4.46) $n = 0.831799443$. Again, the correspondence is quite acceptable, with the differences having no practical consequences. The frequency response, shown in Fig. 5.1, was obtained by combining the synthesized sections in the frequency

domain using the following method: at $\psi = j\phi$, the transfer matrix for each elementary section can be expressed as

$$\mathbf{T}_i(j\phi) = \frac{1}{\sqrt{1-|\rho_i|^2}} \begin{bmatrix} \gamma_i & \rho_i \\ \gamma_i \rho_i & 1 \end{bmatrix} \qquad \text{where} \quad \rho_i := \frac{h_i}{g_i} \quad , \quad \gamma_i = \sigma_i \frac{g_{i*}}{g_i} \tag{5.1}$$

where γ_i is clearly unimodular. The product of two transfer matrices $\mathbf{T}_k = \mathbf{T}_i \mathbf{T}_j$ at any $\psi = j\phi$ can be obtained efficiently by using

$$\gamma_k = \gamma_i^* \gamma_j \frac{(\gamma_i^* + \rho_i^* \rho_j)^*}{\gamma_i^* + \rho_i^* \rho_j} \quad , \quad \rho_k = \frac{\gamma_i^* \rho_i + \rho_j}{\gamma_i^* + \rho_i^* \rho_j} \quad . \tag{5.2a,b}$$

Note that γ_k is also unimodular and, therefore, only its argument needs to be retained. Assuming that ρ_i and ρ_j are given in polar form, only two polar-to-rectangular and two rectangular-to-polar conversions are required to evaluate (5.2). Once the overall reflectance ρ is obtained, the magnitude of the transmittance follows from the complementary-responses property in (2.27) and is given by $\sqrt{1-|\rho|^2}$.

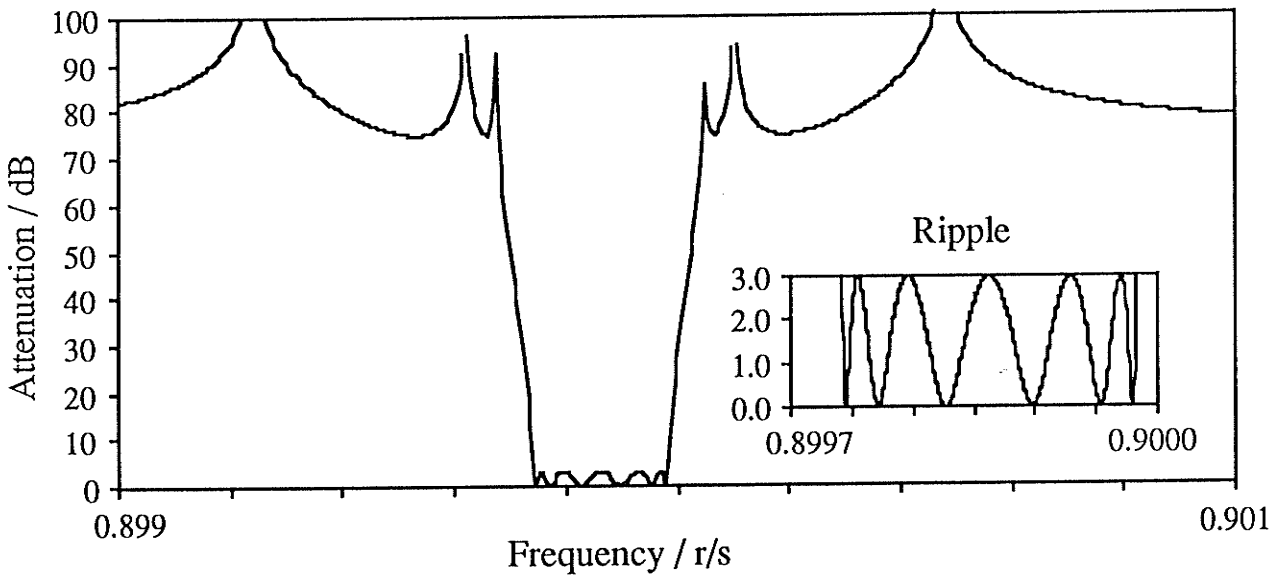

Fig. 5.1 Frequency response for Example 5.1 with the horizontal scale in radians per second.

5.2 Example of an 8th-order Bandpass Filter

The second example is an 8th-order bandpass filter taken from [16, Ex.7.1] and synthesized in the z^{-1}-domain. The transfer function is the result of an optimization with the following specifications: find a bandpass transfer function with two finite transmission zeros and transition regions from 0.325π to 0.35π and from 0.4π to 0.425π such that the passband ripple is within 1.5 dB and the minimum stopband attenuation is as large as possible. The resulting canonic polynomial set $\{f, g, h\}$ that satisfies these specifications is given in Table 5.3, where $T_D = f/g$ is the desired transfer function.

Because WD filters are inherently bidirectional and provide two complementary transfer functions, it is possible to realize a given transfer function as either a transmittance or a reflectance. For this example, the desired transfer function was realized both as a transmittance and as a reflectance to show the differences in stopband sensitivities to multiplier quantizations and the efficiency of the final realizations.

Table 5.3 Canonic polynomials for Example 5.2.

Zeros of f		Zeros of g		Zeros of h	
Radius	Angle/π	Radius	Angle/π	Radius	Angle/π
1	±0.430034232	0.991526647455	±0.350675396513	1	±0.351732711368
1	±0.320538560	0.976757231041	±0.364509517763	1	±0.365109796566
		0.977066484118	±0.385806739120	1	±0.385182448776
		0.991727478015	±0.399341528947	1	±0.398308216049
Constant factor of f		Constant factor of g		Constant factor of h	
0.00090521		1		0.938442111704	

By letting $T_D = f/g$, we have a multiple transmission zero of order 4 at $z^{-1} = 0$, which is characterized using the sample representation described in Section 4.3. The resulting WD circuit parameters for an arbitrarily chosen sequence of transmission zeros are given in Table 5.4. WD circuits for sections **1E** and **2D** can be found in Table 3.8 and Fig. 3.15, respectively. To ensure computability, all sections were chosen with port 2 reflection-free. The parameter for the final 2-port adaptor was obtained using (4.47), and is given by $\cos\theta = -0.9384421117$. We should point out that, initially, the data from [16] did not satisfy $gg_* = hh_* + ff_*$ with sufficient accuracy to permit verification of the given circuit as was evidenced by the three different answers obtained for the final 2-port parameter. The Feltdkeller equation was subsequently resolved to allow a more acceptable match between the results from the three different methods described in Section 4.4.

Table 5.4 WD circuit parameters for Example 5.2 realized as a transmittance.

Section Type	Transmission Zero angle/π	θ_0/π	θ_1/π	θ_2/π	θ_3/π
1E	0		0.61226914	0.50000000	
1E	0		0.87522338	0.50000000	
2D	0.430034232	-0.40234062	1.03255564	0.37250176	1.40234062
1E	0		0.52873577	0.50000000	
1E	0		0.87719940	0.50000000	
2D	0.320538560	-0.39450193	0.96882327	0.37498973	1.39450193

Two types of multiplier quantization schemes were examined: 1) with two quantizations per normalized 2-port adaptor such that passivity is maintained, and 2) each normalized 2-port adaptor was converted to its voltage wave equivalent (see Fig. 2.7) and, wherever possible, the resulting pairs of inverse multipliers were shifted out of the structure. This amounts to replacing Fig. 3.15 with Fig. 3.17 for each **2D** section. Also, every 1E section in Table 5.4 has $\cos\theta_2 = 0$, which implies that the simpler special-case circuit from Table 3.8 can be used with the power wave 2-port adaptor replaced with its voltage wave equivalent. The conversion step reduced the number of sources of passivity from 12 to 2. In total, the circuit requires 13 2-port adaptors and two pairs of multipliers. The resulting frequency responses for multipliers quantized to 8 bits are shown in Fig. 5.2. Note the improved passband response for the voltage wave adaptor circuit. The stopband responses for the quantized voltage and power wave designs are essentially the same as the ideal response

Letting $T_D = h/g$ by interchanging polynomials h and f results in a transmittance with four transmission zeros on the unit circle. The final realization, therefore, consists of four **2D** sections. The choice of $T_D = h/g$ was also used in [16]; a choice, however, constrained by the fact that only a method for extracting noncanonic, reciprocal, and lossless sections was given there, whereas the realization in Table 5.4 requires nonreciprocal lossless sections. The final realization parameters are given in Table 5.5

Table 5.5 WD circuit parameters for Example 5.2 realized as a reflectance.

Section Type	Transmission Zero Angle/π	θ_0/π	θ_1/π	θ_2/π	θ_3/π
2D	0.351732711368	-0.4153885	0.42783062	0.92390509	1.04153848
2D	0.365109796566	-0.0680749	0.57423753	0.06063559	1.06807490
2D	0.385182448776	-0.0684596	1.61677417	0.99804390	1.06845968
2D	0.398308216049	-0.0417846	1.32278945	0.07551627	1.04178456

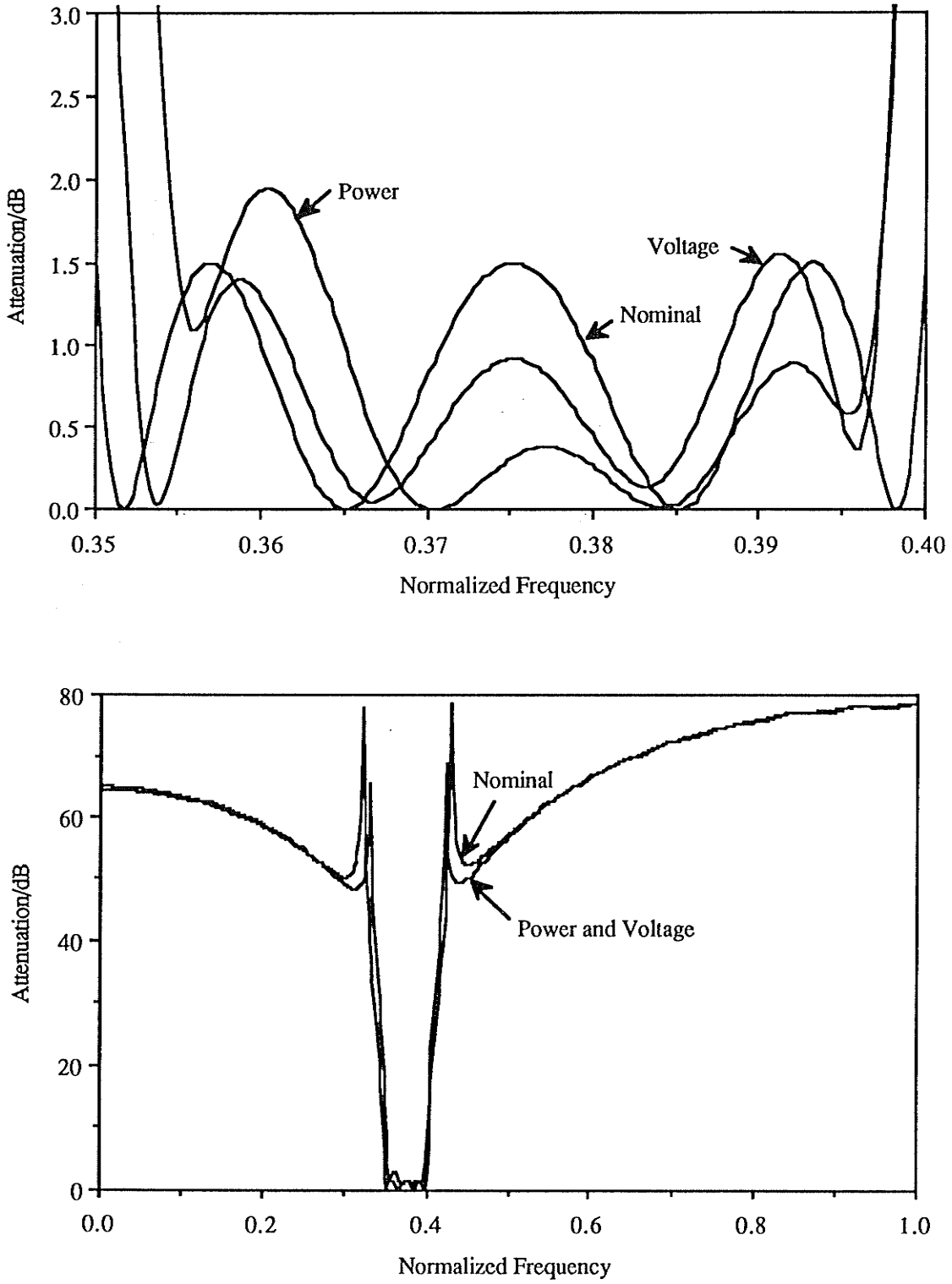

Fig. 5.2 Passband and stopband responses for Example 5.2 realized as a transmittance.

To ensure computability, all **2D** sections were chosen with port 2 reflection-free. From (4.47), the parameter for the final 2-port adaptor is given by $\cos\theta = -0.00090521$. The final realization requires 17 nontrivial 2-port adaptors, which is 4 more than the $T_D = f/g$ realization. The frequency responses for the two types of multiplier quantization schemes are shown in Fig. 5.3

Again, the passband response for the voltage wave realization is superior to the power wave one due to the smaller number (5 vs. 17) sources of passivity. The stopband responses, however, deteriorate substantially for both quantization schemes. This is because, in general, in order to effect a transmission zero with the reflectance, a perfect cancellation of two signals in the first section must occur, i.e.,

$$\frac{b_1}{a_1} = \frac{h_1}{g_1} + \sigma_1 \frac{f_1^*}{g_1}\frac{a_2}{a_1} \tag{5.3}$$

where the second term must equal $-\frac{h_1}{g_1}$. For quantized realizations where the reflectance $\frac{a_2}{a_1}$ is generated by a one-port with several passive sources, such cancellations are difficult to achieve due to the reduced magnitude of $\frac{a_2}{a_1}$ and, hence, the deterioration. Due to the smaller number of passive sources, the voltage wave circuit shows smaller stopband response deterioration in Fig. 5.3 than the power wave design. In conclusion, the realization derived from $T_D = f/g$ is more efficient and has a superior stopband response.

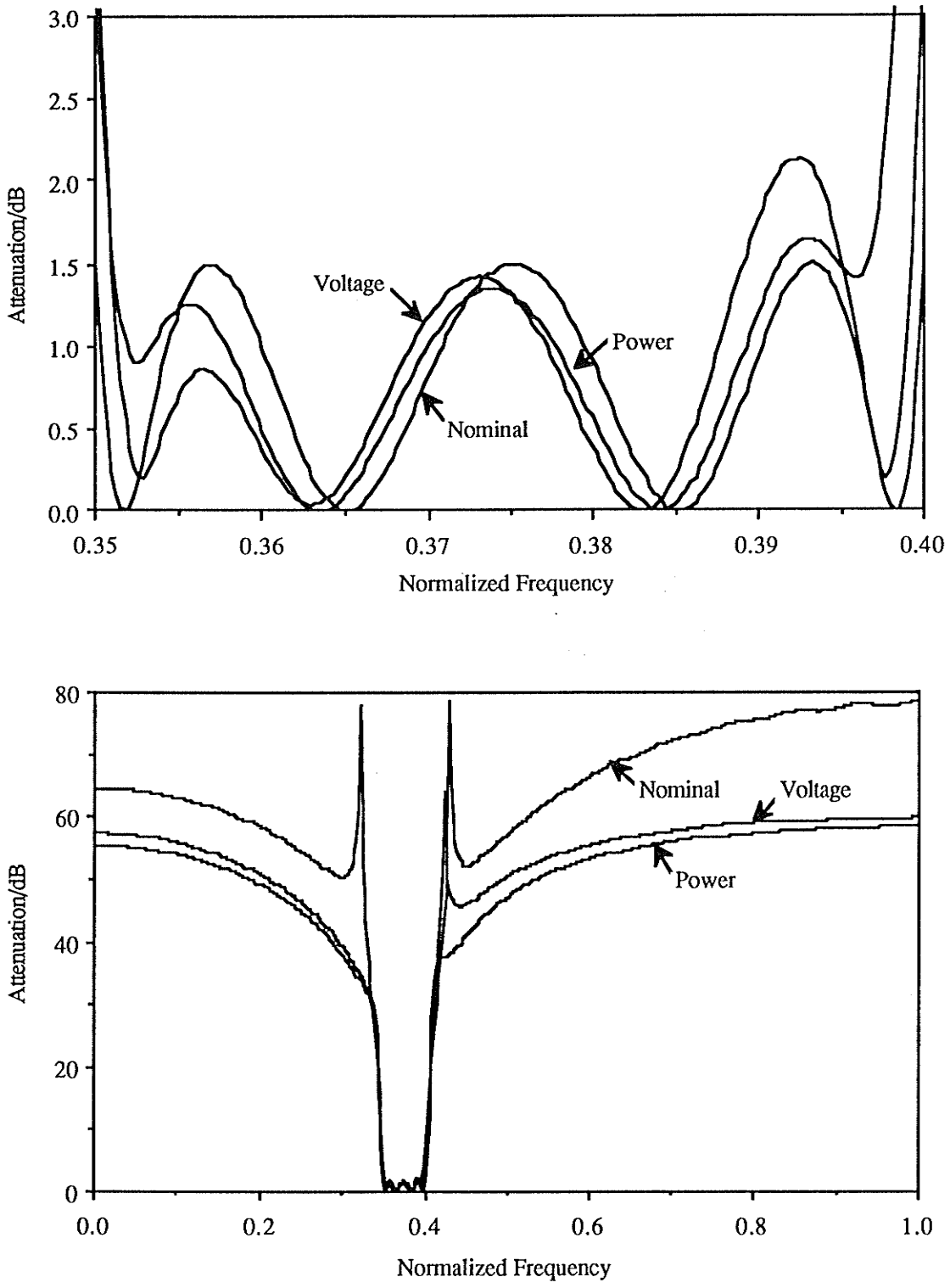

Fig. 5.3 Passband and stopband responses for Example 5.2 realized as a reflectance.

5.3 Example of a 14th-order Bandpass Filter with CCITT specifications

The final example is a design of a 14th-order bandpass filter that in the passband satisfies 1/20 CCITT attenuation specifications with the reference point set at 7.2 kHz (0 dB), as shown in Fig. 5.4a. Filters with these specifications occur frequently in the telephone communication networks; e.g., for the sampling frequency set at 24 kHz, a digital PCM/FDM transmultiplexer [38],[55] requires a digital filter with the above specifications.

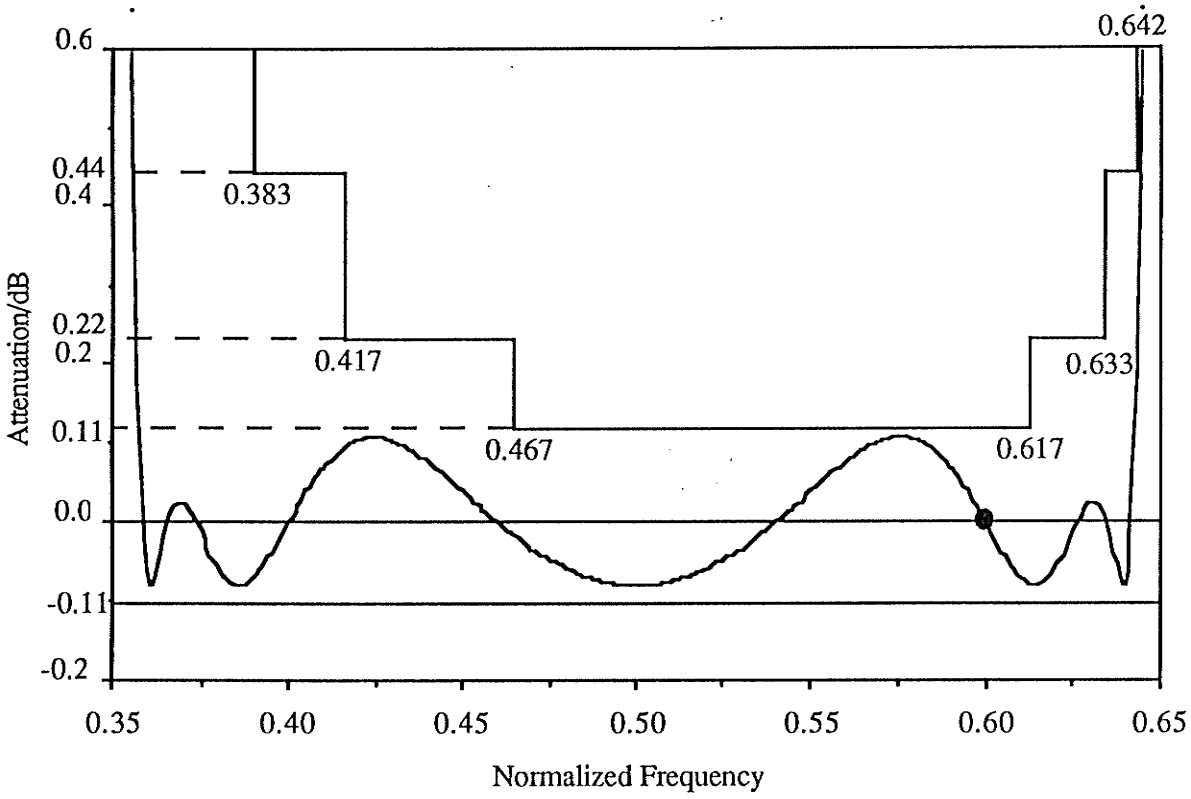

Fig. 5.4a CCITT specifications and the passband response for Example 5.3.

The simplest method of designing a bandpass filter is to start with a lowpass filter and then perform a lowpass-to-bandpass transformation. In the digital domain, this transformation takes on its simplest form, $z \rightarrow z^2$, when the center frequency of the bandpass filter is chosen to be 1/4 the sampling frequency. Since the passband specifications are asymmetrical for the bandpass filter (see Fig. 5.4a), the more stringent half is used in designing the required lowpass filter. We start with a 7th-order canonic analog prototype, as shown in Fig. 5.5, because analog filter design tables are readily available [53]. The canonic network in Fig. 5.5 is obtained from a noncanonic ladder by removing the redundant elements [29].

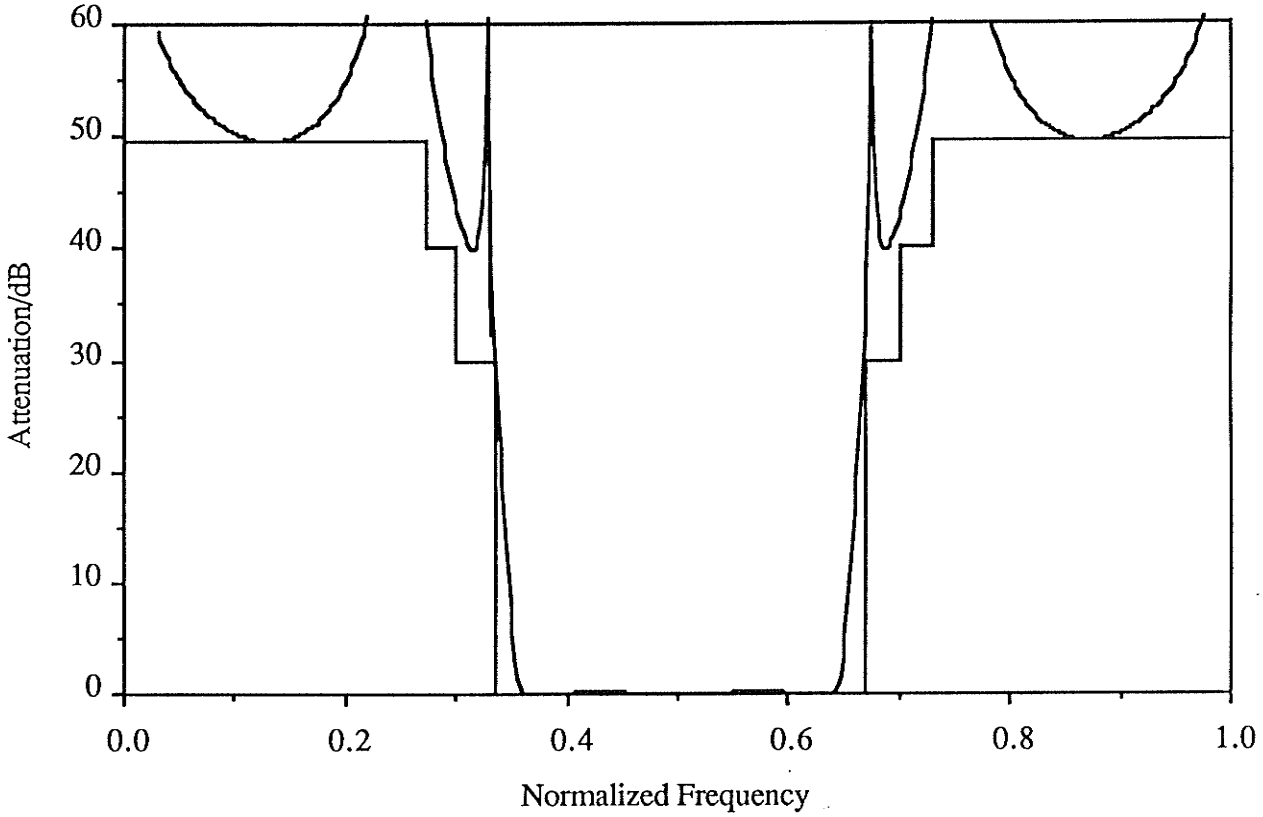

Fig. 5.4b Stopband response for Example 5.3.

A 7th-order elliptic response designated by CC071050 [53] and frequency scaled by $k_f = 0.477$ satisfies the lowpass specifications. As shown in Fig. 5.5, the filter is a cascade of three sections which are characterized by

$$\{\phi_1 , \alpha_1 , d_1\} \quad , \quad \{\phi_2 , \alpha_2 , d_2 , \infty , \pi , d_4\} \quad , \quad \{\phi_3 , \alpha_3 , d_3\}$$

with the middle section corresponding to the quasi-lattice section from Fig. 3.21 which, in effect, combines two elementary sections. A nonlinear optimization algorithm [42] was applied to the filter to induce the constraints from (3.30) for the two Brune sections (i.e., $\alpha_1 = -\omega_1 T$ and $\alpha_2 = \omega_2 T + \pi$ where $\phi_i = \tan \omega_1 T/2$) thereby allowing the simplified circuits from Table 3.7 to be used in the WD realization. Since in the corresponding WD realization the quasi-lattice section must be terminated on both sides with reflection-free sections, the last constant section, which results from this operation, must also be eliminated so as not to cause a delay-free loop between it and the last Brune section. This poses an additional constraint which was included in the optimization. It turns out that for the specifications in Fig. 5.4, all three constraints can indeed be imposed.

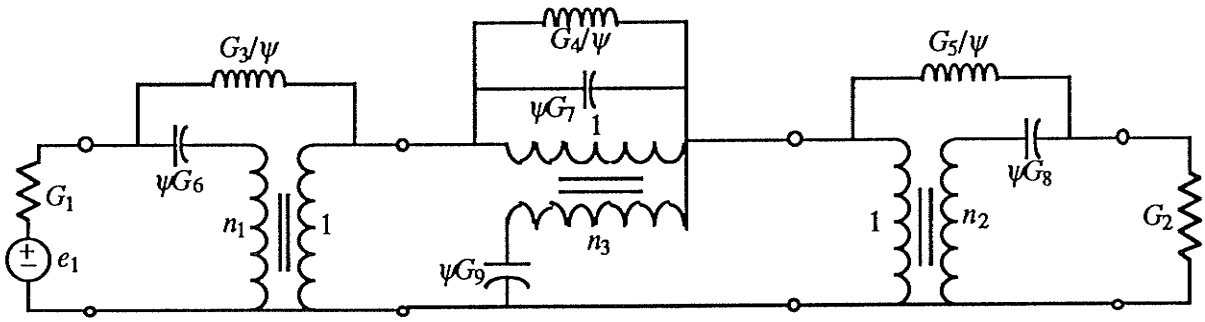

Fig. 5.5 Canonic analog prototype for Example 5.3.

The resulting WD bandpass filter with quantized multipliers is shown in Fig. 5.6, where the most efficient circuit from Fig. 3.3b was used for each matched 4-port adaptor. The quantized solution was obtained through an exhaustive search which is greatly aided by the fact that all multipliers are bounded $-1 < \gamma_i < 1$ and, because the structure is lossless and therefore has low sensitivity, a low number of bits is usually required. The corresponding frequency response is shown in Figs. 5.4a and b with the frequency scale normalized: actual frequency in kHz/12 kHz..

The analog element values that correspond to the lossless and quantized WD circuit are given by

$$G_1 = 4 \quad G_3 = \frac{4}{3} \quad G_6 = \frac{16}{3} \quad n_1 = \frac{1}{4} \quad G_2 = 4 \quad G_5 = \frac{4}{3} \quad G_8 = \frac{16}{3} \quad n_2 = \frac{1}{4}$$

$$G_4 = \frac{36}{23} \quad G_7 = \frac{417}{46} \quad G_9 = \frac{58}{3} \quad n_3 = \frac{1}{2}$$

A parallel adaptor [11] was used to realize the 2nd-order resonant circuit in the quasi-lattice section since it allows more quantized solutions than the circuit in Fig. 2.11a. The overall WD realization requires 19 additions (assuming $a_2 = 0$) and 9 multiplications, most of which are simple binary shifts. The design compares favorably with other solutions such as the one in [56] which requires 40 additions and 12 multiplications, but with two fewer delays. Another solution derived from a noncanonic prototype was given in [57] and requires 30 additions and 9 multiplications (all of which are simple shifts), but 6 more delays are also required. The circuit in Fig. 5.6 is therefore the preferable choice.

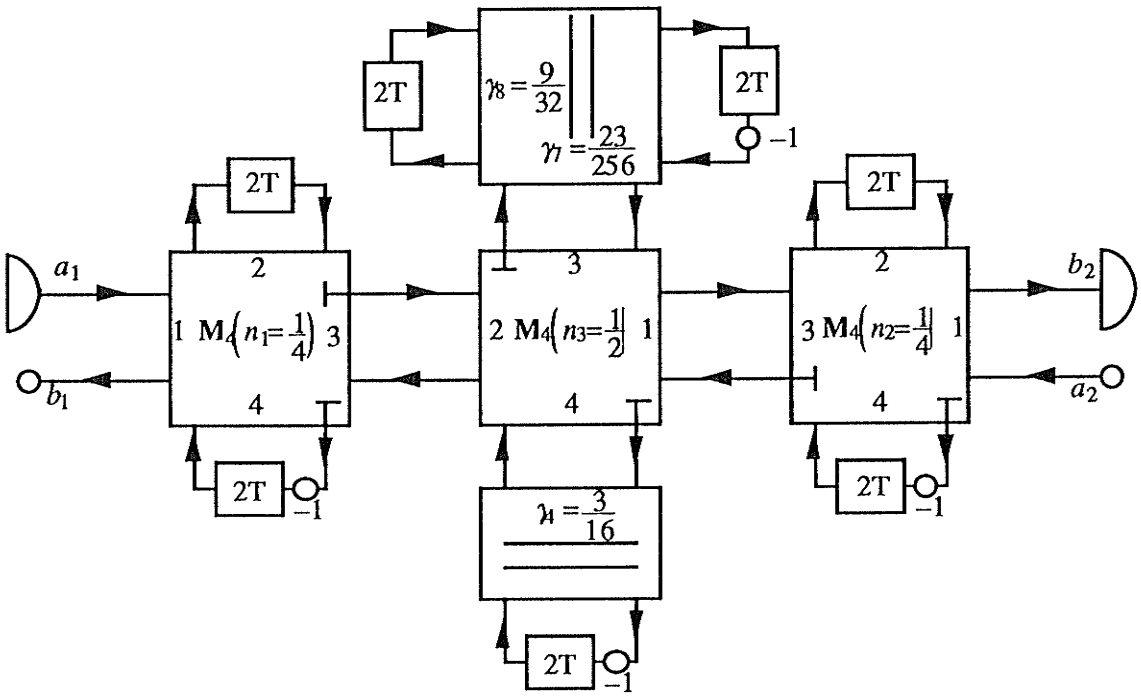

Fig. 5.6 WD circuit for a 14th-order bandpass filter.

VI. CONCLUSIONS AND RECOMMENDATIONS

It has been shown that a particular characterization of every elementary section, which is both simple and minimal, leads to a cascade synthesis algorithm of lossless, real two-port networks that has eliminated the need for performing basic polynomial operations, particularly zero finding. In other words, the decomposition can be achieved without having to obtain intermediate polynomials at any stage during the extraction process.

It is possible to characterize minimally every type of elementary section, reciprocal and nonreciprocal, using a triplet of numbers

$$\{\psi_i\,,\,\rho\,(\psi_i)\,,\,d\,(\psi_i)\} \;\leftrightarrow\; \{z_i^{-1}\,,\,\rho\,(z_i^{-1})\,,\,\delta\,(z_i^{-1})\}$$

where $\psi_i = \dfrac{1 - z_i^{-1}}{1 + z_i^{-1}}$, $\rho\,(\psi_i) = \rho\,(z_i^{-1})$, $d\,(j\phi_i) = (1 + \cos\,\omega_i T\,)\delta\,(e^{-\omega_i T})$

The first number is the location of the transmission zero, the second is the value of the reflectance at the transmission zero, and the third has been shown to be equal to the return group delay and is only required for reciprocal sections. Because of the simple relationship between characterizations in the continuous-time (ψ) and the discrete-time (z) domains, the algorithm can synthesize lumped LC circuits and wave digital filters. The output of the algorithm are the factors comprising the product of L transfer matrices, $\mathbf{T} = \prod_{i=1}^{L} \mathbf{T}_i$, where L is the number of sections and $\mathbf{T} = \frac{1}{f}\begin{bmatrix} \sigma g_* & h \\ \sigma h_* & g \end{bmatrix}$ is the scattering transfer matrix where the set of polynomials $\{f\,,\,g\,,\,h : gg_* = hh_* + ff_*\}$ is referred to as Belevitch's representation. All types and multiplicities of transmission zeros are allowed. This is important in the case of non-minimum phase transfer functions (i.e., ones with right-hand ψ-plane transmission zeros) which become necessary when a design combining high selectivity with a good approximation to phase linearity is desired.

During the extraction step, the triplets that characterize the remaining transmission zeros can be recomputed using two simple algebraic expressions that only require complex multiplications and divisions. If the triplet of the extracted section is equal to the corresponding triplet obtained from the set $\{f\,,\,g\,,\,h : gg_* = hh_* + ff_*\}$, the recomputed triplets characterize a lossless two-port with a lower degree such that the overall realization is canonic, i.e., the number of reactive elements (delays) is equal to the degree of g. It should be possible, however, to alter the synthesis algorithm to allow noncanonic synthesis, i.e., instead of extracting a canonic 2nd-order section with a unimodular $e^{j\alpha}$ reflectance, a 1st-order section is extracted first that sets the recomputed α to either 0 or π, which is then

followed by the extraction of a two-port with a resonant circuit (Tables 3.5-3.6). This procedure would generate analog circuits that are free of ideal transformers.

It has been found convenient to split-up the recomputation step into two stages so that the different requirements for analog and WD circuits can be dealt with simultaneously. The first stage of recomputation uses primitive polynomials whose coefficients are simple functions of the minimal triplet. During the second stage, an ideal transformer $\leftrightarrow$ 2-port adaptor can be extracted that, in the analog domain, annihilates the ideal transformer that was possibly introduced during the primitive stage, and in the WD domain, induces a reflection-free port. The actual choice is up to the user. It has been found experimentally that the two-stage recomputation step accumulates roundoff error more slowly than the nominally equivalent one-stage step. The difference, however, is only significant for extreme designs. The recomputation stage is the only source of roundoff error and it has been found that for noncritical transfer functions the accumulation of roundoff error is negligible.

Because of the purely algebraic nature of the recomputation expressions and the computation of initial triplets, the algorithm can be programmed with relative ease and has a high running speed. For example, it took only a few seconds on a personal (MacII) computer to synthesize the 14th-order bandpass filter in Example 5.1. Such speed makes it feasible to generate many equivalent circuits such that the final realization is optimum.

Realizations for all elementary sections can be derived systematically from a basic 4-port topology that is matched at each port. As a result, the derivations are simple and generate WD circuits whose flowgraphs consist of only normalized 2-port adaptors and delays. Moreover, the number of parameters characterizing each circuit is minimal but the number of multipliers that must be quantized is not minimal, thus necessitating a passive realization. By converting to voltage wave 2-port adaptors, the number of multipliers that must be quantized can be drastically reduced. For general 2nd-order sections with $e^{j\alpha_i} = \pm e^{j\omega_i T}$, the number of quantized multipliers is minimal, the circuit is structurally lossless, and only one multiplier controls the location of the transmission zero. WD filters that are a chain connection of structurally lossless sections have lower sensitivity to multiplier quantizations than passive circuits. It would, therefore, be of interest to examine the possibility of generating an altered set $\{f, g, h : gg_* = hh_* + ff_*\}$ such that the condition $e^{j\alpha_i} = \pm e^{j\omega_i T}$ for each general 2nd-order section can be induced by extracting the simplest kind of the 1st-order nonreciprocal section (see special cases in Table 3.8). This is in direct analogy to the procedure used for generating noncanonic analog circuits.

A new WD circuit, referred to as quasi-lattice, has been derived that is inherently structurally lossless and requires a minimum number of 2-port adaptors. This circuit is a generalization of the WD lattice filter and must be terminated on both sides by sections with reflection-free ports – a condition which can be satisfied by placing the circuit in the middle of the cascade. An example of a realization utilizing this section has been shown to be very efficient.

REFERENCES

[1] V. Belevitch, *Classical Network Synthesis,* San Francisco, CA: Holden-Day, 1968.

[2] H. Baher, *Synthesis of Electrical Networks,* Chichester, Sussex, England: John Wiley 1984.

[3] A. Fettweis, "Factorization of transfer matrices of lossless two-ports", *IEEE Trans. Circuit Theory,* vol. CT-17, pp. 86-94, Feb. 1970.

[4] A. Fettweis, "Cascade synthesis of lossless two-ports by transfer matrix factorization", in *Proc. Nat. Advanced Study Institute in Network Theory,* R. Boite (Ed), Gordon and Breach, New York 1972.

[5] M. Hasler and J. Neirynck, *Electric Filters*, Artech House, Inc. Dedham, MA. 1986.

[6] D. C. Youla, "A tutorial exposition of some key network-theoretic ideas underlying classical insertion-loss filter design', *Proc. IEEE,* vol. 59, No. 5, pp. 760-799, May 1971.

[7] W. Cauer, *Synthesis of Linear Communication Networks,* vols I and II. New York: McGraw-Hill, 1958.

[8] S. Darlington, "Synthesis of reactance 4-poles', *J. Math. Phys.,* vol. 18, pp. 257-353, Sept. 1939.

[9] V. Belevitch, "Four-dimensional transformations of 4-pole matrices with applications to the synthesis of reactance 4-poles', *IRE Trans.* 1956, CT-3, pp. 105-111.

[10] A. Fettweis, "Digital filters related to classical filter networks", *Arch. Elec. Übertragung.,* vol. 25, pp. 79-89, Feb. 1971.

[11] A. Fettweis, "Wave digital filters: theory and practice" (invited paper), *Proc. IEEE,* vol. 74, pp. 270-327, Feb. 1986.

[12] A. Fettweis and K. Meerkötter, "Suppression of parasitic oscillations in wave digital filters", *IEEE Trans. Circuits Syst.,* vol CAS-22, pp. 239-246, Mar. 1975.

[13] K. Meerkötter, "Incremental pseodopassivity of wave digital filters", *Proc. First Europ. Signal Proc. Conf.* (EUSIPCO-80), Lausanne, Switzerland, Sept. 1980, 27-32.

[14] P. Dewilde and E. Deprettere, "Orthogonal cascade realization of real multiport digital filters", *Int. J. Circuit Theory Appl.,* vol. 8, pp. 245-277, June 1975.

[15] S. K. Rao and T. Kailath, "Orthogonal digital filters for VLSI implementation", *IEEE Trans. Circuits Syst.,* vol CAS-31, pp. 933-943, Nov. 1984.

[16] P. P. Vaidyanathan and S. K. Mitra, "Low passband sensitivity digital filters: A generalized viewpoint and synthesis procedures", *Proc. IEEE,* pp. 404-423, April 1984.

[17] A. Fettweis, "Network-theory approach to designing lossless (orthogonal) digital filter structures", *Proc. IEEE Int. Symp. Circuits and Systems,* vol. 1, Philadelphia, PA, 1987, pp. 154-156A.

[18] A. Fettweis, "Passivity and losslessness in digital filtering", *Arch. Elec. Übertragung.*, vol. 42, pp. 1-8, Feb. 1988.

[19] P. P. Vaidyanathan, "A unified approach to orthogonal digital filters and wave digital filters based on LBR two-pair extraction", *IEEE Trans. Circuits Syst.*, vol CAS-32, pp. 673-686, July 1985.

[20] S. K. Mitra, P. P. Vaidyanathan and B. D. O. Anderson, "A general theory and synthesis procedure for low-sensitivity active RC filters", *IEEE Trans. Circuits Syst.*, vol CAS-32, pp. 687-699, July 1985.

[21] B. J. Hosticka, J. Büddefeld, and U. Kleine, "Power-wave digital filters using CORDIC adaptors", *Arch. Elec. Übertragung.*, vol. 39, pp. 242-244, no. 4, 1985.

[22] W.F. Göttlicher, "Beiträge zur rechnergestützten Synthese verlustfreier Zweitore", Ph.D. Thesis, Erlangen, West Germany, 1983.

[23] R. Unbehauen, *Synthese elektrischer Netzwerke*, R. Oldenbourg Verlag, München, 1972.

[24] P. Burrascano, G. Martinelli, and G. Orlandi, "Low-sensitivity digital filters based on zero extraction", *IEEE Trans. Circuits Syst.*, vol CAS-34, pp. 1581-1587, Dec. 1987.

[25] P. P. Vaidyanathan and S. K. Mitra, "Synthesis of arbitrary digital transfer fuctions using allpass-based structures derived via LBR two-pair extraction procedure", *Circuits Systems Signal Process.*, vol. 5, no. 3, 1986 pp. 343-370.

[26] H. J. Orchard, "Low sensitivity in simply and doubly terminated filters", *IEEE Trans. Circuits Syst.*, vol CAS-26, pp. 293-297, Jan. 1979.

[27] D.C. Youla, "A new theory of cascade synthesis", *IRE Trans.*, 1961 CT-8, pp. 244-260

[28] J. Scanlan and J. Rhodes, "Unified theory of cascade synthesis", *Proc. IEE,* vol. 17, no. 4, pp. 665-670, April 1970.

[29] M. Jarmasz and G.O. Martens, "Design of canonic wave digital filters using Brune and matched 4-port adaptors", *IEEE Trans. Circuits Syst.*, vol CAS-34, pp. 480-496, May 1987.

[30] P. Dewilde, "Orthogonal filters, pipelining and VLSI implementation", *Proc. Sixth Eur. Conf. Circuit Th. Design,* Stuttgart, W. Germany, 1983, pp. 400-404.

[31] J. Williamson, "Transfer matrix factorization using product-form polynomial scattering parameters', Master's Thesis, Univ. of Man., 1987.

[32] A. Fettweis, "Digital circuits and systems", *IEEE Trans. Circuits Syst.*, vol CAS-31, pp. 31-48, Jan. 1984.

[33] A. Oppenheim and R. Schafer, *Digital Signal Processing,* Englewood Cliffs, New Jersey: Prentice-Hall 1975.

[34] K.J. Schultz and M.R. Jarmasz, "A VLSI Wave Digital Filter With a Bit-Parallel Architecture", *Proc. Canadian Conf. on VLSI*, Winnipeg, Man., Canada, pp. 255-261, Oct. 1987.

1987.
[36] A. Fettweis, J.A. Nossek, and K. Meerkötter, "Reconstruction of signals after filtering and sampling rate reduction," *IEEE Trans. Acoust., Speech, Signal Processing,* vol. ASSP-33, pp. 893-902, Aug. 1985.
[37] M.R. Jarmasz, V. Shkawrytko, and G.O. Martens, "Application of Wave Digital Filter Structures to Sub-Band Voice Coder Design", Final Report Dept. of Communications, Ottawa, Ont., DSS Contract No. OST85-00192, 85-86.
[38] A. Fettweis, "Transmultiplexers with either analog conversion circuits, wave digital filters, or SC-filters – A review," *IEEE Trans. Commun.,* vol. COM-30, pp. 1575-1586, July 1982.
[39] M.R. Jarmasz, "Progress report on: Wave digital filters," Manitoba Hydro University Post-Graduate Student Research Grant Program.
[40] R. E. Crochiere, "Digital ladder structures and coefficient sensitivity", *IEEE Trans. Audio and Electroacoustics,* vol. AU-20, no. 4, pp. 240-245, Oct. 1972.
[41] S. Y. Kung, H. J. Whitehouse, and T. Kailath, EDS., *VLSI and Modern Signal Processing,* Englewood Cliffs, New Jersey: Prentice-Hall 1985.
[42] J.A. Nelder and R. Mead, "A simplex method for function minimization," *Computer J.*, no. 7, pp.308-313, 1965.
[43] H.J. Orchard, "Inductorless filters," *Electron. Lett.*, vol. 2, pp. 224-225, June 1966.
[44] R. Unbehauen, *MOS Switched-Capacitor and Continuous-Time Integrated Circuits and Systems – Analysis and Design,* Spriger Verlag, Berlin, 1989.
[45] L. Gazsi, "Explicit formulas for lattice wave digital filters", *IEEE Trans. Circuits Syst.,* vol CAS-32, pp.68-88, Jan. 1985.
[46] M. Renfors and E. Zigouris, "Signal processor implementation of digital allpass filters," *IEEE Trans. Acoust., Speech, Signal Processing,* vol. ASSP-36, pp. 714-729, May 1988.
[47] P. A. Regalia, S. K. Mitra, and P. P. Vaidyanathan, "The digital all-pass filter: a versatile signal processing building block", *Proc. IEEE,* vol. 76, pp. 19-37, Jan. 1988.
[48] P. P. Vaidyanathan, S. K. Mitra, and Y. Neuvo, "A new approach to the realization of low-sensitivity IIR digital filters", *IEEE Trans. Acoust., Speech, Signal Processing,* vol. ASSP-34, pp. 350-361, April 1986.
[49] A. Sedlmeyer and A. Fettweis, "Digital filters with true ladder configuration", *Int. J. Circuit Theory Appl.,* vol. 1, pp. 5-10, March 1973.
[50] G. O. Martens and K. Meerkötter, "On n-port adaptors for wave digital filters with applications to a bridged-tee filter", *Proc. IEEE Int. Symp. Circuits and Systems,* vol. 1, Munich, West Germany, 1976, pp. 514-517.
[51] M. Suzuki, N. Miki, and N. Nagai, "New wave digital filters for basic reactance sections", *IEEE Trans. Circuits Syst.,* vol CAS-32, pp.337-348, Apr. 1985.
[52] G. O. Martens and H. H. Lê, "Wave digital adaptors for reciprocal 2nd-order

[51] M. Suzuki, N. Miki, and N. Nagai, "New wave digital filters for basic reactance sections", *IEEE Trans. Circuits Syst.*, vol CAS-32, pp.337-348, Apr. 1985.
[52] G. O. Martens and H. H. Lê, "Wave digital adaptors for reciprocal 2nd-order sections", *IEEE Trans. Circuits Syst.*, vol CAS-25, pp.1077-1083, Dec. 1978.
[53] R. Saal, *Handbook of Filter Design*, AEG Telefunken, Backnang, West Germany, 1979.
[54] G. O. Martens – private communication.
[55] A. Fettweis, "Multiplier-free modulation schemes for PCM to FDM and audio FDM conversion", *Arch. Elec. Übertragung.*, vol. 32, pp. 477-485, Feb. 1978.
[56] W. Wegener, "On the design of wave digital lattice filters with short coefficient word lengths and optimal dynamic range", *IEEE Trans. Circuits Syst.*, vol CAS-25, pp.1091-1098, Dec. 1978.
[57] W. Wegener, "Design of wave digital filters with very short coefficient word lengths", *Proc. IEEE Int. Symp. Circuits and Systems,* vol. 1, Munich, West Germany, 1976, pp. 473-476.
[58] G.O. Martens and M.R. Jarmasz, "Design of Digital Filters with a Diagonal Lyapunov Function Based on Elliptic Reference Filters", *Proc. IEEE Int. Symp. Circuits Syst.*, Rome, Italy, pp. 527-530, 1982.